JOURNAL OF THE AERONAUTICAL SCIENCES

VOLUME 13 APRIL, 1946 NUMBER 4

Effect of Bend Width upon Minimum Bend Radii

GEORGE GERARD*

Republic Aviation Corporation

SUMMARY

Bends of large width occasionally exhibit cracks at the center of the width when minimum bend radii successfully employed on small widths are used. An analysis of the stress condition existing at the center of a large width revealed an unfavorable bi-axial tension stress that reduces the ultimate elongation from that in simple tension. An experimental photogrid strain survey on three aluminum alloys confirmed the results of the analysis and indicated the extent of bi-axiality of stress as the width decreased.

Elongation date from standard tensile coupons were corrected for bi-axiality, and the results were then applied in determining theoretical minimum bend radii for various widths of bend.

INTRODUCTION

DURING A RECENT INVESTIGATION at Republic on the formability properties of certain new aluminum alloys, attention was given to the basic forming problem of minimum bend radii. In evaluating the bend radius test results of this investigation, an attempt was made to correlate the data on Alclad 24S-O (included in the program to provide a basis for comparison with the new materials) with the minimum bend radii in current use at various aircraft companies.

The investigation indicated a marked disagreement on the minimum bend radius for various sheet gages of Alclad 24S-O, although apparently the stated value is the minimum that can be consistently attained in the shops of the various companies. A large share of this disagreement could probably be traced to the different handling techniques employed in each shop, although substantially the same equipment is employed everywhere. Another source of discrepancy may be the consistency of results desired—i.e., some companies were willing to tolerate a small number of rejects in order to realize a smaller bend radius, while others were not. The number of rejects is probably caused by the variations in material properties from one lot of sheet to another.

In spite of these possible causes for disagreement, it was felt that some fundamental factor in establishing minimum bend radii was responsible for the discrepancy. A probable answer was indicated in reference 1, in which test data were presented which showed a marked increase in minimum bend radius as the specimen width (the length of bend normal to the bend cross section) was increased. Since each company probably used different bend widths in establishing minimum bend radii for Alclad 24S-O, this effect as given in reference 1 was serious enough to account for the discrepancy.

Aside from providing a reason for the disagreement on the Alclad 24S-O bend radii, these data provided an explanation of why sections of large bend width, such as stringers or longerons, occasionally crack in central regions when bend radii successfully employed on short

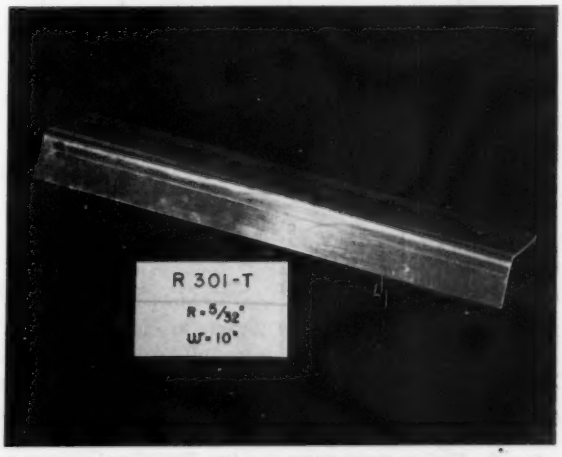

FIG. 1. Characteristic cracking at center of bend width caused by bi-axial tension stress condition.

Received October 13, 1945.

* Senior Research Engineer.

widths are used. This phenomenon is illustrated in Fig. 1 in which a specimen of 0.064-in. R301-T aluminum alloy was formed to a 90° bend. This investigation was initiated, therefore, to determine the seriousness of the width effect on minimum bend radii.

Symbols

σ	= stress, lbs. per sq. in.
ϵ	= strain, in. per in.
x	= coordinate in direction of bend
y	= coordinate in width direction
z	= coordinate in thickness direction
ν	= Poisson's ratio, 0.50 in the plastic range
w	= bend width in
R	= bend radius to neutral axis, in.
R_i	= inside bend radius, in.
t	= thickness, in.
K	= ratio of distance between outside fiber of bend and neutral axis to total thickness
c	= ratio of cladding thickness per face to total thickness
ϵ_x	= strain in bend direction
ϵ_y	= strain in width direction
$\epsilon_{ult.}$	= strain in bend direction under simple tension, i.e., plane stress
$\epsilon_{ult.c}$	= $\epsilon_{ult.}$ corrected for cladding thickness

Stress Condition in Wide Bends

Before an analysis of the stress condition in a bend is presented, it would be well to review some basic concepts of the response of metals to combined stress.

In general, we are only concerned with an element in a two-dimensional stress field, since the stress condition in a bend can be reduced to one of this nature. In Fig. 2, the three principal stress conditions that can be obtained on a two-dimensional element are illustrated and a stress-strain curve for each condition is shown. Each of the combined stress conditions influences the stress-strain curve in a manner such as to ease or aggravate the forming operation. Condition (b) approaches a pure shear condition that is helpful in forming because of the high elongations that can be obtained, whereas condition (c) approaches the highly undesirable bi-axial tension condition in which elongation properties are considerably reduced from those in simple tension (a).

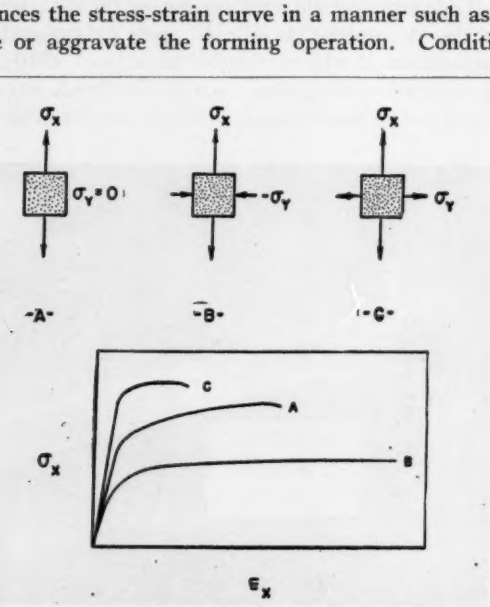

Fig. 2. Various stress states on a two-dimensional element and the effect upon the stress-strain curve.

The principal forming load is often applied in one direction only but the geometry of the part is such that stresses are induced in directions other than that of the applied load. An element elongated in one direction tends to contract in the other two, and if these induced contractions are restrained, stresses are induced in the latter directions. The ratio of this induced lateral deformation to applied axial deformation under an axial load is Poisson's ratio. For aluminum alloys, this ratio has a value of 0.3 in the elastic range and is assumed equal to 0.5 in the plastic range of the material.

Fig. 3 shows the deformation of an element under an applied stress. If the lateral deformation is completely restricted—i.e., $\epsilon_y = 0$—a stress will be induced in this direction. If no lateral restraint is imposed then $\epsilon_y = -\nu\epsilon_x$ and the stress in the lateral direction will be zero.

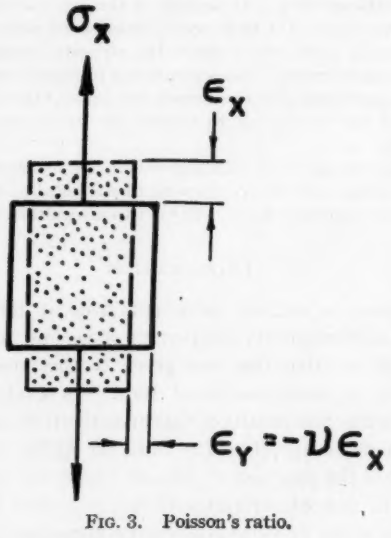

Fig. 3. Poisson's ratio.

Anticlastic Bending

In the bending process, the outer surface of the bend is elongated and the inner surface compressed. Thus, tension and compression forming loads are applied to the outside and inside surfaces, respectively. These forming loads induce strains by Poisson's effect in the width (y) and thickness (z) directions (see Fig. 4) of a magnitude equal to one-half the applied strain, since forming is accomplished in the plastic range. The z-direction strain is not restrained by the geometry of the formed part, and, consequently, in the bending process some thinning can occur.

The strain in the width direction, however, is affected by the bend geometry. The outer fiber strain

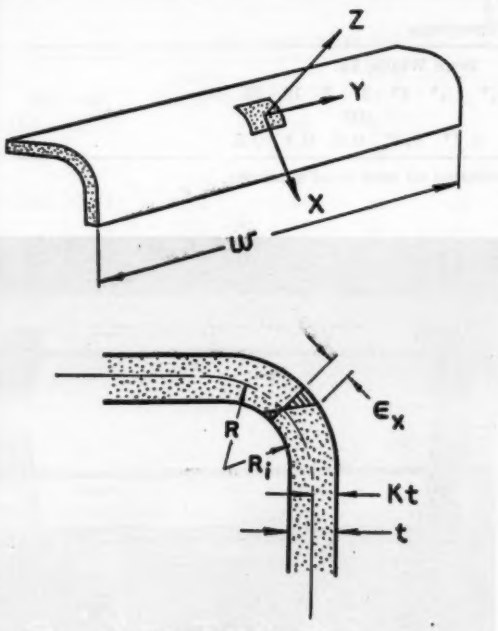

FIG. 4. Bend parameters.

induces a lateral contraction in the width direction, and, similarly, the inner fiber strain induces a lateral elongation. Unless the bend curves in the width direction as shown in Fig. 5, these induced strains will be restrained. The geometry of the bent part is such as to completely restrain this anticlastic curvature because of the relatively large moment of inertia of the flange and the high degree of curvature of the material in the bend region.

Photographs of sections through bend widths are illustrated in Fig. 6. Except for a highly localized curvature at the edge of the large bend widths and the complete anticlastic curvature in the smallest bend widths, the center of the width is straight and, consequently, the width direction strain must be zero.

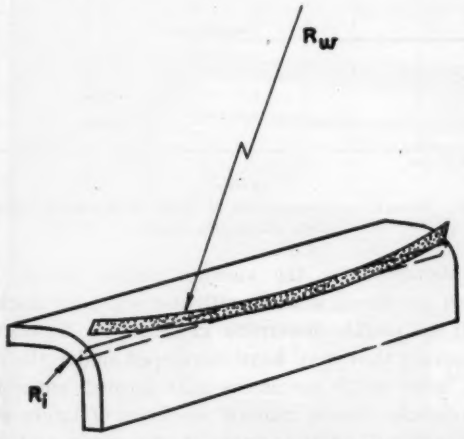

FIG. 5. Anticlastic curvature of bend if no restraint were imposed in the width direction.

Therefore, it can be concluded that the induced stress along the bend width arises from the restriction upon lateral strain. This induced stress corresponds to a strain equal to one-half the strain in the direction of loading.

At the center of the tension side of the bend, there now exists a bi-axial tension condition that is highly unfavorable and reduces the formability of the material. Thus, for bend widths in the usual range employed in aircraft parts, an unfavorable bi-axial tension condition does exist in the central region of the width. The bi-axial stress state reduces to a simple tension at the edges where the anticlastic curvature is not restrained, and, consequently, cracking may be confined only to the central region of the bend width where lowest elongation exists.

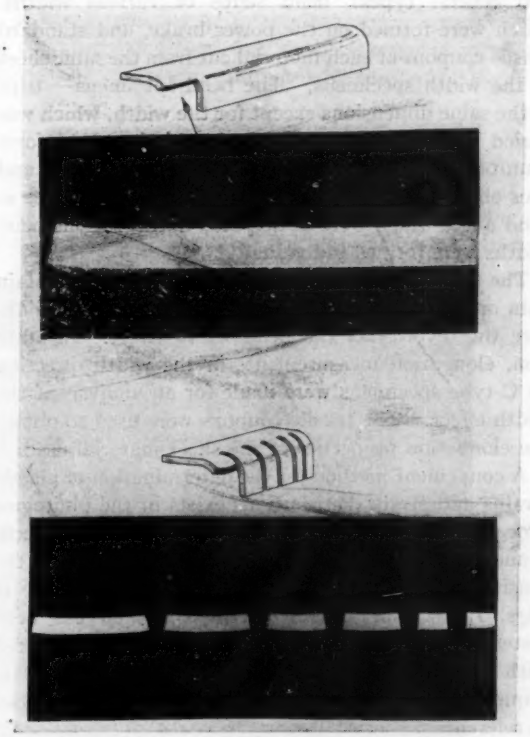

FIG. 6. Section through bend showing (a) anticlastic curvature confined to edge of large width and (b) complete anticlastic curvature of small widths (0.4 to 0.1 in.).

BEND RADIUS TESTS ON VARIOUS WIDTHS

Test Specimens

The bending of large widths—e.g., stringers or longerons—is usually accomplished in a power brake, whereas the hydropress and hand brake are used largely in bending sections of small width. To obtain a complete range of bend widths in this investigation, the froming of all bends was performed on the power brake. Thus, if the effect of bend width upon minumum bend

TABLE 1
Width of Bend Specimens

Material	Bend Width, In.							
0.064 Alclad 24S-T, 0.064 R301-T, 0.064 Alclad 75S-T	Specimens A	1/4*	1/2*	1*	2*	5	10	25	50
	Specimens B	100							
	Specimens C	0.1*	0.2*	0.3	0.4	0.5			

* Two widths of this dimension were included on each bend specimen.

radius were serious, it would be manifest on the power brake where the widest range of widths are attainable.

To limit the scope of the investigation, the test program was restricted to the -T temper of aluminum alloys R301, Alclad 24S, and Alclad 75S. In addition, the specimens were of 0.064-in. sheet only, and no attempt was made to investigate the effect of thickness. The test specimens used in the investigation were of two general types: bend strips of various widths, which were formed on the power brake, and standard tensile coupons of each material cut from the same sheet as the width specimens. The bend specimens—strips of the same dimensions except for the width, which was varied as listed in Table 1—were designed to form simultaneously as many different widths as possible and thus eliminate experimental errors due to variations in bend angle which were anticipated if the various bend widths were formed individually.

The general experimental approach was to obtain data on shop bend tests of specimens A and B to indicate the severity of the bend width effect. In addition, elongation measurements in the width direction on C-type specimens were made for an analysis of the width effect. The tensile coupons were used to obtain the elongation properties of the sheet material used.

A convenient method for the determination of plastic strains and strain distributions exists in the photogrid process. This process, amply described in references 2 and 3, consists of photographing a fine grid on the sensitized surface of the specimen as illustrated in Figs. 7, 10, and 12. After the specimen has been tested, elongations between the grid lines are measured with a cathetometer. An application of this technique in determining minimum bend radii is described in reference 4.

As a preliminary step, a 2-in. grid was printed at the center of each of the widths on one A-type specimen of Alclad 24S-T and the specimen was bent to a 1/8-in. radius. The bent specimen with the grid at the center of a width is shown in Fig. 7. After bending, a strain survey on each width indicated that elongations along the width of the bend were restricted to specimens less than 1 in. Consequently, all subsequent elongation surveys were confined to C-type specimens.

The bend specimens of type A and B were bent 90° to a number of different radii in the region of the minimum radius so as to produce fracture in some widths and satisfactory bends near the minimum in others. Thus the region of the minimum bend radius

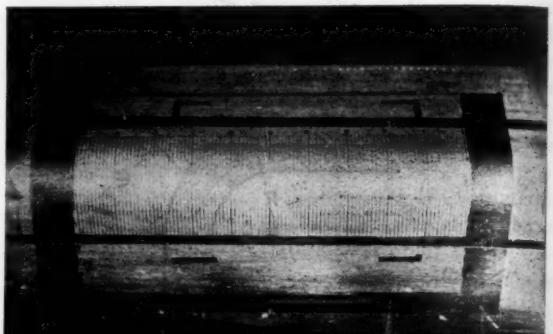

FIG. 7. Photogrid at center of large width.

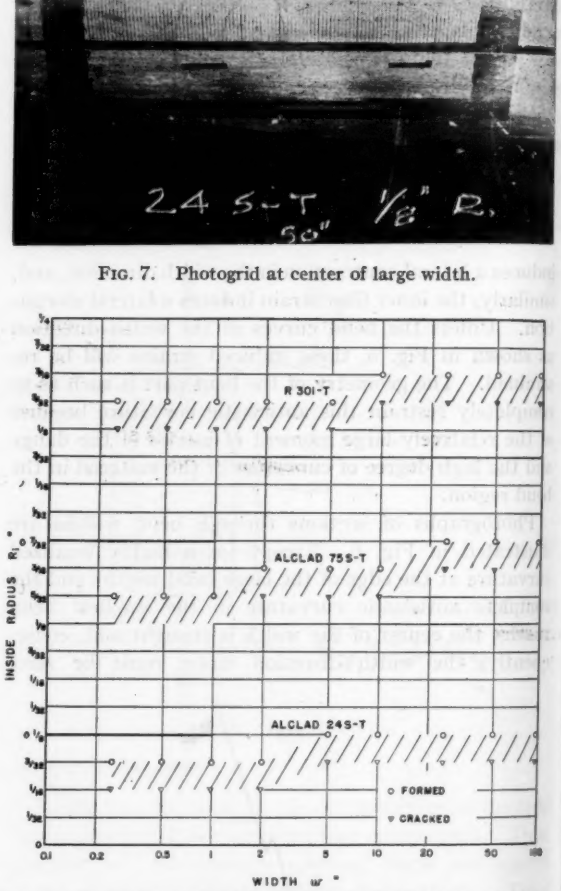

FIG. 8. Experimental variation of bend radius with width for three aluminum alloys.

was blanketed by the various widths tested. The formed specimens were visually inspected for cracking, which was readily discernible in all cases. To discover any cracks that may have developed under the cladding, bend width specimens that formed successfully immediately after a cracked specimen of larger width were sectioned at the center of the width and deep-etched.

TABLE 2

90° Power-Brake Bend Tests on Specimens A and B—0.064-In. Sheet

Material	Inside Radius, In.	R_i/t	Bend Width, In. 1/4	1/2	1	2	5	10	25	50	100
Alclad 24S-T	1/16	0.97	fr	fr	fr	fr	fr	fr	fr	fr	fr
	3/32	1.47	ok	ok	ok	ok*	cr	cr	cr	cr	fr
	1/8	1.95	ok	ok	ok	ok	ok	ok	ok	ok	ok
Alclad 75S-T	5/32	2.44	ok	ok	ok*	fr	fr	fr	fr	fr	..
	3/16	2.94	ok	ok	ok	ok	ok	ok*	cr	cr	..
	7/32	3.42	ok	ok	ok	ok	ok	ok	ok	ok	ok
	1/4	3.90	..	..	..	..	..	..	..	..	ok
R301-T	1/8	1.95	fr	fr	fr	fr	fr	fr	fr	fr	..
	5/32	2.44	ok	ok	ok	ok	ok*	cr	fr	cr	cr
	3/16	2.94	ok	ok	ok	ok	ok	ok	ok	ok	ok

* Specimens sectioned at center of width and deep-etched.

NOTE: ok—specimen formed successfully; cr—specimen cracked in center region of bend; fr—specimen fractured along entire bend line.

Power-brake equipment for making bends in the shop varies in steps of 1/32-in. radius. Consequently, it was impossible to determine exactly the minimum bend radius for each width specimen. At best, the minimum radius could be bracketed, and thus the radius was approached within a maximum tolerance of $\pm 1/32$ in.

The shop bend tests are tabulated in Table 2, and these data are plotted on Fig. 8.

It was interesting to observe the progressive severity of cracking along the bend line as the specimen width increased. A typical example is illustrated in Fig. 9.

ELONGATION SURVEYS

Type C Specimens

As previously stated, the elongation survey was confined to type C specimens. Photogrids were printed

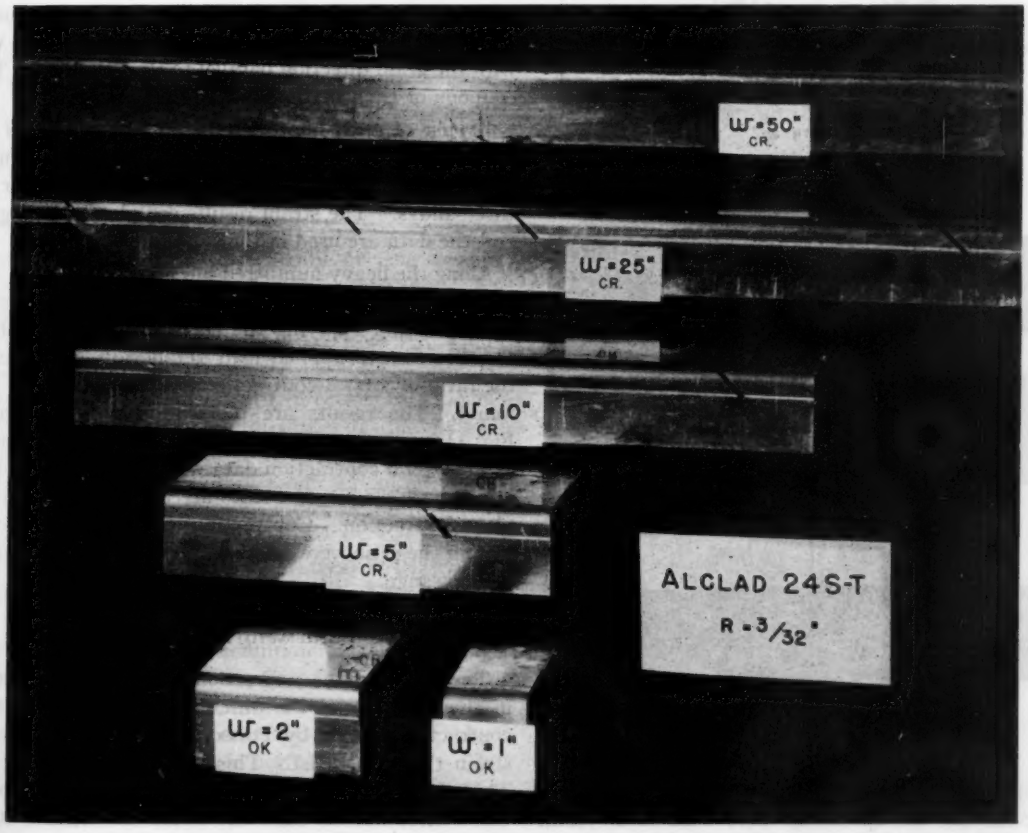

FIG. 9. Progressive severity of anticlastic cracking as bend width increases.

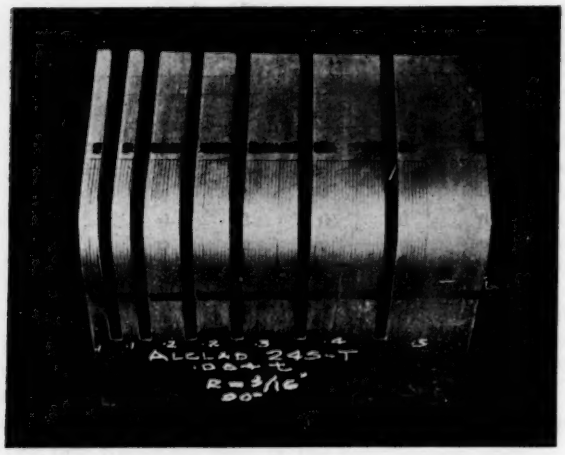

FIG. 10. Type C bend specimen showing photogrid on surface.

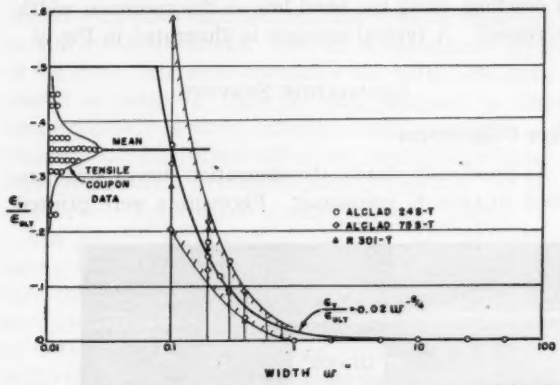

FIG. 11. Lateral strain at center of bend width for various bend widths.

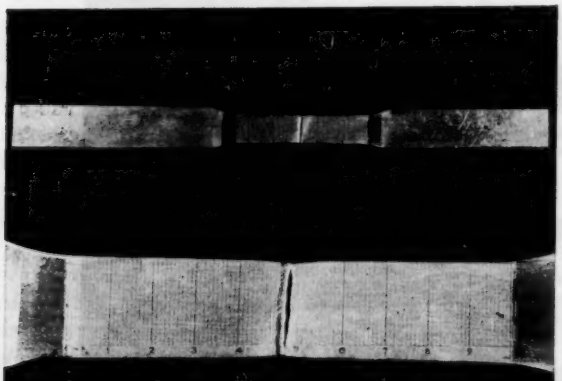

FIG. 12. Gridded tensile coupon showing enlarged fracture region.

on one specimen for each of the three alloys as shown in Fig. 10, and the specimens were bent to a $^3/_{16}$-in. radius. The strain along the width, ϵ_y, was then determined by measuring the elongation between successive pairs of grid lines.

The elongation data from these small width specimens are plotted on Fig. 11, with $\epsilon_y/\epsilon_{ult.}$ as the ordinate and the specimen width as the abscissa. The ratio $\epsilon_y/\epsilon_{ult.}$ is the strain in the width direction relative to the simple tensile strain in the bend direction. The latter strain, $\epsilon_{ult.}$, is determined theoretically for the particular sheet thickness and bend radius according to the analysis presented in reference 4.

Because of rather large scatter in the test data, it was thought desirable to group all data for the three alloys on one curve as shown in Fig. 11. On this curve, the elongation data obtained from the grid survey on an A-type specimen is also plotted to complete the range of widths tested.

A curve was fitted to the test data as shown by the heavy line on Fig. 11. The equation of this curve expressing the relationship between the lateral strain ratio and the width is

$$\epsilon_y/\epsilon_{ult.} = -0.02w^{-1/4} \qquad (1)$$

Theoretically, the limiting value of the ratio $\epsilon_y/\epsilon_{ult.}$ is 0.5, which is Poisson's ratio in the plastic range.

Tensile Coupons

Standard tensile coupons were cut cross-grain to duplicate the grain direction of the bend strips, viz., with the grain direction parallel to the bend line. Two coupons of each material were used.

By use of grids photographed on the surface of the tensile coupons as shown in Fig. 12, the ultimate strain in various gage lengths was determined[4] for the three alloys. The strain results are plotted in Fig. 13 and the data are used in the subsequent analysis.

Along the heavy numbered lines of the grid (Fig. 12), the lateral contraction was determined for each tensile specimen, and applying the correction to the strain in the direction of applied load detailed in Appendix A, the ratio of lateral contraction ϵ_y to elongation $\epsilon_{ult.}$ was found. The results are plotted on the ordinate of Fig. 11 in the form of a distribution curve. The mean of the lateral contraction data was 0.35, indicating that in a tensile coupon the sides are restrained from complete contraction. Contraction would have been complete if the ratio were equal to 0.5, Poisson's ratio in the plastic range.

Bend Width Analysis

The strain in the y-direction which induces a stress in this direction is the difference between the lateral contraction arising by Poisson's effect and the actual strain that does exist. This is illustrated on Fig. 14. This stress, in turn, tends to produce a contraction in the x-direction so that the maximum tensile strain that can be attained is

$$\epsilon_z = \epsilon_{ult.} - \nu[\epsilon_y - (-\nu\epsilon_{ult.})]$$

Simplifying

$$\epsilon_z = \epsilon_{ult.}(1 - \nu^2) - \nu\epsilon_y \qquad (2)$$

The relation between $\epsilon_y/\epsilon_{ult.}$ and width has been empirically determined from lateral contraction measurements on C-type specimens. From Eq. (1),

$$\epsilon_y = \epsilon_{ult.}(-0.02w^{-1/4})$$

Combining the latter with Eq. (2) leads to

$$\epsilon_z = \epsilon_{ult.}(1-\nu^2) + \nu\epsilon_{ult.}(0.02w^{-1/4})$$

Simplifying,

$$\epsilon_z = \epsilon_{ult.}[1 - \nu(\nu - 0.02w^{-1/4})] \qquad (3)$$

It has been shown in reference 4 that the ultimate strain in the gage length of the bend can be predicted from ultimate strain-gage length data such as presented in Fig. 13. These data are for a stress condition approaching simple tension and, consequently, are inapplicable for predicting minimum bend radii for wide bend specimens.

By applying Eq. (3) to these data, however, the ultimate strain-gage length curves can be modified to account for the effect of the width. For a given width, w, this equation reduced to the form

$$\epsilon_z = \epsilon_{ult.}(1 - K)$$

where K is a constant for each width. Thus, the basic strain-gage length curve derived from tensile coupons can be corrected for the width effect, and the corrected curve can be used in solving for the minimum bend radius.

Tensile Coupon Stress Condition

Lateral contraction measurements on the tensile coupons showed the mean lateral contraction to be 0.35 of the strain in the direction of applied load. Since the lateral contraction was less than 0.5, some restraint must have existed in the y-direction (Appendix A) similar to that in the width direction of a bend. This restraint in the width direction of the tensile specimen was probably caused by the geometry of the coupon in this plane. Lateral contraction measurements in the thickness direction indicated no restraint upon necking in this direction.

In addition to the width direction stress on the tensile coupon, some restraint was imposed in the lateral directions when necking occurred. However, since the tensile specimens were of -T condition material, necking is usually insignificant. Consequently, the restraint due to necking as outlined in reference 5 is small, and since scatter of the lateral contraction data was relatively large, the correction was neglected.

On Fig. 11, the mean lateral contraction of 0.35 for the tensile specimens corresponded to a bend width of 0.1 in. Thus, the bend width for which minimum bend radii are theoretically determined was established.

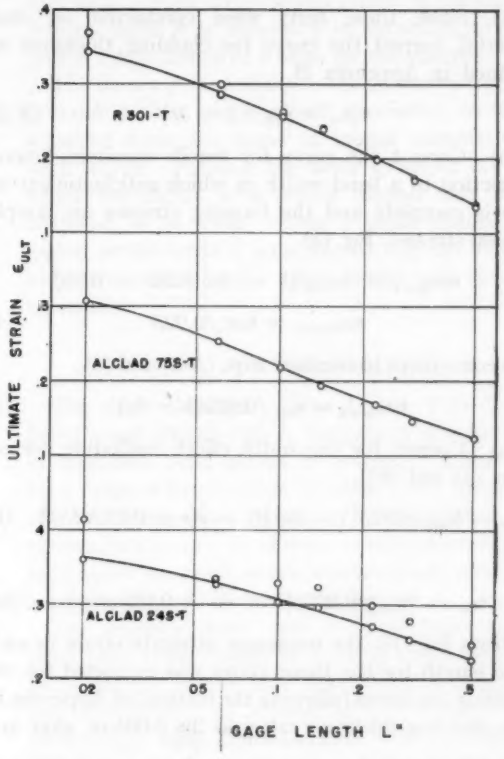

FIG. 13. Ultimate strain in various gage lengths. Data obtained from gridded tensile coupons.

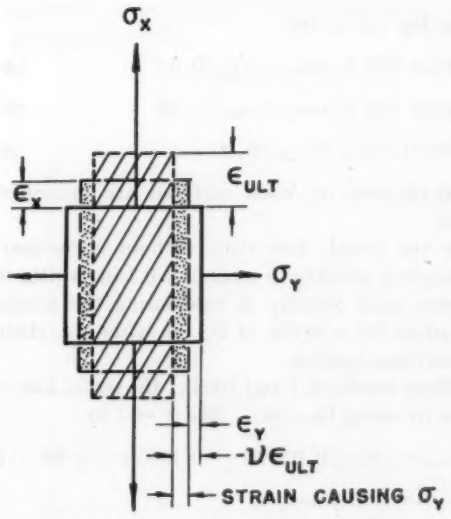

FIG. 14. State of strain in a wide bend.

Summary of Analysis and Theoretical Results

To determine the minimum bend radius for a bend of a given width, the following calculations are performed with the ultimate strain-gage length data of Fig. 13:

(a) Since these tests were conducted on clad material, correct the curve for cladding thickness as outlined in Appendix B.

$$\epsilon_{ult._c} = \epsilon_{ult.}/(1 - 2c) \qquad \text{(A-3)}$$

(b) Correct the curve for tensile specimen lateral restriction to a bend width in which anticlastic curvature is complete and the forming stresses are simple tension stresses, Eq. (3).

$$\epsilon_{ult._{w=0}} = \epsilon_{ult._c}/[1 - 0.5(0.50 - 0.35)$$

$$\epsilon_{ult._{w=0}} = \epsilon_{ult._c}/0.925 \qquad (4)$$

It is convenient to combine Eqs. (A-3) and (4).

$$\epsilon_{ult._{w=0}} = \epsilon_{ult.}/0.925(1 - 2c) \qquad (5)$$

(c) Correct for the width effect (including corrections (a) and (b)),

$$\epsilon_{x_w} = [\epsilon_{ult.}/0.925(1 - 2c)][1 - \nu(\nu - 0.02/w^{3/4})] \qquad (6)$$

or

$$\epsilon_{x_w} = (\epsilon_{ult._c}/0.925)[1 - \nu(\nu - 0.02/w^{3/4})] \qquad (6a)$$

From Fig. 13, the minimum ultimate strain in each gage length for the three alloys was corrected for the cladding thickness following the method of Appendix B. The cladding-thickness ratios in the 0.064-in. gage are:

Alclad 24S-T	$c = 0.025$
Alclad 75S-T	0.040
R301-T	0.050

Using Eq. (A-3), for

Alclad 24S-T, $\epsilon_{ult._c} = \epsilon_{ult.}/0.95$ (A-3a)

Alclad 75S-T, $\epsilon_{ult._c} = \epsilon_{ult.}/0.92$ (A-3b)

R301-T, $\epsilon_{ult._c} = \epsilon_{ult.}/0.90$ (A-3c)

The calculations for each material are presented in Table 3.

Since the tensile test data without correction for width applied directly to a bend of 0.1-in. width, these data were used directly in calculating the minimum bend radius for a width of 0.1 in. after the cladding correction was applied.

For bend widths of 1 and 100 in., the strain data were reduced by using Eq. (6a). For $w = 1$ in.:

$$\epsilon_{x_{w=1}} = (\epsilon_{ult._c}/0.925)[1 - 0.5(0.5 - 0.02/1)]$$

$$\epsilon_{x_{w=1}} = 0.822\ \epsilon_{ult._c} \qquad (6b)$$

for $w = 100$ in.:

$$\epsilon_{x_{w=100}} = 0.811\ \epsilon_{ult._c} \qquad (6c)$$

These calculations are also presented in Table 3.

These ultimate strain-gage length data are plotted on Fig. 15. The minimum bend radii for the 0.064-in. gage materials were determined by the nomographic solution detailed in reference 4, the results of which are presented in Table 4.

TABLE 3

Cladding and Width Corrections for Ultimate Strain-Gage Length Data

Gage Length, In.	$\epsilon_{ult.}$ (Fig. 13)	$w = 0.1$ in. $\epsilon_{ult._c}$ Eq. (A – 3a, b, c)	$w = 1$ in. $\epsilon_{ult._c}$ Eq. (6b)	$w = 100$ in. $\epsilon_{ult._c}$ Eq. (6c)
Alclad 24S-T				
0.02	0.360	0.379	0.312	0.307
0.06	0.330	0.347	0.285	0.281
0.10	0.306	0.322	0.264	0.261
0.14	0.301	0.317	0.260	0.257
0.22	0.274	0.288	0.236	0.233
0.30	0.256	0.269	0.221	0.218
0.50	0.230	0.242	0.199	0.196
Alclad 75S-T				
0.02	0.308	0.334	0.274	0.271
0.06	0.257	0.279	0.229	0.226
0.10	0.219	0.238	0.196	0.193
0.14	0.194	0.211	0.173	0.171
0.22	0.170	0.185	0.152	0.150
0.30	0.149	0.162	0.133	0.131
0.50	0.130	0.141	0.116	0.114
R301-T				
0.02	0.344	0.382	0.322	0.318
0.06	0.285	0.317	0.260	0.257
0.10	0.256	0.284	0.233	0.230
0.14	0.238	0.264	0.217	0.214
0.22	0.197	0.219	0.180	0.177
0.30	0.170	0.189	0.155	0.153
0.50	0.135	0.150	0.123	0.121

TABLE 4

Theoretical Minimum Bend Radii for Various Widths

	w, In.	R_i, In.	$R_{i/t}$
Alclad 24S-T	0.1	0.092	1.44
	1	0.101	1.57
	100	0.121	1.90
Alclad 75S-T	0.1	0.182	2.85
	1	0.252	3.93
	100	0.272	4.24
R301-T	0.1	0.144	2.25
	1	0.208	3.24
	100	0.225	3.52

The results presented in Table 4 are plotted on Fig. 16 to indicate the agreement between theory and the experimental data of Table 1.

Because of the small number of specimens used in the testing program, the results presented herein must be considered qualitative in nature. Definite trends were indicated by the investigation, but several parameters that may be of some importance were neglected. It is felt, however, that the results are sufficiently indicative to obviate further time-consuming investigation, although the subject is of sufficient academic interest to warrant considerable study.*

* An intensive investigation of the entire bending problem is a current project of the Office of Scientific Research and Development being conducted at the Case School of Applied Science under Dr. George Sachs.

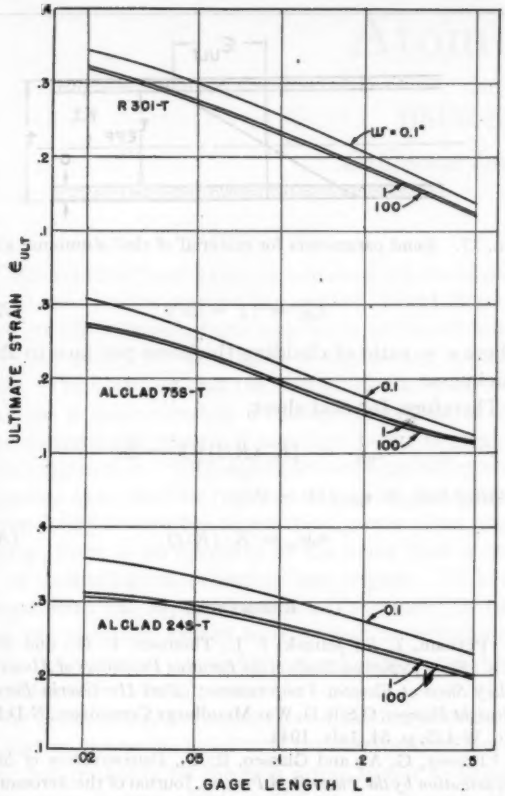

FIG. 15. Ultimate strain data in various gage lengths corrected for bi-axiality of stress existing in bends of several widths.

One specimen of each type of material was tested at the various bend radii, and thus no attempt was made to account for variations in test results which may arise from different sheet lots. For a given width of bend, this anticipated variation may result in a different minimum bend radius, but it is expected that the indicated trend of increase in bend radius with width is unaffected.

The effect of sheet thickness upon the results was not investigated, but this parameter is thought to have little influence on the width effect. The thickness is of fundamental importance in establishing minimum bend radii, but since the width effect arises from the stress condition imposed in attaining the minimum radius, the thickness should have little effect per se.

Because of the small number of specimens used, no attempt is made to find any difference in width effect among the three alloys tested. However, from stress-strain considerations in the plastic range, it appears that the material with the smallest degree of strain hardening may be the most seriously affected by the width effect.

The agreement between theory and test data (Fig. 16) is good for Alclad 24S-T, but the theory predicts considerably conservative bend radii for R301-T and Alclad 75S-T. This may be partially due to errors in test data. Such errors would reflect in the theoretical results, since it is necessary to establish certain empirical relationships as a basis for the analysis.

The theory gives a sharp rise in minimum bend radius in small widths and levels off thereafter, as would be expected from the trend of lateral contraction data with width. Possibly the bend width of 0.1 in., for which correlation with tensile coupon data has been obtained, is in error. Even a small change in this region would cause a large decrease in minimum bend radii predictions in the large widths and yield better agreement.

CONCLUSIONS

The three aluminum alloys tested, R301-T, Alclad 24S-T, and Alclad 75S-T, indicate a definite increase in minimum bend radius of between $^1/_{32}$ and $^1/_{16}$ in. for a range of bend widths between 1 and 100 in. This effect of width upon minimum bend radius is not too serious, but it may be of some consequence when bend radii based on small width specimens are used on long sections, such as stringers or longerons.

The practice often used is to establish minimum bend radii from results of tests on small width specimens because of the ease with which such specimens can be handled. As a result of work herein, it is suggested that, when minimum bend radii are established, specimens of large widths be included in the test program. If the minimum bend radius varies considerably over the width range, it may then be desirable to establish a set of bend radius minimums for smaller and larger widths.

(*Continued on page 170*)

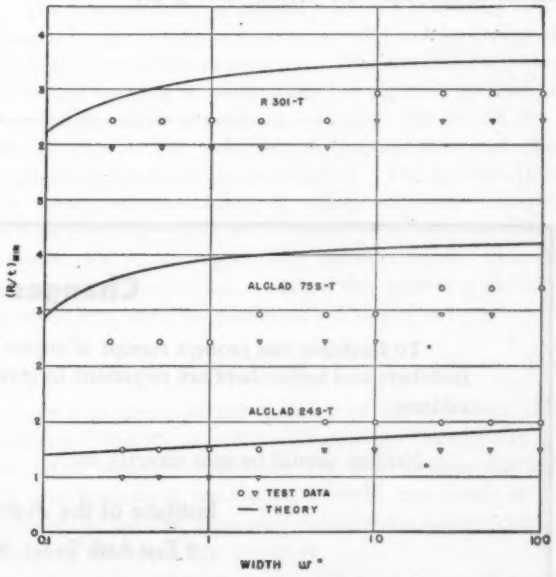

FIG. 16. Agreement between theory and test data on variation of minimum R/t with width.

Appendix A

Reduction of Tensile Coupon Elongation Data

In a tensile coupon, a restriction exists in the direction normal to the applied load similar to that in a wide bend. The state of strain in the tensile coupon is considered identical to that shown in Fig. 14. Hence, the strain measured in the x-direction is decreased from the ultimate value

$$\epsilon_x = \epsilon_{\text{ult.}} - \nu[\epsilon_y - (-\nu\epsilon_{\text{ult.}})]$$

To find the strain under simple tension,

$$\epsilon_{\text{ult.}} = (\epsilon_x + \nu\epsilon_y)/(1 - \nu^2)$$

or to determine the ratio $\epsilon_y/\epsilon_{\text{ult.}}$

$$\epsilon_y/\epsilon_{\text{ult.}} = \epsilon_y(1 - \nu^2)/(\epsilon_x + \nu\epsilon_y)$$

Since $\nu = 0.5$,

$$\epsilon_y/\epsilon_{\text{ult.}} = 0.75\epsilon_y/[\epsilon_x + (\epsilon_y/2)] \qquad \text{(A-1)}$$

Appendix B

Correction of Ultimate Strain Data for Cladding Thickness

Cladding material is a low yield strength alloy capable of sustaining much larger ultimate strains than the base metal. Consequently, it is assumed that when the base material reaches the ultimate strain it will fracture underneath the cladding, as shown in Fig. 17. With continued application of load complete fracture will result.

From reference 4, the ultimate strain in the gage length of the bend is

$$\epsilon_{\text{ult.}} = K/(R/t_{\text{eff.}})$$

The effective thickness subjected to the ultimate strain is less than the actual sheet gage,

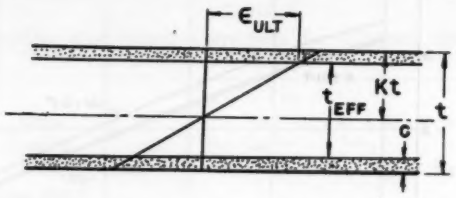

FIG. 17. Bend parameters for material of clad aluminum alloy.

$$t_{\text{eff.}} = (1 - 2c)t \qquad \text{(A-2)}$$

where c = ratio of cladding thickness per face to sheet thickness.

Therefore, for clad sheet,

$$\epsilon_{\text{ult.}} = [K/(R/t)](1 - 2c)$$

letting $\epsilon_{\text{ult.}_c} = \epsilon_{\text{ult.}}/(1 - 2c)$,

$$\epsilon_{\text{ult.}_c} = K/(R/t) \qquad \text{(A-3)}$$

References

[1] Putnam, J. A., Jelinek, J. J., Thomsen, E. G., and Dorn, J. E., *Final Report on Study of the Forming Properties of Aluminum Alloy Sheet at Elevated Temperatures: Part II—Guerin Forming Straight Flanges*, O.S.R.D. War Metallurgy Committee, N.D.R.C. No. W-115, p. 54, July, 1944.

[2] Brewer, G. A., and Glassco, R. B., *Determination of Strain Distribution by the Photo-Grid Process*, Journal of the Aeronautical Sciences, Vol. 9, No. 1, pp. 1–8, November, 1941.

[3] Shanley, F. R., *Elastic Theory in Sheet Metal Forming Problems*, Journal of the Aeronautical Sciences, Vol. 9, No. 9, pp. 313–333, July, 1942.

[4] Gerard, G., *Determining Bend Radii—Via Analytical Approach*, Aviation, Vol. 44, No. 3, pp. 152–155, March, 1945.

[5] Bridgman, P. W., *Stress Distribution at the Neck of a Tension Specimen*, American Society for Metals Preprint, 1943.

Changes of Address

To facilitate the prompt receipt of copies of the JOURNAL OF THE AERONAUTICAL SCIENCES, members and subscribers are requested to give the Institute 30 days' notice of any change of address.

Notices should be sent directly to:

Institute of the Aeronautical Sciences, Inc.
2 East 64th Street, New York 21, New York

Atomic Energy

HSUE-SHEN TSIEN*

California Institute of Technology

Introduction

The spectacular results achieved by the use of atomic bombs toward the end of World War II have greatly stimulated the interest in the possibilities of atomic energy in other fields of engineering applications. The very fact that the energy release by nuclear reactions is approximately a million times that of the more conventional chemical reactions seems to stagger one's imagination. Although there are wide differences in opinion as to the time required to develop this branch of new-found knowledge to practical power-plant engineering, there is no diversity in the belief that a new era of technological evolution has begun. To keep abreast with the expected rapid advancement in this field, the engineers should have a clear understanding of the fundamental concepts involved as advocated by von Kármán in a recent article.[1]

The aeronautical engineers have a further interest in the matter due to the belief that the aeronautical power plant will probably be the first prime mover to utilize the atomic energy. This belief is based upon the following fact: For stationary power plants, the criterion for economic operation is the cost to produce one kilowatt-hour and thus the cost of the fuel, be it chemical or atomic, is of prime importance instead of the weight of the fuel. For automotive applications and especially aeronautical applications, the weight of the fuel is extremely important. In case of the projected supersonic flight at extreme speeds, it seems that only the use of atomic energy will make such flight economically feasible by reducing the fuel load and increasing the pay load.

This article is a digest of the basic concepts in this branch of knowledge as an introductory study of this new field. The enormous energy release of nuclear reaction is explained through the binding energy of the atomic nuclei, with the energy generation in the stars and the atomic bombs as typical examples. Frequent comparison between molecular reaction and nuclear reaction will be made to guide the exploration of an unfamiliar land.

The Equivalence of Energy and Mass

The astonishing amount of energy released by the nuclear reactions can be easily understood through the still greater energy potential in the atom itself represented by its mass. Therefore, one of the fundamental concepts of the atomic energy is the concept of the equivalence of energy and mass. This concept was first announced by Einstein as a conclusion of his special theory of relativity. This theory deals with the comparison of measurements made by observers who are assumed to be in unaccelerated relative motion and in a region of space and time where the action of gravitation can be neglected. The basis of the theory can be conveniently regarded as the two following fundamental postulates:[2]

(a) It is impossible to measure or detect the unaccelerated translatory motion of a system through free space or through any ether-like medium that might be assumed to pervade it.

(b) The velocity of light in free space is the same for all observers, independent of the relative velocity of the source of light and the observers.

The first postulate is derived from the failure to detect the ether drift of the motion of the earth through the space, and the second postulate can be derived from both astronomical evidences and laboratory experiments. Therefore, although Einstein's theory is often disseminated by popular science writers as an abstruse mathematical theory, it really is solidly founded on observational facts. In this sense, the relativity theory is just as empirical as a stress-strain curve drawn through test points obtained on a steel specimen.

The first postulate of special relativity is already contained in the Newtonian dynamics and can be accepted as part of everyday experience. The second postulate, although familiar in wave theory of light, is somewhat beyond the daily experience. In fact, one would generally expect the velocity of propagation and the velocity of the source to be additive. The combination of these two postulates of widely different natures would certainly lead to entirely new results. This expectation is, of course, fully substantiated. One of the results of deduction is that, if the mass of a particle is m_0 at rest, then its mass m at velocity V is

$$m = m_0/\sqrt{1 - (V^2/c^2)} \qquad (1)$$

where c is the constant velocity of light. Since the velocity of light is about a million times the velocity of sound at ordinary conditions, for all velocities realized in the terrestrial macroscopic world the mass m is practically the rest mass m_0. The kinetic energy calculated by the relativity theory is

$$E = c^2(m - m_0) \qquad (2)$$

Received September 29, 1945.

* Daniel Guggenheim Aeronautical Laboratory.

For small velocities—i.e., $V \ll c$—the preceding equation reduces to the familiar form $E = {}^1/_2 m_0 V^2$.

This close relationship between energy and mass, as well as other evidences, prompted Einstein to take a revolutionary step. He says that there is no difference between energy and mass. One is just a form of the other. They are closely associated with each other. The energy E associated with any mass m is $E = mc^2$. Any energy E has a mass $m = E/c^2$ associated with it. In other words, a complete equivalence of energy and mass is achieved here. The old concept of separate conservation of energy and mass is thus merged into one single concept of conservation of "energy-mass."

Since the velocity of light is generally given as approximately 3×10^{10} cm. per sec., 1 lb. of mass is equivalent to

$$\left(\frac{1}{g}\right)c^2 = \left(\frac{1}{32.2}\right)\left(\frac{1}{778}\right)\frac{(3 \times 10^1)_0}{10^2} \times (3.280)^2 = 3.86 \times 10^{13} \text{ B.t.u.} = 1.130 \times 10^{10} \text{ kwh.} \quad (3)$$

The problem is then how to transform the mass into energy or how to release the energy intrinsically bounded with the mass.

Atomic Structure

The problem is similar to that of releasing the chemical energy, intrinsically bounded with a mixture of hydrogen and oxygen. Until a device for igniting this gaseous mixture is discovered, the chemical reaction, although known to be possible, cannot be started and no chemical energy of this mixture will be released. Thus, the central problems of converting mass into energy are first to discover the type of reactions which can perform this mass-energy transformation and then to find the means of "igniting" or starting such reactions. The only known reactions that will transform mass into energy are nuclear reaction or the reactions with the atomic nuclei as the participants. Before entering into the discussion of the nuclear reaction, it is thus profitable to study the structure of atoms first.

The atom is composed of the central core or the nucleus and the outer collection of electrons. The mass of the atom is mostly concentrated in the nucleus. The electrons are extremely light. The mass of an electron at rest is 9.035×10^{-28} g., and in the physical atomic weight* scale it is 0.000549. The total mass of the electrons is only several thousandths that of the nucleus. The charge of the nucleus is positive and that of the electrons is negative. For a normal atom the positive charge of the nucleus is just equal to the negative charge of the electrons and thus gives a neutral atom.

* In the physical atomic weight scale, the atomic weight of O^{16}, or the oxygen atom with 8 protons and 8 neutrons, is exactly 16. Because of a slight amount of heavier atoms in natural oxygen, the usual atomic weight scale or the chemical atomic weight scale is slightly larger (by about 1 part in 4,000).

Table 1
Electronic Quantum States

Shell	Orbital Quantum States						
K	1s(1)						
L	2s(1)	2p(3)					
M	3s(1)	3p(3)	3d(5)				
N	4s(1)	4p(3)	4d(5)	4f(7)			
O	5s(1)	5p(3)	5d(5)	5f(7)	5g(9)		
P	6s(1)	6p(3)	6d(5)	6f(7)	6g(9)	6h(11)	
Q	7s(1)	7p(3)	7d(5)	7f(7)	7g(9)	7h(11)	7i(13)

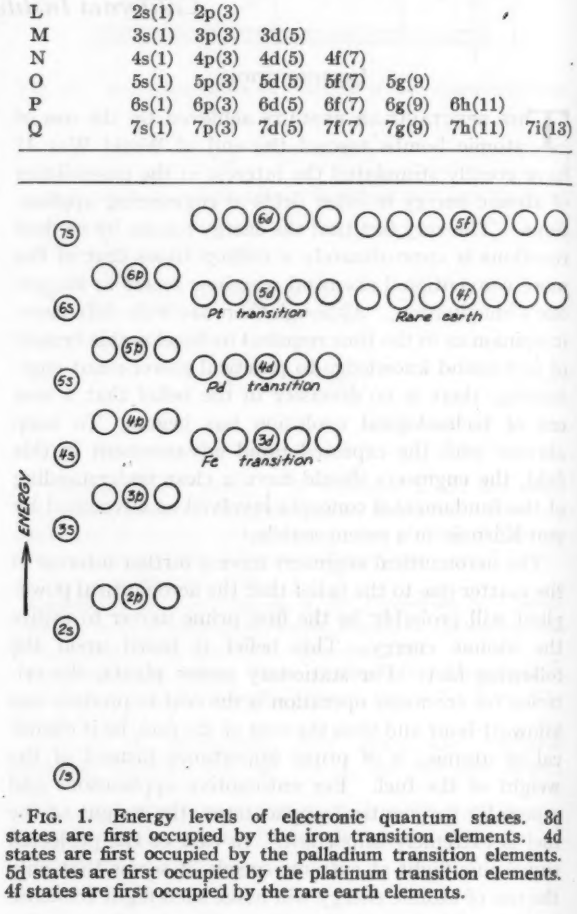

Fig. 1. Energy levels of electronic quantum states. 3d states are first occupied by the iron transition elements. 4d states are first occupied by the palladium transition elements. 5d states are first occupied by the platinum transition elements. 4f states are first occupied by the rare earth elements.

The electrons are arranged in "shells" around the nucleus. In terms of atomic scales there is an enormous distance between the nucleus and the first shell. This is indicated by the fact that the diameter of the nucleus is less than ${}^1/_{10,000}$ of the diameter of the atom. The shells are named as K, L, M, N, O, P, Q. The states of motion the electron might occupy are designated by three-positional or orbitual quantum numbers and a "nonclassical" spin quantum number. For each orbitual quantum number there are two spin quantum numbers. These quantum numbers, together with the energy of the corresponding states of motion, can be determined either experimentally by measuring the spectrum of the element or theoretically by calculation with the rules of quantum mechanics assuming Coulomb forces between the electrons and the nucleus. In fact, the excellent agreement between the theory and the experiment is one of the major triumphs of modern physics. It is also found that no two electrons can occupy a state with the same four quantum numbers,

according to the "Pauli exclusion principle." The orbital states are listed in Table 1. The number in the parentheses is the number of orbital states. Since there are two spin numbers with each orbital state, the number of electron positions is twice the number shown in the parentheses.

With increasing atomic weight, the nucleus gets heavier, and the charge of the nucleus is increased with increase in the number of electrons attached to it. In other words, the shells of electrons gradually fill up. The states or "positions" with the lowest potential is filled up first. The potential ladder is shown in Fig. 1. Hydrogen uses one of the 1*s* electron positions. Helium uses both of the 1*s* electron positions and completes the K shell. Hence, helium shows little tendency to draw electrons of other atoms to form chemical compounds and is an inert gas. Neon completes the L shell and becomes an inert gas. Now, the chemical property of the atom is mainly determined by the outmost shell. Since the Fe, Pd, Pt, transition elements, and the rare earth elements are made by filling up the inner shells with 3d, 4d, 5d, and 4f positions, respectively, and without changing the outer shell, their respective similarity in chemical property is expected.[3] For the same reason, the similarity between the elements U, Np,* Pu,* indicate that they may be the elements made by filling up the 5*f* positions in the O shell with the two electrons in the Q shell unchanged. These elements then might constitute the beginning of a new series similar to the rare earth elements.[4]

The nucleus is now generally considered as composed of neutrons and protons. They have about the equal mass, with the neutron being slightly heavier, and are approximately 1,840 times heavier than electrons. In the physical atomic weight scale, a neutron is 1.00893 and a proton is 1.00757. Similar to the electron, their states are determined by the orbitual numbers and the two spin numbers. Since only the proton has a unit positive charge, the number of protons in the nucleus must be equal to the number of electrons. This number is the atomic number Z. Hydrogen has the atomic number 1 and uranium 92. The total number of neutrons and protons in the nucleus is the mass number A. Thus $N = A - Z$ is the number of neutrons in the nucleus. Since the mass of neutrons or protons is approximately unity in the scale of atomic weight, A is also roughly the atomic weight. Therefore, the nucleus of the hydrogen is a proton. The nucleus of deuterium is deuteron, or a proton and a neutron. The nucleus of helium is usually called the α-particle and is composed of two neutrons and two protons. Elements with equal number Z are called "isotopes." Thus, hydrogen and deuterium are isotopes. Similarly, the uranium isotopes U-235 and U-238 are composed of 92 protons and 133 and 136 neutrons, respectively.

* Np and Pu stand for neptunium and plutonium, two new elements beyond uranium with 93 and 94 electrons, respectively (atomic numbers 93 and 94).

The neutrons and protons in the nucleus are not a loose assemblage but are tightly bound together. In fact, their bounds are much stronger than the bounds between the nucleus and the electrons in the outer shells. For instance, while it takes only 13.53 volts to remove the electron from the hydrogen atom—i.e., a binding energy of 13.53 ev.†—the binding energy between a proton and a neutron is approximately 2.15×10^6 ev. The average binding energy per particle for heavier elements is even higher, being approximately 8.5×10^6 ev. The ratio for these two types of bounds is thus roughly 10^6. The ordinary chemical energy released by molecular reactions is linked with the rearrangement of electrons in the molecules. For instance, the electrons in hydrogen molecules and in oxygen molecules are bound to the hydrogen nuclei and the oxygen nuclei, respectively. By rearranging the electrons so that they are bound to both the hydrogen nucleus and the oxygen nucleus at the same time, water molecules are formed. The closer binding between the electrons and the nuclei in the water molecule corresponds to the chemical energy released during the combustion of hydrogen with oxygen. Therefore, if nuclear reaction involving rearrangements of the particles in nuclear structure is realized, then the associated energy released must be of the order of the nuclear binding energy—i.e., approximately a million times that of chemical or molecular reaction. This difference in the order of magnitude between the nuclear reactions and the molecular reactions is basic and will occur frequently in the subsequent discussions.

Nuclear Reactions

The nuclear reactions known up until 1939 are reactions produced by the bombardment of the atoms with various kinds of projectiles, such as α-particle, proton, neutron, and deuteron. The result of this bombardment is either absorption of the bombarding particle with emission of short wave-length electromagnetic waves or γ-ray, or disintegration of the atom with emission of other particles. The reactions can be classified as in Table 2. For instance, in 1932 J. D. Cockcroft and E. T. S. Walton of Rutherford's laboratory, bombarded a target of lithium with protons of 700 kv. energy and found that α-particles were ejected from the target as a result of the bombardment. The nuclear reaction that occurred can be written symbolically as

$$ {}_3\mathrm{Li}^7 + {}_1\mathrm{H}^1 \rightarrow {}_2\mathrm{He}^4 + {}_2\mathrm{He}^4 \qquad (4) $$

where the subscript represents the atomic number Z and the superscript the mass number A. In a chemical equation, the number of atoms of any element entering into the reaction must be equal to the number of atoms

† ev. is the abbreviation for electron-volt—i.e., the energy spent in moving a unit electron charge through a potential of 1 volt. 1 ev. $= 4.45 \times 10^{-26}$ kwh.

of that element in the product. In a nuclear reaction as shown in Eq. (4), the number of the nuclear particles, protons, and neutrons must be the same on both sides. Thus the sum of subscripts is four and the sum of superscripts eight on each side.

Neither mass nor energy has been included in this equation. In general, the sum of the masses of the incident proton and the lithium atom will not be precisely the same as the sum of the masses of the α-particles produced. According to Einstein's law of conservation of energy-mass, the sums of mass and energy taken together should be the same before and after the reaction. The masses were known from mass spectra. On the left ($Li^7 + H^1$) they totaled 8.0241; on the right ($2He^4$), 8.0056, so that 0.0185 unit of mass had disappeared in the reaction. The experimentally determined energies of the α-particles were approximately 8.5 Mev.* each, a figure compared to which the kinetic energy of the incident proton could be neglected. Thus, 0.0185 units of mass are 3.07×10^{-26} g. or 17.2 Mev. according to Einstein's equation. Therefore the experimental results have completely proved Einstein's mass energy equivalence.

As stated, the protons for the lithium reaction are accelerated by 700 kv. or have 0.7 Mev. energy per particle. Such an amount of kinetic energy gives the proton an appreciable probability of penetrating into a lithium nucleus and causing a reaction. However, out of a million accelerated protons there still is only one that will make a successful hit; the others will be slowed down by collisions with atoms without producing the desired reaction, and their kinetic energy will be lost by transforming into heat. Thus 0.7×10^6 Mev. energy is required to accelerate a million protons to produce one reaction giving 17 Mev. energy. Hence, 40,000 times more energy is spent than recovered. It is obviously impracticable to use this nuclear process to produce energy. The situation could be compared to that of a hypothetical molecular reaction where an inefficient igniting device has to be used for *every* pair of molecules. Then the chemical reaction, even if it were an energetic one, cannot be practically utilized for energy production.

There is a special class of nuclear reactions which does not involve incident particles. This means that the nuclei automatically disintegrate with the emission of particles. This phenomenon is called the radioactivity and is discovered actually earlier than the usual nuclear reactions described above. The emitted particles could be the α-particles, the protons, the electrons, and the positrons, positive electrons, as shown in Table 2. The emission of electrons and positrons are found, however, to give continuous spectra of the kinetic energy of the emitted particles, while the energy states of the nuclei are found to be discrete. This is in contradiction to the law of conservation energy-mass, which is observed to hold in all other cases. To preserve this law, a neutral particle with spin but of practically zero mass called neutrino is assumed by W. Pauli. The neutrino is, so far, not directly detected. However, because of the assumed existence of neutrinos, part of the energy could be transferred to them, and the continuous spectra of electron energy in radioactivity is explained. The kinetic energy of the neutrinos is "lost" because it cannot be detected.

* 1 Mev. is one million electron-volts or 10^6 ev. and is equivalent to 4.45×10^{-20} kwh.

TABLE 2
Types of Nuclear Reaction

	Incident Particle	Emitted Particle	Z Becomes	A Becomes
Reactions by Particle Bombardments	α	Proton	$Z+1$	$Z+3$
	α	Neutron	$Z+2$	$A+3$
	Proton	....	$Z+1$	$A+1$
	Proton	α	$Z-1$	$A-3$
	Proton	Neutron	$Z+1$	A
	Proton	Deuteron	Z	$A-1$
	Deuteron	Proton	Z	$A+1$
	Deuteron	Neutron	$Z+1$	$A+1$
	Deuteron	α	$Z-1$	$Z-2$
	Neutron	....	Z	$A+1$
	Neutron	Proton	$Z-1$	A
	Neutron	α	$Z-2$	$A-3$
Radio-activity	....	α	$Z-2$	$A-4$
	....	Proton	$Z-1$	$A-1$
	....	Electron	$Z+1$	A
	....	Positron	$Z-1$	A

NUCLEAR STRUCTURE—BINDING ENERGY

An entirely new type of nuclear reactions is the breaking up of a heavy nucleus into two approximately equal fragments. This is called the nuclear fission reaction. It was discovered by L. Meitner, O. Hahn, and F. Strassmann toward the end of 1938. To understand the reaction one must look into the structure of the nucleus in more detail.[5]

In studying nuclear structure one is, however, faced with the difficulty of not knowing the character of the forces between the nuclear particles. The desired information must be deduced from the scanty experimental data. First, by plotting the atomic number Z against the mass number A for all known elements, there is an obvious relation between these two quantities. This relation is, of course, not precise because of the variations by isotopes. For instance, with the same atomic number 1 for hydrogen and deuterium, the mass numbers are 1 and 2, respectively. However, for light elements, the value of A is approximately twice that of Z. This is exactly true for ${}_6C^{12}$, ${}_7N^{14}$, ${}_8O^{16}$, etc. This means that the stable light nuclei are composed of equal numbers of protons and neutrons. Then, the binding force between the nuclear particles must be the greatest between the proton and the neutron. If the force between protons were stronger, the stable nucleus would contain more protons than neu-

trons. If the force between the neutrons were stronger, the stable nucleus would contain more neutrons. However, the fact that the force between the neutron and the proton is the strongest does not exclude the possibility of forces between neutrons themselves and protons themselves. But if such binding force between the like particles exists, they cannot be widely different, because, if the binding force between a pair of neutrons were much higher than that between a pair of protons, then the stable nucleus would again have a preponderance of neutron instead of the observed equality in numbers of these two kinds of particles. Of course, there will be Coulomb repulsion between two protons. But this repulsion can be shown to be small in comparison with the specifically nuclear forces. In fact, it is generally assumed that aside from the Coulomb force, the force between a pair of neutrons is equal to the force between a pair of protons.

The α-particle, or the nucleus of the helium atom, consists of two protons and two neutrons. The binding energy per particle of this nucleus is found to be much higher than the deuteron. Furthermore, a nucleus of five particles, by adding either a proton or a neutron to the α-particle, is never observed. This means that a nucleus of five particles is highly unstable and its lifetime is so short that its detection by experiment is highly unlikely. This great stability of the helium nucleus and the difficulty of adding another particle to it show the saturation of the binding forces in helium nucleus. The situation is similar to that of the helium atom with the two electrons in the same orbital quantum state but different spin states. The resultant closed K-shell structure refuses to combine with additional electrons from other atoms to form molecules. Thus, similarly, the two neutrons must be in the same orbital quantum state with different spin states, and the two protons must be in the same orbital quantum state with different spin states. But the large binding energy of the helium nucleus requires that there is binding force between every pair of the particles in this nucleus. Hence, the binding force between a proton and a neutron and the binding force between the like particles cannot depend to any considerable extent upon the relative spin directions of the interacting particles.

If there is binding energy between *every* pair of interacting particles, then, since the number of pairs in a nucleus is $(1/2)A(A-1)$, the total binding energy of a nucleus must be proportional to the square of A. However, experimental data show a practically linear relation between the binding energy and the mass number A. This is the same as the relation between molecular binding energy of a liquid drop containing many molecules. It is known that the force between the molecules in liquid or solid shows saturation. In other words, a molecule is attracted only to the other molecules in its immediate neighborhood. Thus, the intermolecular forces can be said to be short ranged, speaking in terms of the dimension of the drop. This character of the binding force greatly limits the number of effectively interacting pairs of particles and makes the total binding energy proportional to the number of particles. The nuclear forces then must show a similar saturation character. Here, a neutron or a proton only interacts strongest toward another particle of nearest orbitual quantum states. As the number of the particles increases with increasing mass number A, the number of particles having nearly a given orbitual quantum state does not increase, since only two particles of the same kind can occupy the same orbitual quantum states, according to Pauli's exclusion principle. Then the nuclear forces can also be said to be short-ranged in terms of the dimension of the nucleus. Thus, the number of effectively interacting pairs is limited in a similar manner as in the liquid drop, and the total binding energy is only proportional to the total number of particles instead of proportional to the square of the number of particles.

This liquid drop analogy is also useful in two other connections. First, since the volume of the liquid drop is proportional to the number of molecules, the volume of a nucleus must also be proportional to the number of nuclear particles, since they are similarly held together. This means that the radius of a nucleus is proportional to $A^{1/3}$. This is found to be true experimentally. Secondly, a liquid drop exhibits the well-known surface tension phenomenon. This is due to the existence of a free surface where the molecules are only attracted by the molecules within the drop. Therefore, for the molecules on the surface, only half of their binding force is satisfied, and their contribution to the total binding energy of the drop is not so large as the molecules within the drop. A similar situation exists for the nucleus, where the protons or neutrons on the surface of the nucleus contribute much less binding energy than the particles within the nucleus. For a heavy nucleus, the ratio of the particle at the surface to the total number of particles is reduced and the binding energy per particle should be increased. In other words, the surface tension effect indicates an increase in binding energy per particle with increasing mass number A.

So far, the effect of Coulomb repulsion between protons is neglected. A simple calculation shows that the average energy due to this effect is $1/4$ Mev. per pair of protons. The average binding energy due to nuclear forces is $8\,1/2$ Mev. per particle. Thus the Coulomb repulsion is negligible if compared on the basis of a single pair of protons. However, the nuclear forces show saturation, and the binding energy due to nuclear forces is approximately proportional to A. The number of protons in the nucleus and, thus, the total proton charge are also approximately proportional to A. The radius of the nucleus is proportional to $A^{1/3}$. Hence, the total repulsion energy is proportional to $A \times A/A^{1/3}$ or $A^{5/3}$. This difference of the Coulomb repulsion energy from the energy due to nuclear forces is, of

course, the result of nonsaturation character of the Coulomb forces. The ratio of these two energies is thus proportional to $A^{2/3}$. Therefore, for a large nucleus, the Coulomb repulsion energy is important in spite of its smallness for one pair of protons. Then the total binding energy of the nucleus will be increased and the nucleus made more stable by substituting some of the protons by neutrons. This is actually found to be the case: The uranium nucleus has a neutron-proton ratio N/Z equal to 1.6, while for light nuclei this ratio is 1 as stated before. Furthermore, the effect of the Coulomb repulsion will also make the total binding energy increase less rapidly as the increase in number of particles A. This effect is thus opposite to the surface tension effect. However, for small nuclei, the Coulomb repulsion is unimportant. Hence, the binding energy per particle will increase with A in this range. For large nuclei, or large A, the binding energy per particle will again decrease as the surface tension effect is overcome by the Coulomb repulsion.

To actually calculate the nuclear binding energy from the experimental data, one can proceed as follows: An atom of atomic number Z and mass number A contains Z protons and Z electrons together with $N = A - Z$ neutrons. Because of the negligible binding energy between electrons and the nucleus, the mass of Z protons and Z electrons is equal to Z times the mass of hydrogen atom. The atomic mass of hydrogen and the mass of neutrons are 1.00813 and 1.00893, respectively, in the physical scale. Therefore, the mass of components that go into the structure of the atom is $1.00813Z + 1.00893N$. If the actually measured atomic weight of the element is M, then the mass defect is $1.00813Z + 1.00893N - M$. This mass defect must represent the binding energy of the atom according to Einstein's law of equivalence of energy and mass. Since the binding energy of the electrons to the nucleus is negligible, the mass defect is practically the binding energy of the nucleus. Generally, a different parameter is introduced. This parameter is called the packing fraction f defined as

$$f = (M - A)/A \tag{6}$$

The binding energy per particle is then

$$\frac{1.00813Z + 1.00893N - M}{A} = -f + 0.00813\frac{Z}{A} + 0.00893\frac{N}{A} = -f + 0.01706\frac{Z}{A} - 0.00893 \tag{7}$$

By neglecting the small variation of the ratio Z/A, the binding energy per particle is given by the negative of the packing fraction f. Therefore, for increasing binding energy per particle, the packing fraction increases. According to the discussion given in the previous paragraph, the binding energy per particle must show a maximum for medium heavy nuclei. Thus, the packing fraction must show a minimum for the medium values of the mass number A. This is seen in Fig. 2.[5]

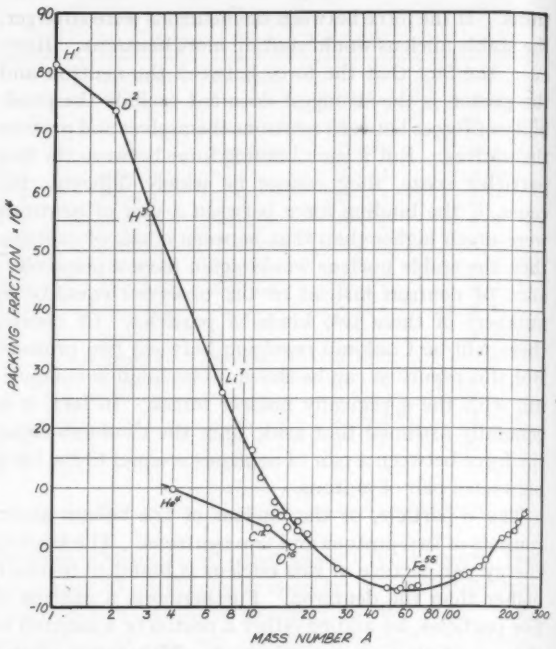

FIG. 2. Packing fraction f as a function of mass number A.

By examining the graph for the packing fractions (Fig. 2), it is seen that very large energy can be released by either of the two methods: manufacture of the medium heavy elements out of light elements, or breakdown of an extremely heavy element into the medium heavy elements. In other words, by going from the two ends of the periodic table toward the middle, closer packing of the nucleus can be achieved with the release of the enormous binding energy. Nature provides an example for each case. The manufacture of helium from hydrogen is of the first type and is carried out in the center of the main sequence stars such as the sun. The fission of uranium is of the second type. This reaction is used in the atomic bomb. These two typical examples will be examined in more detail presently.

Energy Production in the Stars

In the laboratory nuclear transmutations are produced by accelerating a few particles to high kinetic energy. The resultant poor efficiency is explained under "Nuclear Reactions." In stars, different conditions prevail: Because of the high temperature in the interior of stars, all protons in the stars have high kinetic energies. Moreover, they are not slowed down by collisions with other atoms because all atoms have equally high energies. Therefore, unlike the laboratory nuclear reaction, no energy need be spent in accelerating the bombarding particles such as protons, and any energy released by the nuclear reaction is a net gain.

On the other hand, the kinetic energies of the nuclei in stars are small compared with those used in the laboratory. It is true that the temperature is about 20,000,000°C. at the center of sun, and the atomic nuclei are therefore traveling with much greater speed than the molecules in the terrestrial atmosphere. However, their average kinetic energy is still only about 0.003 Mev.—200 times smaller than the energies commonly used in the laboratory. Therefore, their probability of penetrating into the nucleus of the bombarded atom is much smaller. This is, however, remedied by the presence of enormous numbers of bombarding protons, and the net reaction rate is not small.

Through a careful examination of the probable reaction, Bethe[7] picked out a series of the nuclear reactions as follows:

$$_6C^{12} + {}_1H^1 \rightarrow {}_7N^{13} + \gamma \tag{8}$$

$$_7N^{13} \rightarrow {}_6C^{13} + {}_1e^0 \tag{9}$$

$$_6C^{13} + {}_1H^1 \rightarrow {}_7N^{14} + \gamma \tag{10}$$

$$_7N^{14} + {}_1H^1 \rightarrow {}_8O^{15} + \gamma \tag{11}$$

$$_8O^{15} \rightarrow {}_7N^{15} + {}_1e^0 \tag{12}$$

$$_7N^{15} + {}_1H^1 \rightarrow {}_6C^{12} + {}_2He^4 \tag{13}$$

Here γ represents the emission of γ-rays and ${}_1e^0$ represents the positron that is emitted together with neutrinos, as explained previously. This series of reactions is remarkable in that it reproduces the carbon atom after six reactions. This is important, since the content of carbon in the stars is not high while hydrogen is plentiful. The net result is the manufacture of an α-particle and two positive electrons from four protons. The two positive electrons will react with two ordinary electrons to disappear into γ-ray, the so-called annihilation of electron pairs. Then the net energy released per cycle is that given by the difference in mass of four protons plus two electrons, and an α-particle. Since the binding energy between the electron and nuclei particles is negligible, this difference is the same as the difference between four hydrogen atoms (four protons plus four electrons) and the helium atom (α-particle plus two electrons). This difference is equivalent to 27 Mev. A small fraction 2 Mev. of this energy goes into neutrinos and is lost. The remainder goes into radiation, which is finally emitted from the sun.

Thus about 25 Mev. are set free for each helium nucleus produced in the stars, or 6 Mev. for each proton destroyed. One gram of sun material has been calculated to contain about 2×10^{23} protons. Therefore, if all the protons can be converted into helium, the available energy supply is 1.2×10^{24} Mev. per g. At present, the sun radiates about 1.2×10^{6} Mev. per g. per sec. At this rate, the energy supply will last about 30,000,000,000 years. The rate of energy release can also be approximated by calculations based upon the reactions (8) to (13) and laboratory measured constants. Thus Bethe's "carbon cycle" is indeed the energy process in the sun. In fact, the "carbon cycle" is found to be the energy process for all the "main-sequence stars" from "red dwarfs" to "blue giants."

On the physical atomic weight scale, four protons and two electrons total 4.0215 units. This means that 4.0215 g. of the reacting material in stars will carry out 6.064×10^{23} processes, each of which generates 25 Mev. energy. The energy generated by 1 lb. of the reacting substance is then

$$[1/(0.0040215 \times 2.205)] \times 25 \times 6.064 \times 10^{23} \times 4.45 \times 10^{-20} \times 3{,}413 = 2.59 \times 10^{11} \text{ B.t.u.} \tag{14}$$

By comparing this value with that given by Eq. (3), it is seen that the helium manufacturing process is able to transform 0.67 per cent of the original reacting mass into energy. While this percentage may seem to be small, because of an enormous conversion factor from mass to energy, the "heat value" per pound of reacting material is still tremendous. One of the most energetic molecular reactions is the combustion of hydrogen with oxygen. The heat value of the stoichiometric mixture is 6,850 B.t.u. per lb. The heat value of the nuclear reaction given in Eq. (14) is thus 3.78×10^{7} times larger than that of the molecular reaction. This confirms the previous surmise that the ratio of energy releases for the nuclear reaction and the molecular reaction must be of the order of a million.

Nuclear Fission—Chain Reaction

The second method of energy release by breaking down the extremely heavy elements depends upon the instability of the heavy nuclei under external excitation. The liquid drop model of the nucleus is also useful in the stability considerations for this nuclear fission reaction. In fact, by assuming that the drop is composed of an incompressible fluid of radius R and of volume $(4\pi/3)R^3 = (4\pi/3)\, r_0{}^3A$, uniformly electrified to a charge Ze and possessing a surface tension O, the critical excitation energy, E_f, for separating into two equal nuclei is shown by Bohr and Wheeler[8] to be expressed by

$$E_f = 4\pi r_0{}^2 O A^{2/3} f[(Z^2/A)/(Z^2/A)_{\text{limiting}}] \tag{15}$$

r_0 is the radius of a single nuclear particle and $(Z^2/A)_{\text{limiting}} = 47.8$, limiting value for Z^2/A giving instability for infinitesimal deformation of the "drop." E_f is actually the height of the barrier which leads to instability. In other words, if a certain excitation has an energy of less than E_f, the nucleus is stable against splitting into two fragments. If a certain excitation has an energy in excess of E_f, then the nucleus can be deformed to such an extent that it can be further deformed into two fragment nuclei without additional energy expenditure. The situation is similar to that of rolling a ball against a hump of ground. In order to pass the hump, one must apply sufficient energy for the

TABLE 3
Excitation of Heavy Nuclei by Neutron Capture

Initial Nucleus	Produce Nucleus	Z^2/A	x	E_f	E_c	$E_f - E_c$
$_{92}U^{234}$	$_{92}U^{234}$	36.00	0.753	$5.0M_V$	$5.4M_V$	$-0.4M_V$
$_{92}U^{235}$	$_{92}U^{236}$	35.86	0.750	5.2	6.4	−1.2
$_{92}U^{238}$	$_{92}U^{239}$	35.40	0.741	5.9	5.2	+0.7
$_{94}Pu^{239}$	$_{94}Pu^{240}$	36.80	0.770	4.0	6.2	−2.2
$_{90}Th^{232}$	$_{90}Th^{233}$	34.76	0.727	6.9	5.2	+1.7
$_{91}Pa^{231}$	$_{91}Pa^{232}$	35.70	0.747	5.5	5.4	+0.1

ball to reach the hump, then further motion of the ball is automatic.

Consider now what would happen if a neutron were added to such a near unstable nucleus. The value of E_f is calculated by Bohr and Wheeler and the result included in Table 3. After the capture of a "zero" kinetic energy neutron (thermal neutron), the equilibrium of the collection of neutrons and protons is disturbed. In general, a readjustment is possible with the subsequent release of energy to excite the product nucleus. The energy of excitation E_e of the compound nucleus is then the binding energy between the initial nucleus and the neutron. This is also calculated by Bohr and Wheeler and the result listed in Table 3. Therefore, the threshold energy of neutrons required for producing the splitting of fission of a given compound nucleus is obtained by subtracting the excitation energy of zero kinetic energy neutron from the critical energy for fission. The result for this energy of the bombarding neutrons is listed in Table 3 as $E_f - E_c$ for different bombarded nuclei. The negative values for U^{235}, U^{234}, and Pu^{239} mean that these nuclei will undergo fission *after capture* of thermal neutrons. These theoretical results are in full agreement with experiments.

However, there are other competitive reactions that could happen to an excited nucleus. These reactions are: (a) emission of γ-ray, (b) emission of α-particle, and (c) re-emission of the neutron. To estimate the relative probability of occurrence, one must turn to the statistical mechanics of the excited nucleus. It is found that, for energies of excited nucleus below, or not far above, the critical value, radiation of γ-ray will predominate. With increasing energy the probability of fission will increase rapidly. The probability of fission will not increase indefinitely, however, because at still higher energies the re-emission of neutrons becomes the predominant process.

Now there still remains the problem of making the capture possible. Of course, the nuclei will be bombarded with neutrons, but the probability of actual absorption depends upon the kinetic energy of the bombarding neutron and the character of the bombarded nucleus. This probability is generally expressed as a "cross section" σ defined by

$$N = n\nu\sigma \tag{16}$$

N is the number of occurrences of the kind in question (fission) per sq.cm. of bombarded surface per sec.; n is the number of bombarding particles per sq.cm. per sec. (normal incidence around); and ν is the number of atoms of the kind involved per sq.cm. of surface. The situation is as if each atom presented a target area σ. If the target is struck, the effect in question occurs; if not, nothing happens. It is apparent that σ gives a sort of averaged probability of occurrence of an effect for a random spatial distribution of impinging particles.

It is thus evident for the successful fission process that two conditions must be satisfied: (a) a large cross section of capture of neutrons of proper energy; (b) the energy of the neutron must be such that the excitation energy of the compound nuclei, after capture of neutrons, is above the critical barrier energy. It is found that $_{92}U^{235}$ and $_{94}Pu^{239}$ can be split by either thermal neutrons or fast neutrons. Then, as explained before, a very large energy release is expected. In fact, the measured energy release per fission for $_{92}U^{235}$ is approximately 177 Mev.[9] Since 1 gram mole or 235 g. of $_{92}U^{235}$ contains 6.064×10^{23} atoms, the energy generated by 1 lb. of $_{92}U^{235}$ with complete fission is

$$[1/(0.235 \times 2.205)] \times 177 \times 6.064 \times 10^{23} \times 4.45 \times 10^{-20} \times 3{,}413 = 3.14 \times 10^{10} \text{ B.t.u.} \tag{17}$$

By comparing with the value given by Eq. (3), it is seen that the fission of U-235 is able to convert 0.081 per cent of the original mass into energy. Thus, the reaction is not so efficient as that of helium manufacture from hydrogen, treated in the previous section. This is, of course, expected from the diagram for the packing fraction (Fig. 2), which shows a much greater change in binding energy per nuclear particle from hydrogen to helium than from uranium to medium heavy elements. Nevertheless, the "heat value" of the U-235 is still approximately 1.5×10^6 times the heat value of gasoline, which is the most powerful fuel used today.

However, to make the fission process a really going process, a continuous supply of neutrons of proper energy is necessary. This is actually accomplished by slowing down the fast neutrons released by the fission fragments themselves. For $_{92}U^{235}$, the compound nucleus $_{92}U^{236}$ first breaks down into $_{56}Ba$ and $_{36}Kr$ of unequal mass, since this splitting involves smaller potential barriers. The product nuclei would be highly excited because of the energy released and would contain more neutrons than stable equilibrium requires, because the ratio of neutron to proton is much higher in uranium than for atoms of medium atomic weight. These extra neutrons will be "vaporated" or emitted with high energy and a small time delay of about 1 sec. For one fission, more than one neutron is thus generated. If these neutrons can be slowed down to proper energy for fission of new $_{92}U^{235}$ atoms without absorbing so many of them as to reduce the desired neutron to less than one per fission, the reaction becomes a chain reaction. The chain carrier is the neutron of proper energy.

Then the reaction will tend to build up to explosive violence.

The agents for slowing down the fast neutrons are called moderators. They must not absorb the neutrons above the desired energy; otherwise the useful yield will be extremely small. They must also be light elements so that they can effectively share the kinetic energy of fast neutrons by collision and thus slow down the neutrons with but few collisions. The thickness and the bulk of the moderator can thus be reduced. Hydrogen is good because it is the lightest element, but it is undesirable for slow neutron fission because of its large capture cross section of slow neutrons. Deuterium is best from this aspect, and heavy water is a good moderator.

Besides the absorption of neutrons by the moderator, there is another loss due to escape of the neutrons out of the reacting mass. This is proportional to the surface of the mass. Therefore, by increasing the size of the reacting mass, this loss can be cut down relative to the production, which is proportional to volume. Hence, if a small quantity of fission material and moderator cannot carry on the chain reaction, a large quantity of the same material might be able to do so. For any given geometrical arrangement and effective composition, there is thus a *critical size*. Generally, single fission can be produced automatically or by cosmic ray; therefore, once the critical size is reached, the mass will react by itself or explode. The atomic bomb is based essentially on the principle of bringing parts of subcritical size together quickly to build up the reaction. The rate of reaction and particularly the rate of building up the reaction are controlled by the diffusion of the neutrons through the moderator to the fission nuclei. For fast build-up in explosion, fast neutrons are preferred.

Engineering Approach to the Nuclear Reaction

The previous discussion clearly shows that the fundamental concepts involved in a nuclear reaction—such as collision, capture, excitation, and energy barrier—are all familiar to students of molecular reactions. The study of the molecular reactions or chemical reaction from kinetic point of view is, however, only a recent development. Its consideration by engineers is even more so. For instance, the power-plant engineers learned to design large boiler installations burning tons of coal per hour without any concept of molecular physics. The design of internal combustion engines was no exception, until the difficulty caused by detonation became serious. Then the investigation of the slow oxidation of the hydrocarbons by chain reactions is helpful. However, the study of nuclear reactions took a different road. Here, the effort was concentrated immediately on the detailed dynamic processes and on the development of a fundamental theory for the nuclear dynamics to explain these processes. This, of course, is the natural result of the emphasis by physicists on the understanding of the fundamentals.

For an engineer, his assignment is not so much to understand a particular phenomenon as to learn to utilize it. Electrical engineers knew how to design long-distance transmission lines before the development of satisfactory physical theory for the conduction of electricity. A similar situation will certainly appear in the engineering utilization of atomic energy. A satisfactory fundamental theory for nuclear structure will no doubt be a great help in "atomic engineering," but to wait for such a theory is certainly unwise and unnecessary. Then shall the *ad hoc* experiments without coordination be encouraged? Such an approach would not only be uneconomical but extremely dangerous because of possible uncontrollable explosion with greater violence. A better approach would be a semi-empirical one. In other words, first the performance of each *elementary process* should be determined experimentally. Then the kinetic theory of reaction developed for the chemical kinetics can be used to predict the performance of the overall reaction involving these elementary processes.

For instance, the basic knowledge required for predicting the fission reaction is the fission cross section; the elastic scattering cross section; the inelastic scattering cross section of the atoms U-234, U-235, U-238, and Pu-239 as a function of the energy of the neutrons; the number and energy of neutrons emitted by fission and its dependence on the energy of incident neutron; etc. With these *empirical data*, the fission reaction in an atomic bomb can be calculated. To those familiar with the theory of chemical kinetics, the extreme complexity of the treatment due to the great variety of possible molecules is well known. The application of kinetic theory to nuclear reactions, however, may be much simpler, since the total number of possible nuclei is only several hundred, while the number of known molecular compounds may be hundreds of thousands. The reacting components that need to be considered in a nuclear reaction will certainly be fewer than for the case of molecular reactions.

According to H. D. Smyth's report[4] on the development of the atomic bomb, this semi-empirical approach is actually followed. Similar methods must be used for the development of the general utilization of atomic energy to determine the optimum process or processes and then finally test the validity of calculation by experiments. This approach would certainly eliminate, as far as humanly possible, the danger and the waste that through improper handling might be associated with the release of energy a million times as great as the conventional combustion process of molecular reaction. It is seen then that the concept of nuclear power engineering is necessarily somewhat different from its counterpart in pure science, the nuclear physics.

REFERENCES

[1] von Kármán, Th., *Atomic Engineering?* Mechanical Engineering, Vol. 67, p. 672, 1945.

[2] See, for instance, Tolman, R. C., *Relativity, Thermodynamics and Cosmology*, Chapter II, Part I, and Chapter III, Part 1, Oxford, 1934.

[3] For a complete tabulation of electron positions in various atoms, see pp. 275 and 276 of the *Handbook of Chemistry and Physics*, 25th Ed:, 1941.

[4] Smyth, H. D., *A General Account of the Development of Methods of Using Atomic Energy for Military Purposes under the Auspices of the United States Government 1940–45*, 1945.

[5] The treatment given follows closely that by Bethe, H. A., *Nuclear Physics—A Stationary State of Nuclei*, Reviews of Modern Physics, Vol. 8, pp. 92–97, 1936.

[6] The figure is based upon data given in the following papers: Oliphant, M. L., *Masses of Light Atoms*, Nature, Vol. 137, pp. 396–397, 1936; Dempster, A. J., *The Energy Content of the Heavy Nuclei*, Physical Review, Vol. 53, pp. 869–874, 1938.

[7] Bethe, H. A., *Energy Production in Stars*, American Scientist, Vol. 30, pp. 243–264, 1942; *Energy Production in Stars*, Physical Review, Vol. 55, pp. 434–456, 1939.

[8] Bohr, N., and Wheeler, J. A., *The Mechanism of Nuclear Fission*, Physical Review, Vol. 56, pp. 426–450, 1939.

[9] Henderson, M. C., *The Heat of Fission of Uranium*, Physical Review, Vol. 58, pp. 774–780, 1940.

Letter to the Editor

Dear Sir:

The following comments on the Wright Brothers Lecture ("British Aircraft Gas Turbines," by Dr. H. Roxbee Cox, JOURNAL OF THE AERONAUTICAL SCIENCES, Vol. 13, No. 2, p. 53, February, 1946) are submitted to you as my personal points of view and do not necessarily correspond to those of the Bureau of Aeronautics.

As a history of gas-turbine developments in England the paper is an extraordinarily interesting document and contains some material with which I was not familiar heretofore. The early history of the struggle for favorable consideration of such devices is not unlike similar history in this country. For example, the conclusions of a special panel formed in 1939 to investigate the application of gas turbines to aircraft is worthy of note: "In its present state, and even considering the improvements possible when adopting the higher temperatures proposed for the immediate future, the gas turbine could hardly be considered as feasible of application to airplanes mainly because of the difficulty in complying with the stringent weight requirements of aeronautics.

". . . . The minimum weight for gas turbines even when taking advantage of higher temperatures appears to be approximately 13 to 15 pounds per horsepower." The Navy was fortunate in having officers like Captain Kauffman of sufficient vision to proceed, despite this lugubrious outlook, to the planning of, and final contracting for, a gas turbine, the first such project in this country for aviation purposes. These studies led to a joint Navy-A.A.F. project under Navy cognizance started early in 1941. Later in the same year the first United States turbojet project was undertaken by the Navy at Westinghouse. I do not doubt that this information, or part of it, was known to Dr. Cox, but it does illustrate the difficulties involved in getting new ideas into development.

It may have occurred to some persons to wonder why the United States did not follow the British example in setting up a collaboration committee. Surely the excellent results obtained by this method in England is a strong argument in favor of such a procedure. However, it was, and still is, my opinion that the idea would not have worked so well in this country. The difference in the situation here and in England as to urgency, available facilities, and methods of handling design and development problems are obvious. In this country we depended on liaison officers like Lieutenant Commander Bollay of the Navy and Colonel Keirn of the Army Air Forces to effect proper distribution of essential design information and development experiences. If this system delayed our progress somewhat, it nevertheless resulted in several distinct designs, each having its own merits. It has long been my contention that competition is an essential to proper development in any field where competition can be achieved. There is little doubt that collaboration between England and the United States in this field was complete and of great value to both countries.

In considering Dr. Cox's detail comments on troubles experienced in gas-turbine development, our difficulties seem to correspond closely with the British with minor exceptions. I do not feel that we have completely licked the turbine disc problems in this country, although we have had little recent trouble. However, I shall not consider the problem completely solved until such time as we have suitable turbine discs that can be manufactured on a high production basis. The annular combustion chamber appears to be successful in Westinghouse engines, somewhat contrary to British experiences. I do not feel that the convenience of the multiple chamber from a development and handling standpoint should be a primary design consideration if the engine suffers in any respect thereby as an engine. Naturally the axial flow engine can less afford the increased size arising from the use of multiple chambers, since small diameter is one of its major advantages.

The facilities described as being available to Power Jets are comparable to those available in the component test laboratory at Westinghouse and at other places in this country. However, it is my opinion that more extensive facilities for the test and development of full-scale engines is essential to eventual success in this field. Although the Navy has used flying test beds for some time to determine at altitude such things as starting characteristics, stable combustion ranges, and minimum speeds, this type of test equipment is too severely limited to be considered as other than an adjunct to laboratories capable of full-scale altitude test work.

The question of thoroughly integrated airplane and engine design is one that arises from time to time in everyone's mind. Steps taken in this direction in past years have resulted in major improvements, such as new types of cowling, quickly removable power plants, etc., as well as revisions of engine shape and arrangement. However, a completely integrated engine and airplane has never been built in this country. Nor does it appear probable that the advent of the gas turbine will appreciably change the situation. There are gas-turbine designs that will permit some rearrangement of components to fit specific airplane designs, but, in general, gas turbines are no more suitable for such treatment than are reciprocating engines. In my opinion, the desire for standardized engines applicable to a wide variety of airplanes will always prohibit separate engine designs for specific airplanes. It is possible that ram jets or rockets may readily lend themselves to such treatment, particularly in pilotless aircraft, but even here standardization and ease of production must be

carefully considered. The views of the airplane and engine people are normally at almost complete divergence on this question, and naturally so. The engine manufacturer must build in competition the best engine as an engine; the airplane manufacturer realizes that all too frequently the success or failure of his airplane depends on the efficiency of his power-plant installation.

It is perfectly true, as the paper points out, that there is inadequate evidence to indicate the superiority of either centrifugal or axial flow blowers at the moment. However, centrifugal blowers are limited as to pressure ratios if multiple staging is not used, and it would appear that the greater capacity of the axial flow blower may limit the use of centrifugal blowers to moderate powers in order to remain within reasonable engine diameters. On the other hand, the axial blower suffers from two plaguing difficulties for which complete cures are not yet available. The first is its narrow operating range, which leads to instability and surge at altitude, and the second is its starting difficulties due, in part, to its narrow operating range and, in part, to the little assistance obtained from ram airflow as well as to its normally higher design pressure ratio.

The discussion of the relative merits of turbojets, gas turbines, and ducted fans is interesting and, in general, corresponds to U.S. Navy ideas. Comparing the three systems alone, the turbojet appears to be most generally applicable to the highest speeds; the other two, to the greatest ranges. Such a generalization is not particularly pertinent, however. All things considered, the gas turbine appears to me to be most suitable for U.S. Navy use, offering the most advantages and the fewest disadvantages. Present indications are that propeller efficiencies may be increased markedly at high Mach numbers. If this proves to be true the turbojet airplane will offer little advantage in high speed and will be inferior in take-off, climb, range, endurance, and general flexibility of operation.

As the paper points out, the consideration of how to select the best engine for a particular design is based on a wide variety of factors, only one of which is the engine power curve with its corresponding fuel consumption curve. All things being equal the commercial "useful load ton-miles per gallon" is a better criterion in the selection of an engine for a given design than is pounds of fuel per pound of thrust. That number includes consideration of take-off power, part throttle performance, differences in engine weight and fuel weight, variations in fuel consumption and in drag, etc. It cannot be expected to cover such things, however, as desirable operating altitudes; penalties acceptable for higher operating speeds; or desired airplane characteristics such as endurance (as contrasted to range), maneuverability, flexibility of loading and operation, stability, etc. Nor can it cover extraneous considerations such as whether or not a flying fuel tank can make an acceptable military airplane.

For commercial aircraft, economy would appear to be a prime consideration, but economy must include consideration of first cost, reliability of operation, maintenance costs, and premiums to be expected from higher operating speeds, in addition to the usual "ton-miles per gallon." The military operator must define economy primarily in terms of losses of aircraft and crews in combat, although he must also consider, from the U.S. Navy standpoint, day-by-day operational readiness. It is obvious that an airplane that must remain on deck from a lack of engine reliability or durability or from lack of fuel is worse than useless and that an airplane is just as surely lost if it has inadequate endurance or if it cannot be safely operated as it is if it has inadequate performance.

Of interest in this connection might be a summary I prepared several years ago near the beginning of the Navy's gas-turbine program.

"From the standpoint of thermal efficiency alone, true jet propulsion is at one end of a scale which has the propellered engine at the other, most efficient, end. The difference is very marked, being on the border of three to one. Assuming equal weights and drag, a conventional airplane which has a range of 1,000 miles will have a range of only 300 miles as a true jet propulsion airplane. The difference in endurance is even more marked, being on the border of the ratio of 1 to 4 hours at equivalent percentage powers. Basically the true jet propulsion unit is a full throttle engine and, hence, suffers in endurance. A possible way of reducing this discrepancy would be to have multiple units so that the airplane could be operated at full throttle on whatever percentage of units would be required to obtain the desired power. At best, however, there must always be considerable loss in efficiency, assuming always, of course, that the propeller does not lose too much efficiency at higher speeds (which does not seem unreasonable at the speeds we are now discussing).

"In weight again the true jet propulsion is at one end of the scale, possibly as low as half pound per equivalent brake horsepower, the propellered engine being 1.1 to 1.6 lbs. per b.hp.

"From the standpoint of airplane design the true jet propulsion machine offers several advantages. Its small size leads to smaller fuselages and possibly better streamlining than the conventional propellered airplane. Furthermore, since propeller clearance is not involved, the landing gear need only be big enough to keep the fuselage off the deck, and therefore the landing gear weight is considerably reduced. In this connection it should be pointed out that a propeller need not be of the conventional design now familiar but could readily be a shrouded (pro) impeller, an axial fan, or an exhaust inducer, and therefore part of this advantage can be eliminated.

"From a performance standpoint the jet propulsion unit, for the same weight airplane and assuming the airplane is still below the critical compressibility range, will give substantially constant speed up to its critical altitude. However, for the same weight, a turbosupercharged engine will produce more (equivalent) brake horsepower at altitudes about 35,000 ft. and, assuming reasonable propeller efficiency, more speed. Hence, in speed ranges up to perhaps 450 m.p.h., the jet propulsion unit shows tremendous advantages of speed and climb at low and intermediate altitudes but approaches equality at high altitudes. For speeds above 500 m.p.h. it is probable that propeller efficiency will be so low as to nullify any advantage at high or low altitudes, except in cruising. The take-off with a true jet propulsion unit will be poor in any case and must be augmented in some form. The range question has already been considered in paragraph 2.

"From the standpoint of a usable airplane the true jet propulsion aircraft must necessarily await the solution of the following problems: controllability; balance; handling characteristics at low and high speeds; take-off; carrier approach; and gas disposal, particularly with regard to damage to other airplanes in carrier take-offs and to flame visibility. In this connection a compromise solution in which part of the power is absorbed in a propeller will reduce the energy in the jet and may reduce the above problems considerably.

"After due consideration of all the factors involved, this Section recommends as an eventual desirable solution a compromise power plant in which the division of power between the propeller and the jet approximates the theoretical best division—i.e., 75 per cent to the propeller and 25 per cent to the jet. This setup might include a means of adjusting this percentage in the air so that the pilot may elect to get high speed low range at sea level, or long range, or any compromise between the two. The propeller, as previously pointed out, may take the form of a fan or impeller. Pending this eventual solution, it is recommended that true jet units be installed as accessories to conventional internal combustion engines in order to obtain better low-altitude performance without sacrificing too much in range or endurance. It is the present hope of this Section to have one or more such units of different types ready for the flight test in early 1943. A true jet propulsion installation is not recommended at this time." Qualitatively, this analysis still appears valid.

The lecture presents some ideas relative to possible airplane changes because of the advent of the gas turbine. Unquestionably, some changes will be called for by the advent of long, small diameter power plants and by higher airplane speeds. That those changes will result in tail first or no tail airplanes is open to considerable question. We are all more or less familiar with the defects of this type of aircraft, particularly from a military standpoint. Furthermore, available test data indicate the slipstream effect at high speeds to be small either as a pusher or as a tractor. The maximum slipstream drag is probably no more than 2 per cent of the total drag in the extremely high-speed condition. The tractor arrangement is preferable at low speeds, as in the approach condition, because of the much lower stalling speeds available with tractor propellers with power on.

One effect not covered as such in the paper is the radical change in center of gravity location, which may be expected in airplanes whose major useful load is in fuel, between the full load and no load condition. Stability and controllability at low speeds is likely to be an extremely serious problem in turbojet airplanes in which the designer tries to obtain ranges and endurances comparable to those obtainable in propellered aircraft. The Me 163 is an exaggerated example of this effect, since it is a rocket airplane, but that airplane is almost uncontrollable at low speeds with no fuel.

It is assumed that the paper omits a discussion of the so-called compound engine, since that arrangement is not considered a true gas turbine. However, combinations of reciprocating engines and gas turbines have much to recommend them. The use of an Otto or Diesel cycle engine as compressor and combustion chamber offers higher overall efficiencies than appear obtainable in other ways. The free piston compressor, if applied to a gas turbine, would be, in effect, a combination of reciprocating engine and turbine. Admittedly, the result of such a marriage is a complicated and bulky engine, but, if past experience is a suitable criterion, simplicity will always give way to performance.

S. B. SPANGLER
Captain, U.S.N.
Bureau of Aeronautics
Navy Department

Library Facilities of the Institute of the Aeronautical Sciences

To serve Institute members and others in the aeronautical industry, the Institute of the Aeronautical Sciences offers the facilities of:

The W. A. M. Burden Library
2 East 64th Street
New York 21, N.Y.

The facilities of this library are available for reference study at the Institute.

The Paul Kollsman Lending Library
2 East 64th Street
New York 21, N.Y.

This library loans books without charge to members and others in the United States over eighteen years of age. Full information will be sent on request.

The Pacific Aeronautical Library
6715 Hollywood Boulevard
Hollywood 28, Calif.

This is a service and reference library for West Coast organizations. Full information as to its facilities will be sent on request.

Flapping Characteristics of Rigid Rotor Blades

RALPH W. ALLEN

Consulting Engineer

SUMMARY

The influence of blade stiffness on rotor blade flapping is investigated and equations are developed which describe the blade motion. The blade lag angle is also obtained and an example calculation is given.

It is found that blade stiffness has a marked influence on blade lag and flapping amplitude and that there exists a possible resonant condition for the semirigid type of rotor blades. Increasing the blade stiffness decreases the magnitude of flapping and reduces blade lag. The stiffness effects are especially noticed in the transition from a freely hinged blade to a semirigid blade.

INTRODUCTION

BEFORE THE AERODYNAMICS or structural quantities of the present helicopter rotor blade systems can be properly determined, it is necessary to know the characteristic motions of the blades as they rotate. An important motion of the blade system is flapping, which occurs mostly when the helicopter is in motion. Blade flapping is generally brought on by the differences of lift distribution between the advancing blade and the retreating blade. Each blade tends to seek its equilibrium position in the vertical direction and in doing so causes the blade to flap. The flapping changes the angle of attack of the blade thereby changing the lift distribution. These changes occur in a cyclical manner around the azimuth.

The majority of the present helicopters have their blades hinged somewhere near the center of rotation, thus permitting the blade to flap freely and seek its own equilibrium position in the vertical direction. The investigation of the flapping motion of the hinged rotor blade has been developed not only in theory but has been experienced in many flight tests.[1] Recently, there has been a definite swing toward rigid-type rotor blade construction, and the flapping motion of this type of blade has not been greatly investigated. In the rigid-type blades, such as is used in many coaxial-type rotor blade systems, the flapping motion of the blade is restrained by the elasticity of the blade material and will, therefore, have a different flapping pattern about the azimuth. The positions of maximum and minimum flapping will be different in the rigid blade than in the hinged blade. This paper analyzes the flapping motions of a rigid-type rotor blade and determines the angle of lag, which is defined as being the azimuth angle between the maximum thrust position and maximum flapping position of the rotor blade.

Received April 30, 1945.

DEVELOPMENT OF THE FUNDAMENTAL EQUATIONS

In order to simplify the equations, it is assumed that the blade in this analysis is perfectly rigid and develops all of its bending at the root section of the blade. The elasticity of the material at the root section is represented by a torsional spring of stiffness factor K. A rotor blade system that mechanically duplicates an actual rotor blade motion is schematically shown in Fig. 1.

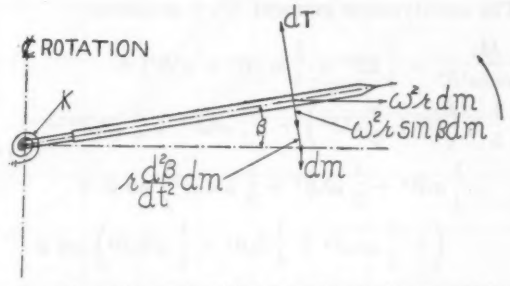

FIG. 1. Schematic setup of blade flapping mechanics and forces acting on blade.

NOMENCLATURE

β	=	flapping angle
ψ	=	azimuth angle measured from downwind direction
a_0, a_1, b_1	=	flapping constants
I	=	moment of inertia of blade in flapping
t	=	time
K	=	blade stiffness constant
ω_0	=	natural frequency of blade in bending
ω	=	rotational velocity of rotor blade
M_t	=	thrust bending moment
M_w	=	blade weight bending moment
R	=	blade radius
c	=	blade chord
a	=	lift slope factor
λ	=	down-wash factor
θ_0	=	blade pitch
θ_1	=	blade twist factor
μ	=	tip speed ratio
B	=	blade tip loss factor
ψ_1	=	blade lag angle

The moment due to the centrifugal force is

$$\int \beta\omega^2 r^2 dm = \beta\omega^2 I$$

Assuming $\cos \beta = 1$,

$$\sin \beta = \beta$$

The moment produced by the inertia force is

$$\int (D^2\beta/Dt^2) r^2 dm = (D^2\beta/Dt^2) I$$

The restoring moment of the spring is $K\beta$.

These moments sum up to the left side of the differential Eq. (4).

The flapping angle β is expressed in the form of a trigonometric series

$$\beta = a_0 - a_1 \cos\psi - b_1 \sin\psi - a_2 \cos 2\psi - b_2 \sin 2\psi \quad (1)$$

Neglecting second harmonic terms β becomes:

$$\beta = a_0 - a_1 \cos\psi - b_1 \sin\psi \quad (2)$$

Eq. (2) is sometimes written in the form

$$\beta = a_0 - a_1 \cos(\psi - \psi_1) \quad (3)$$

The differential equation expressing the relationship of the aerodynamic moments to the mechanical moments is

$$I(d^2\beta/dt^2) + K\beta + I\omega^2\beta = M_t - M_w \quad (4)$$

The aerodynamic moment M_t is as follows:

$$\left.\begin{aligned}\frac{M_t}{{}^1/_2\rho c a \omega^2 R^4} = {} & \frac{1}{3}\lambda B^3 + \frac{1}{4}\theta_0 (B^4 + \mu^2 B^2) + \\ & \frac{1}{5}\theta_1 \left(B^5 + \frac{5}{6}\mu^2 B^3\right) + \left(\frac{2}{3}\mu\theta_0 B^3 + \frac{1}{2}\mu\theta_1 B^4 - \right. \\ & \left. \frac{1}{4}a_1 B^4 + \frac{1}{2}\mu\lambda B^2 + \frac{1}{8}\mu^2 a_1 B^2\right)\sin\psi + \\ & \left(-\frac{1}{3}\mu a_0 B^3 + \frac{1}{4}b_1 B^4 + \frac{1}{8}\mu^2 b_1 B^2\right)\cos\psi\end{aligned}\right\} \quad (5)$$

The gravity moment M_w is neglected in this analysis, for its magnitude is far less than the aerodynamic moment and therefore negligible error should be introduced.

Solution of the Differential Equation

The solution of Eq. (4) is found by substituting the value of B into Eq. (4) and equating coefficients of like trigonometric functions; thus

$$d^2\beta/dt^2 = \omega^2(a_1 \cos\psi + b_1 \sin\psi) \quad (6)$$

Substituting Eqs. (6) and (3) into Eq. (4) yields

$$\omega^2(a_1 \cos\psi + b_1 \sin\psi) + \Omega^2(a_0 - a_1 \cos\psi - b_1 \sin\psi) = M_t/I \quad (7)$$

where $\omega^2 + \omega_0^2 = \Omega^2$ and $\omega_0^2 = K/I$.

Equating coefficients of like trigonometric functions, the following values for the constants are obtained:

$$\left.\begin{aligned}a_0 = {} & \frac{\gamma}{I\Omega^2}\left[\frac{1}{3}\lambda B^3 + \frac{1}{4}\theta_0 (B^4 + \mu^2 B^2) + \right. \\ & \left. \frac{1}{5}\theta_1 \left(B^5 + \frac{5}{6}\mu^2 B^3\right)\right] \\ \gamma = {} & {}^1/_2\rho c a \omega^2 R^4\end{aligned}\right\} \quad (8)$$

$$a_1(\omega^2 - \Omega^2)\frac{I}{\gamma} = -\frac{1}{3}\mu B^3 a_0 + \frac{1}{4}b_1 B^4 + \frac{1}{8}\mu^2 b_1 B^2 \quad (9)$$

$$b_1(\omega^2 - \Omega^2)\frac{I}{\gamma} = \frac{2}{3}\mu\theta_0 B^3 + \frac{1}{2}\mu\theta_1 B^4 - \frac{1}{4}a_1 B^4 + \frac{1}{2}\mu\lambda B^2 + \frac{1}{8}\mu^2 a_1 B^2 \quad (10)$$

From Eqs. (8), (9), and (10) a_1 and b_1 are obtained.

$$a_1 = \left\{-\frac{1}{3}\mu B^3 a_0\left[\frac{I}{\gamma}(\omega^2 - \Omega^2)\right] + \frac{1}{6}\mu\theta_0 B^7 + \frac{1}{8}\mu\theta_1 B^8 + \frac{1}{8}\mu\lambda B^6\right\} \Big/ \left[\frac{I^2}{\gamma^2}(\omega^2 - \Omega^2)^2 + \frac{1}{16}B^8\right] \quad (11)$$

For a blade with no twist and neglecting μ^2 terms

$$a_1 = \left\{\mu B^3\left[-\frac{1}{3}(\omega^2 - \Omega^2)\frac{I}{\gamma}a_0\right] + \frac{1}{6}\theta_0 B^4 + \frac{1}{8}\lambda B^5\right\} \Big/ \left[\frac{I^2}{\gamma^2}(\omega^2 - \Omega^2)^2 + \frac{1}{16}B^8\right] \quad (12)$$

Neglecting μ^2 terms

$$b_1 = \left[\frac{I}{\gamma}(\omega^2 - \Omega^2)\left(\frac{2}{3}\mu\theta_0 B^3 + \frac{1}{2}\mu\lambda B^2 + \frac{1}{2}\mu\theta_1 B^4\right) + \frac{1}{12}\mu B^7\theta_0\right] \Big/ \left[\frac{I^2}{\gamma^2}(\omega^2 - \Omega^2)^2 + \frac{1}{16}B^8\right] \quad (13)$$

with μ^2 terms included, b_1 becomes

$$b_1 = \left[\frac{I}{\gamma}(\omega^2 - \Omega^2)\left(\frac{2}{3}\mu\theta_0 B^3 + \frac{1}{2}\mu\lambda B^2 + \frac{1}{2}\mu\theta_1 B^4\right) + \frac{1}{12}\mu B^7\theta_0\right] \Big/ \left[\frac{I^2}{\gamma^2}(\omega^2 - \Omega^2)^2 + \frac{1}{16}B^8 - \frac{1}{32}\mu^2 B^6 + \frac{1}{32}\mu^2 B^6\right] \quad (14)$$

For a blade with no twist

$$b_1 = \left[B^2\frac{I}{\gamma}\mu(\omega^2 - \Omega^2)\left(\frac{2}{3}\theta_0 B + \frac{1}{2}\lambda\right) + \frac{1}{12}B^5\theta_0\right] \Big/ \left[\frac{I^2}{\gamma^2}(\omega^2 - \Omega^2)^2 + \frac{1}{16}B^8\right] \quad (15)$$

Substituting the equations for b_1 and a_1 and into Eq. (2) completes the solution of the flapping motion of the blade.

$$\beta = \frac{{}^1/_2\rho caR^4}{I}\left[\frac{1}{1+(\omega_0^2/\omega^2)}\right]\left(\frac{1}{3}\lambda B^3 + \frac{1}{4}\theta_0 B^4\right) - \left\{\left[\left(\frac{{}^1/_3\mu B^3 a_0 I}{{}^1/_2\rho caR^4}\right)\left(\frac{\omega_0^2}{\omega^2}\right) + \frac{1}{6}\mu\theta_0 B^7 + \frac{1}{8}\mu\lambda B^6\right] \div \left[\left(\frac{I}{{}^1/_2\rho caR^4}\right)^2\left(\frac{\omega_0^2}{\omega^2}\right)^2 + \frac{1}{16}B^8\right]\right\}\cos\psi - \left\{\left[\frac{-I}{{}^1/_2\rho caR^4}\left(\frac{\omega_0^2}{\omega^2}\right)\left(\frac{2}{3}\mu\theta_0 B^2 + \frac{1}{2}\mu\lambda B^2\right) + \frac{1}{12}\mu B^7 a_0\right] \div \left[\left(\frac{I}{{}^1/_2\rho caR^4}\right)^2\left(\frac{\omega_0^2}{\omega^2}\right)^2 + \frac{1}{16}B^8\right]\right\}\sin\psi \quad (16)$$

The minimum flapping position is found by differentiating Eq. (16) and setting to zero; thus

$$\tan\psi_1 = \frac{(-I/{}^1/_2\,\rho caR^4)(\omega_0^2/\omega^2)({}^2/_3\,\mu\theta_0 B^2 + {}^1/_2\,\mu\lambda B^2) + {}^1/_{12}\,\mu B^7 a_0}{({}^1/_3\,\mu B^3 I a_0/{}^1/_2\,\rho caR^4)(\omega_0^2/\omega^2) + {}^1/_8\,\mu\theta_0 B^7 + {}^1/_8\,\mu\lambda B^6} \quad (17)$$

This equation is shown in curve form in Fig. 3, for untwisted blade.

Example Calculation

An example calculation is made to show the effects in curve form of the parameter ω_0/ω. The necessary data for the blade are as follows:

I = 334 slugs ft.^{2}
R = 22.5 ft.
C = 1.25 ft.
θ_0 = 0.06 rad.
μ = 0.5
ρ = 0.0021 slug per ft.^{3}
a = 5.58

The equations that develop from substituting the data into Eq. (16) are

$$\frac{\omega_0}{\omega} = 0,\ \beta = 0.12190 - 0.10000\cos\psi - 0.08193\sin\psi$$

$$\frac{\omega_0}{\omega} = 1,\ \beta = 0.06090 - 0.15020\cos\psi - 0.0079640\sin\psi$$

$$\frac{\omega_0}{\omega} = 2,\ \beta = 0.02430 - 0.17550\cos\psi - 0.02357\sin\psi$$

$$\frac{\omega_0}{\omega} = 10,\ \beta = 0.001219 - 0.001675\cos\psi - 0.00024996\sin\psi$$

These equations are shown in curve form in Fig. 2.

The lag angle is found by substituting the necessary data into Eq. (17). The results are shown in curve form in Fig. 3.

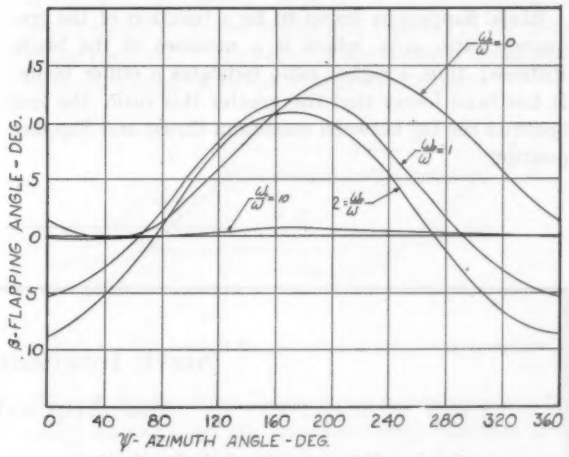

FIG. 2. Blade flapping around the azimuth.

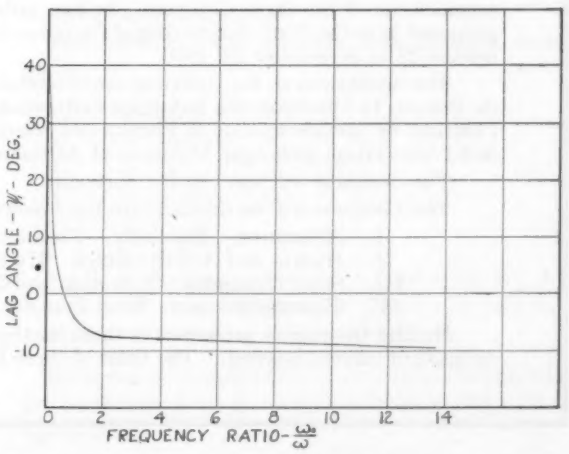

FIG. 3. Blade lag angle with variation of frequency ratio ω_0/ω measured from the down-wind direction.

Procedure in Design Analysis

In the preliminary design of rotary aircraft it is necessary to know the flapping characteristics of the rotor blades. Aside from structural reasons, interference between blades, as in the coaxial-type rotor system, and aerodynamic efficiency are some of the important information needed in the proper design of present-day rotary aircraft.

The procedure necessary for the analysis of blade flapping consists of, first, setting up the design criteria—that is, such fixed quantities as weight of aircraft, speed of rotation, blade radius, number of blades, airfoil section, maximum ceiling, and maximum speed. From this information the factors θ_0, λ, and μ can be found. Knowing these factors, the flapping coefficients a_0, a_1,

and b_1 can be obtained. By substituting the coefficients into the flapping equation for an assumed I and ω/Ω,

$$\beta = a_0 - a_1 \cos \psi - b_1 \sin \psi$$

the flapping amplitude can be found and the maximum and minimum position along the azimuth obtained. If the results are not desirable in accordance with the particular design, the process is repeated using different values of I and ω/Ω until the necessary and proper blade flapping characteristic is determined. The mass moment of inertia and blade frequency will then be found and, from this, the blade weight. The blade is then designed to meet these values.

Conclusions

Blade flapping is found to be a function of the frequency ratio ω_0/ω, which is a measure of the blade stiffness; thus a higher ratio indicates a stiffer blade. It has been found that the greater this ratio, the less becomes the lag between maximum thrust and flapping position.

Apparently, the transition from a freely hinged blade to a semirigid blade produces marked changes in the lag angle, as shown in Fig. 3; however, as the blade stiffness is greatly increased the lag angle change is small.

The amplitude of flapping is reduced by increasing the blade stiffness, other factors remaining the same. From the curves in Fig. 2, the flapping amplitude is negligible under a frequency ratio of $\omega_0/\omega = 10$. It is also noted that the flapping angle reaches fairly high negative values, indicating that there exists a critical flapping condition that occurs near a frequency ratio of 2 for this particular example. It is, therefore, important to investigate, in the preliminary blade design stages, the flapping characteristics of the rotor blades so that a critical resonant flapping condition will not persist. This is especially needed for semirigid blades.

Reference

[1] Wheately, John B., *An Aerodynamic Analysis of the Autogyro Rotor with a Comparison Between Calculated and Experimental Results*, N.A.C.A. T.R. No. 487, 1934.

Sixth International Congress for Applied Mechanics

At a meeting initiated by Dr. J. C. Hunsaker and Dr. Th. von Kármán, acting as joint secretaries of the Fifth International Congress for Applied Mechanics, a committee was formed for the organization of the Sixth Congress. In line with the decision reached at Cambridge in 1938, it is proposed that the Sixth International Congress for Applied Mechanics be held in Paris, from September 22 to September 29, 1946.

The invitations to the Congress are extended on behalf of l'Académie des Sciences de l'Institut de France, la Direction des Relations culturelles, le Centre national de la Recherche scientifique, l'Institut de Méchanique de la Faculté des Sciences de Paris, la Société française des Mécaniciens, and l'Association technique Maritime et Aéronautique.

The Congress will meet at the Sorbonne.

The Congress will be divided into the following Sections:

I. Structures. Elasticity. Plasticity.
II. Hydro- and Aerodynamics. Hydraulics.
III. Solid Dynamics. Vibration and Sound. Friction and Lubrication.
IV. Thermodynamics. Heat Transfer. Combustion. Fundamentals of Nuclear Energy.

Besides the papers presented in these Sections, a number of General Lectures will be given on subjects of current interest. The titles of these Lectures will be made known in a later notice.

Buckling of a Flanged Plate

HENRY L. LANGHAAR*

Consolidated Vultee Aircraft Corporation

ABSTRACT

This investigation treats the buckling of an axially compressed isotropic elastic rectangular plate that is hinged on the ends, supported but subjected to elastic rotational restraint on one longitudinal edge, and flanged but otherwise free on the remaining edge. A numerical procedure with a rigorous mathematical basis is proposed for solving elastic stability problems of this type.

INTRODUCTION

THE GENERAL PROBLEM under consideration presents no inherent mathematical difficulties, but it leads to a finite equation that is too complicated to be directly useful for engineering stress analysis. The following work relieves the labor that is encountered in individual solutions of the problem by the use of numerical tables of the transcendental functions that constitute the snarl in the algebraic result. The tabulations may be regarded as an extension of data charted by Timoshenko[1] for solving special problems of the present type —namely, problems wherein the elastic rotational restraint of the supported edge is infinite (clamped edge). It should be observed that the condition of simple support at the ends of the plate is not an essential restriction if the plate is long, since the buckling stress of a long plate is nearly independent of the end conditions.

The results that are presented are a logical basis for treating certain aircraft structural problems, such as the buckling of the outstanding leg of a lipped or a bulbed angle. With a view to these applications, it may be mentioned that a practice that has been adopted by many aircraft stress analysts is to present plate-buckling data throughout the elastic and the semiplastic ranges by a single curve of σ_{cr} versus $b/(t\sqrt{K})$, the abscissa $b/(t\sqrt{K})$ being derived from the universal plate-buckling formula

$$\sigma_{cr} = KE(t/b)^2 \qquad (1)$$

just as the column-curve abscissa $L/(\rho\sqrt{C})$ or L'/ρ is derived from the Euler column formula. It is not within the scope of this study to pursue theoretical or experimental investigations of the accuracy of this procedure nor to inquire whether variation of the coefficient K is required when the proportional elastic limit is exceeded. Nevertheless, it is pertinent to note that there is, at present, no more reliable method for predicting buckling stresses of highly loaded plates than to ascribe to the coefficient K a significance beyond the confines of elasticity theory.

Received July 17, 1945.

* Structural Research Engineer.

GENERAL EQUATION FOR THE BUCKLING COEFFICIENT

A plate (Fig. 1)—hinged on the edges $x = 0$ and $x = a$, supported and subjected to elastic rotational restraint on the edge $y = 0$, and flanged on the edge $y = b$ —is buckled by an axial compression stress σ_{cr}. The thickness of the plate is t, and its flexural rigidity is $D = Et^3/12(1 - \nu^2)$. The cross-section area of the flange is ω, and the moment of inertia of the flange cross section with respect to its centroidal axis parallel to the plane of the plate is I. The depth of the flange is assumed to be small compared to the width b of the plate.

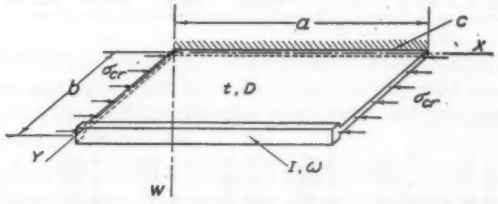

FIG. 1. Diagram of flanged plate showing nomenclature.

The deflection of the plate due to buckling is w. The spring constant for the rotational edge restraint is C; i.e., the moment M_y per unit length on the edge $y = 0$ is $M_y = -C(\partial w/\partial y)$. The number of half waves in the buckled plate is m.

The following dimensionless nomenclature is employed:

$$\begin{aligned}
\xi &= \pi x/a,\ \eta = y/b \\
\gamma &= (m\pi b/a)^2 \\
A &= 12(1 - \nu^2)[I/(bt^3)] \\
B &= \omega/(bt) \\
\kappa &= Cb/D \\
\lambda &= \sigma_{cr}tb^2/D \\
f, g, h &= \text{functions of } \lambda \text{ and } \gamma \text{ defined by Eq. (15) and tabulated in Tables 1, 2, and 3} \\
F(\lambda) &= \text{a function defined by Eq. (4)}
\end{aligned} \qquad (2)$$

By virtue of its definition, the variable λ is related to the coefficient K of the buckling formula (Eq. (1)) by the equation

$$K = \lambda/12(1 - \nu^2) \qquad (3)$$

The theory of elasticity (see Appendix) furnishes the following equation for the coefficient λ:

$$A\gamma - B\lambda + \frac{\lambda + g + \kappa f/\gamma}{h - \kappa} \equiv F(\lambda) = 0 \qquad (4)$$

The quantities f, g, and h are functions of the two vari-

TABLE 1
The Function $F(\lambda, \gamma)$. ($\nu = 0.30$)

γ \ λ	3	5	10	15	20	25	30	35	40	45	50	55	60
0.0	−3.00	−3.00	−3.00	−3.00	−3.00	−3.00	−3.00	−3.00	−3.00	−3.00	−3.00	−3.00	−3.00
0.2	−3.15	−3.07	−2.83	−2.59	−2.34	−2.10	−1.86	−1.62	−1.38	−1.13	−0.85	−0.62	−0.57
0.4	−3.33	−3.15	−2.68	−2.19	−1.69	−1.21	−0.70	−0.21	+0.28	+0.80	+1.38	+1.86	+2.03
0.6	−3.52	−3.26	−2.54	−1.80	−1.04	−0.30	+0.46	+1.23	+2.01	+2.81	+3.69	+4.47	+4.81
0.8	−3.74	−3.38	−2.42	−1.42	−0.40	+0.60	+1.63	+2.71	+3.79	+4.90	+6.09	+7.21	+7.79
1.0	−3.97	−3.52	−2.31	−1.06	+0.23	+1.51	+2.84	+4.21	+5.62	+7.06	+8.55	+10.1	+11.0
1.2	−4.23	−3.68	−2.22	−0.71	+0.86	+2.44	+4.08	+5.77	+7.49	+9.28	+11.2	+13.2	+14.6
1.4	−4.51	−3.86	−2.14	−0.37	+1.48	+3.36	+5.32	+7.36	+9.43	+11.6	+14.0	+16.5	+18.4
1.6	−4.81	−4.05	−2.09	−0.04	+2.09	+4.28	+6.58	+8.98	+11.4	+14.0	+16.9	+19.9	+22.4
1.8	−5.12	−4.26	−2.05	+0.27	+2.69	+5.20	+7.84	+10.6	+13.5	+16.6	+20.0	+23.5	+26.7
2.0	−5.45	−4.50	−2.03	+0.56	+3.28	+6.11	+9.11	+12.3	+15.6	+19.2	+23.2	+27.3	+31.4
2.2	−5.80	−4.75	−2.02	+0.85	+3.88	+7.01	+10.4	+14.0	+17.8	+21.9	+26.6	+31.4	+36.6
2.4	−6.17	−5.02	−2.04	+1.12	+4.46	+7.92	+11.7	+15.8	+20.0	+24.8	+30.1	+35.8	+42.1
2.6	−6.55	−5.31	−2.07	+1.37	+5.02	+8.82	+13.0	+17.5	+22.3	+27.7	+33.8	+40.4	+47.9
2.8	−6.95	−5.62	−2.12	+1.60	+5.56	+9.71	+14.3	+19.3	+24.7	+30.8	+37.6	+45.2	+54.1
3.0	−7.37	−5.94	−2.19	+1.81	+6.09	+10.6	+15.6	+21.1	+27.1	+33.9	+41.5	+50.4	+60.8
4.0	−9.72	−7.82	−2.82	+2.58	+8.47	+15.0	+22.2	+30.4	+40.0	+51.2	+64.4	+82.4	+106
5.0	−12.5	−10.1	−3.95	+2.85	+10.4	+18.9	+28.6	+40.1	+54.0	+71.5	+94.9	+128	+181
6.0	−15.8	−12.9	−5.57	+2.57	+11.7	+22.2	+34.6	+49.7	+69.0	+94.8	+133	+197	+332
7.0	−19.3	−16.1	−7.68	+1.75	+12.5	+25.0	+40.0	+59.0	+84.3	+121	+181	+305	+750
8.0	−23.3	−19.7	−10.3	+0.37	+12.6	+27.0	+44.7	+67.6	+99.4	+149	+241	+493	+6,030
9.0	−27.6	−23.7	−13.3	−1.53	+12.1	+28.2	+48.4	+75.2	+114	+178	+315	+869	
10.0	−32.2	−28.1	−16.8	−3.97	+10.9	+28.7	+51.2	+81.6	+127	+207	+402	+1,880	
11.0	−37.2	−32.8	−20.6	−6.88	+9.11	+28.4	+53.0	+86.8	+138	+234	+499	+9,948	
12.0	−42.5	−37.7	−24.9	−10.2	+6.77	+27.5	+53.8	+90.6	+148	+258	+600		

TABLE 2
The Function $g(\lambda, \gamma)$. ($\nu = 0.30$)

γ \ λ	3	5	10	15	20	25	30	35	40	45	50	55	60
0.0	−4.20	−4.20	−4.20	−4.20	−4.20	−4.20	−4.20	−4.20	−4.20	−4.20	−4.20	−4.20	−4.20
0.2	−4.42	−4.38	−4.26	−4.14	−4.02	−3.92	−3.77	−3.65	−3.52	−3.41	−3.27	−3.14	−3.01
0.4	−4.65	−4.58	−4.34	−4.09	−3.84	−3.64	−3.34	−3.09	−2.84	−2.59	−2.31	−2.03	−1.76
0.6	−4.89	−4.78	−4.42	−4.05	−3.68	−3.35	−2.92	−2.53	−2.13	−1.74	−1.30	−0.88	−0.44
0.8	−5.14	−4.98	−4.52	−4.02	−3.52	−3.05	−2.50	−1.96	−1.41	−0.86	−0.26	+0.34	+0.96
1.0	−5.40	−5.20	−4.62	−4.00	−3.38	−2.74	−2.08	−1.39	−0.68	+0.05	+0.83	+1.62	+2.46
1.2	−5.67	−5.42	−4.74	−3.99	−3.25	−2.46	−1.66	−0.81	+0.07	+0.98	+1.96	+2.99	+4.16
1.4	−5.95	−5.65	−4.86	−4.00	−3.12	−2.20	−1.24	−0.23	+0.83	+1.95	+3.15	+4.42	+5.91
1.6	−6.24	−5.89	−5.00	−4.02	−3.01	−1.95	−0.82	+0.36	+1.61	+2.95	+4.38	+5.93	+7.73
1.8	−6.52	−6.14	−5.14	−4.04	−2.91	−1.70	−0.42	+0.94	+2.40	+3.97	+5.67	+7.51	+9.65
2.0	−6.82	−6.39	−5.29	−4.08	−2.82	−1.47	−0.02	+1.53	+3.20	+5.03	+7.02	+9.20	+11.7
2.2	−7.12	−6.66	−5.45	−4.13	−2.74	−1.24	+0.38	+2.13	+4.02	+6.12	+8.43	+11.0	+14.0
2.4	−7.43	−6.93	−5.62	−4.19	−2.66	−1.02	+0.77	+2.72	+4.85	+7.23	+9.90	+13.0	+16.5
2.6	−7.74	−7.21	−5.80	−4.26	−2.60	−0.82	+1.15	+3.31	+5.70	+8.38	+11.4	+15.0	+19.1
2.8	−8.06	−7.49	−5.98	−4.34	−2.56	−0.62	+1.52	+3.90	+6.55	+9.57	+13.0	+17.1	+21.8
3.0	−8.38	−7.78	−6.18	−4.43	−2.52	−0.44	+1.88	+4.48	+7.41	+10.8	+14.7	+19.3	+24.8
4.0	−10.1	−9.32	−7.29	−5.04	−2.53	+0.31	+3.57	+7.36	+11.9	+17.3	+24.2	+33.0	+45.1
5.0	−11.9	−11.0	−8.59	−5.90	−2.83	+0.74	+4.96	+10.1	+16.4	+24.7	+36.0	+52.5	+79.2
6.0	−13.8	−12.8	−10.1	−6.98	−3.40	+0.84	+6.01	+12.5	+21.0	+32.8	+50.6	+81.1	+147
7.0	−15.7	−14.6	−11.7	−8.25	−4.24	+0.62	+6.66	+14.5	+25.3	+41.4	+68.6	+126	+332
8.0	−17.8	−16.6	−13.4	−9.70	−5.32	+0.06	+6.90	+16.1	+29.2	+50.2	+90.3	+202	+2,680
9.0	−19.8	−18.6	−15.2	−11.3	−6.61	−0.79	+6.74	+17.1	+32.4	+58.8	+116	+352	
10.0	−22.0	−20.7	−17.2	−13.1	−8.09	−1.91	+6.18	+17.5	+34.9	+66.6	+145	+752	
11.0	−24.1	−22.8	−19.2	−14.9	−9.74	−3.28	+5.25	+17.4	+36.6	+73.2	+177	+3,920	
12.0	−26.3	−24.9	−21.2	−16.8	−11.5	−4.87	+3.99	+16.7	+37.3	+78.1	+207		

ables λ and γ. These functions have been tabulated for the case in which Poisson's ratio is equal to 0.30 (Tables 1, 2, and 3).

In any specific problem the numerical values of the quantities A, B, and κ are determined by Eq. (2). It may here be noted that the area ω is introduced in the theory only for the determination of the net load $\omega\sigma_{cr}$ that exists in the flange. *Hence, Eq. (4) also furnishes the solution in cases where the plate and the flange are unequally stressed if the parameter B is modified by a factor that represents the ratio of the flange stress to the plate stress.*

In general, the quantity γ is not precisely determined by Eq. (2) because it depends upon an unknown integer m. This circumstance requires that several determinations of λ be performed with different integral values of m until the value is found that furnishes a minimum to λ. The number of trials may be reduced by a good intuitive estimate of the wave length of the buckled form. In a specific trial calculation, the numerical value of γ is known, and therefore there is essentially only one unknown in Eq. (4)—namely, λ. Thus, Eq. (4) may be symbolically written $F(\lambda) = 0$.

The nature of the function $F(\lambda)$ is shown by Fig. 2. In general, $F(\lambda)$ is a decreasing function that is positive for small positive values of λ but which approaches a vertical asymptote as λ increases. Values of λ that lie beyond the asymptote have no practical significance,

TABLE 3

The Function $h(\lambda, \gamma)$. ($\nu = 0.30$)

γ \ λ	3	5	10	15	20	25	30	35	40	45	50	55	60
0.0	−3.00	−3.00	−3.00	−3.00	−3.00	−3.00	−3.00	−3.00	−3.00	−3.00	−3.00	−3.00	−3.00
0.2	−3.07	−3.06	−3.05	−3.03	−3.01	−2.99	−2.97	−2.95	−2.92	−2.91	−2.89	−2.87	−2.84
0.4	−3.14	−3.12	−3.09	−3.06	−3.02	−2.97	−2.93	−2.90	−2.85	−2.81	−2.77	−2.72	−2.68
0.6	−3.20	−3.19	−3.14	−3.08	−3.03	−2.96	−2.90	−2.84	−2.77	−2.72	−2.65	−2.58	−2.51
0.8	−3.27	−3.25	−3.18	−3.11	−3.04	−2.95	−2.87	−2.79	−2.70	−2.61	−2.52	−2.42	−2.33
1.0	−3.34	−3.31	−3.23	−3.14	−3.05	−2.94	−2.84	−2.74	−2.62	−2.51	−2.39	−2.26	−2.13
1.2	−3.41	−3.37	−3.28	−3.17	−3.06	−2.93	−2.81	−2.69	−2.54	−2.40	−2.25	−2.09	−1.91
1.4	−3.48	−3.44	−3.33	−3.20	−3.08	−2.93	−2.78	−2.64	−2.46	−2.29	−2.11	−1.90	−1.69
1.6	−3.55	−3.50	−3.38	−3.24	−3.09	−2.92	−2.75	−2.58	−2.38	−2.18	−1.96	−1.71	−1.45
1.8	−3.62	−3.57	−3.43	−3.27	−3.11	−2.92	−2.72	−2.53	−2.30	−2.06	−1.80	−1.51	−1.20
2.0	−3.69	−3.63	−3.48	−3.30	−3.12	−2.92	−2.70	−2.48	−2.22	−1.94	−1.64	−1.30	−0.93
2.2	−3.76	−3.69	−3.53	−3.34	−3.14	−2.92	−2.68	−2.43	−2.13	−1.82	−1.47	−1.07	−0.62
2.4	−3.83	−3.76	−3.58	−3.38	−3.16	−2.92	−2.66	−2.38	−2.05	−1.69	−1.30	−0.83	−0.29
2.6	−3.90	−3.82	−3.64	−3.41	−3.18	−2.92	−2.64	−2.32	−1.96	−1.56	−1.11	−0.58	+0.05
2.8	−3.97	−3.89	−3.69	−3.45	−3.20	−2.92	−2.62	−2.27	−1.88	−1.43	−0.92	−0.31	+0.41
3.0	−4.04	−3.95	−3.74	−3.49	−3.22	−2.93	−2.60	−2.22	−1.79	−1.30	−0.72	−0.03	+0.80
4.0	−4.38	−4.28	−4.01	−3.71	−3.37	−2.98	−2.53	−2.00	−1.36	−0.58	+0.41	+1.69	+3.46
5.0	−4.71	−4.60	−4.30	−3.95	−3.55	−3.08	−2.52	−1.82	−0.95	+0.20	+1.78	+4.12	+7.93
6.0	−5.04	−4.92	−4.59	−4.21	−3.76	−3.22	−2.55	−1.69	−0.56	+1.03	+3.46	+7.65	+16.7
7.0	−5.36	−5.23	−4.88	−4.48	−3.99	−3.39	−2.63	−1.63	−0.23	+1.88	+5.48	+13.1	+41.0
8.0	−5.67	−5.54	−5.18	−4.75	−4.24	−3.59	−2.76	−1.62	+0.03	+2.71	+7.88	+22.4	+345
9.0	−5.97	−5.84	−5.47	−5.04	−4.50	−3.82	−2.93	−1.68	+0.20	+3.47	+10.7	+40.4	
10.0	−6.26	−6.13	−5.76	−5.32	−4.77	−4.07	−3.14	−1.81	+0.27	+4.10	+13.7	+88.2	
11.0	−6.55	−6.41	−6.04	−5.60	−5.05	−4.34	−3.38	−2.00	+0.23	+4.54	+16.8	+464	
12.0	−6.82	−6.69	−6.32	−5.88	−5.33	−4.62	−3.65	−2.24	+0.09	+4.77	+19.8		

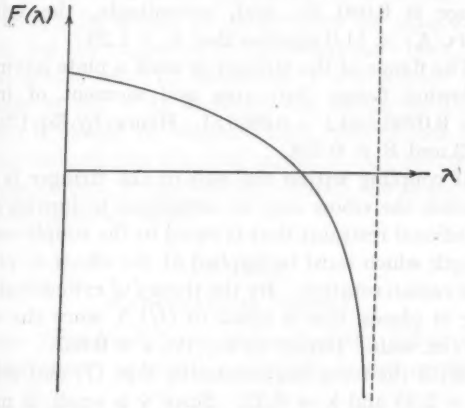

FIG. 2. Curve showing character of the function $F(\lambda)$.

since the object is to find the first intersection of the curve with the λ axis. In nearly all cases this intersection may be located with sufficient accuracy by a linear interpolation* between two computed points that lie on the curve on opposite sides of the λ axis. The procedure will be illustrated by some elementary examples.

EXAMPLE 1

All Edges Simply Supported

This condition is realized if the elastic rotational restraint is zero and the stiffness of the flange is infinite; i.e., $\kappa = 0$ and $A = \infty$. Eq. (4) is consistent with these conditions only if $h = 0$. If the plate becomes infinitely long, the sequence of values of γ becomes dense, and therefore λ is the smallest value for which h can vanish without restriction of γ. Inspection of Table 3 shows that this value of λ lies between 35 and 40, and, by linear interpolation, it is found that $\lambda = 39.3$; whence, by Eq. (3), $K = 3.60$.

If the plate is short, then Eq. (2) restricts γ to a set of discrete values. For example, if $a/b = 1.5$ and $m = 1$, Eq. (2) yields $\gamma = 4.38$. With this value of γ, the following values are interpolated from Table 3:

$$(\lambda = 45, h = -0.28), (\lambda = 50, h = 0.93)$$

Hence, by interpolation, it is found that h vanishes when $\lambda = 46.1$, and it follows from Eq. (3) that $K = 4.22$. Logically it should be shown that a larger value is obtained with $m = 2$, but it is intuitively evident that a plate with aspect ratio 1.5 buckles into a single lobe.

EXAMPLE 2

One Edge Simply Supported and the Other Edge Free

This condition is realized if the elastic rotational restraint is zero and the flange is absent; i.e., $\kappa = 0$ and $A = B = 0$. Then Eq. (4) becomes $F(\lambda) = (\lambda + g)/h = 0$, whence $\lambda + g = 0$. Inspection of Table 2 shows that the smaller the value of γ, the smaller is the value of λ that satisfies this equation. Hence, a plate with these edge conditions always buckles into a single lobe ($m = 1$). If γ is unrestricted (i.e., if the plate is infinitely long) the smallest solution of the equation $\lambda + g = 0$ is evidently $\lambda = 4.20$; whence, $K = 0.38$.

On the other hand, if, for example, $a/b = 1$, Eq. (2) yields $\gamma = 9.87$, and the solution of the equation $\lambda + g = 0$ evidently lies between 10 and 15. Interpolation of data from Table 2 yields:

$$(\lambda = 10, \lambda + g = -6.9), (\lambda = 15, \lambda + g = 2.1)$$

* Milne-Thompson has proposed a refinement of this method which rests upon Newton's general interpolation formula. See Milne-Thompson, L. M., *The Calculus of Finite Differences*, 1st Ed., p. 4; The Macmillan & Co. Ltd., London, 1933.

Hence, by interpolation, the expression $\lambda + g$ is found to vanish when $\lambda = 13.8$. It follows that $K = 1.27$.

Example 3

One Edge Clamped and the Other Edge Free

This condition is realized if the elastic rotational restraint is infinite and the flange is absent; i.e., $\kappa = \infty$ and $A = B = 0$. Then Eq. (4) becomes $F(\lambda) = -f/\gamma = 0$; whence, $f = 0$. It is seen from Table 1 that when γ is unrestricted, the smallest value of λ which satisfies this equation lies between 10 and 15. Interpolation of data from the table yields $\lambda = 12.6$. Thus, for an infinitely long plate, $K = 1.15$.

If, instead of an infinitely long plate, one considers a plate with aspect ratio a/b equal to π, the admissible values of γ are the squares of the integers; i.e., $\gamma = m^2$. For the values $\gamma = 1$, 4, and 9, the following solutions of the equation $f = 0$ are obtained by interpolation of data from Table 1:

$$\lambda_1 = 14.1,\ \lambda_2 = 12.6,\ \lambda_3 = 15.6$$

Thus, the smallest buckling stress is obtained with a two-loop mode for which the coefficient λ is 12.6. Since this is the same coefficient that was obtained for an infinitely long plate, it may be inferred that an extremely long plate breaks up into lobes whose complete wave lengths are approximately π times the width of the plate.

Approximate Algebraic Solution

If the data of Tables 1, 2, and 3 are plotted, it is seen that the functions f, g, and h are approximately linear in the range $\gamma < 1$. Coefficients determined by least-square adjustment of the data corresponding to $\gamma = 1$ furnish the following approximate expressions for the functions f and g:

$$f = -3.00 - 2.10\gamma + 0.270\lambda\gamma \qquad (5)$$
$$g = -4.20 - 1.90\gamma + 0.139\lambda\gamma$$

The function h may be roughly approximated by the first term in its MacLaurin expansion; i.e., $h = -3.00$. These linear formulas for the functions f, g, and h determine, with Eq. (4), a linear equation in λ which has the following solution:

$$\lambda = \frac{[A(\kappa + 3) + 1.90]\gamma + (2.10\kappa + 4.20) + 3\kappa/\gamma}{1 + B(\kappa + 3) + 0.139\gamma + 0.270\kappa} \qquad (6)$$

If the plate is short, the parameter γ is limited to a few discrete values, and the value that furnishes a minimum to λ is most quickly determined by trial. On the other hand, if the plate is long, the range of γ may be considered to be a continuum, and the minimum value of λ is obtained when γ has approximately the following value:

$$\gamma = \sqrt{3\kappa/[A(\kappa + 3) + 1.90]} \qquad (7)$$

This result is obtained by ignoring the term 0.139γ in the denominator of Eq. (6) and then equating the derivative to zero. Observe that γ is determined by Eq. (2) rather than by Eq. (7) if the plate is short.

Eqs. (6) and (7) are not always sufficiently accurate for engineering calculations, but, when γ is small (say $\gamma < 2.00$), these equations form a useful adjunct to the numerical methods described in the preceding section.

Example

Zee Stringer

As an example of the application of the preceding equations, it is proposed to ascertain if the outstanding flange of a 24S-T84 Zee-type stringer (Fig. 3) is stable when the stringer is subjected to 50,000 lbs. per sq.in. stress. An experimentally determined buckling curve for this material shows that the required stability exists only if the parameter $b/(t\sqrt{K})$ is less than 11.0. It seems reasonable and consistent with methods that have been successfully utilized for hat-stringer design[1] to measure the width b between the centroid of the elbow and the centroid of the lip. This dimension is indicated on Fig. 3 to be 1.00 in. The thickness of the flange is 0.080 in., and, accordingly, the criterion $b/(t\sqrt{K}) < 11.0$ signifies that $K > 1.29$.

The flange of the stringer is itself a plate having the following flange (lip) area and moment of inertia: $\omega = 0.0286$ and $I = 0.000151$. Hence, by Eq. (2), $A = 3.23$ and $B = 0.358$.

If coupling within the web of the stringer is disregarded, the elbow may be considered to furnish elastic rotational restraint that is equal to the couple per unit length which must be applied at the elbow to produce one radian rotation. By the theory of cylindrical bending of plates, this is equal to $D/1.5$, since the web is $1^1/_2$ in. wide. Hence, by Eq. (2), $\kappa = 0.667$.

With the foregoing constants, Eqs. (7) and (6) yield $\gamma = 0.38$ and $\lambda = 6.32$. Since γ is small, it may be expected that this result is fairly accurate.

More refined calculations may be based upon Eq. (4) and Tables 1, 2, and 3. The algebraic results indicate that γ lies in the neighborhood of the value 0.40

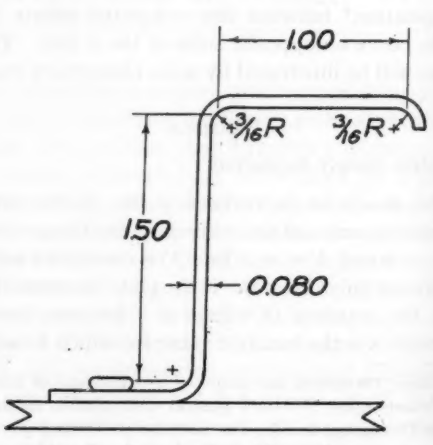

Fig. 3. Cross section of Zee stringer.

and that λ lies between 5 and 10. Hence, for any specified value of γ, the zero of $F(\lambda)$ may be determined by a linear interpolation between $F(5)$ and $F(10)$. Thus, the following values are obtained:

γ	0.2	0.4	0.6	0.42	0.38
λ	7.12	6.13	6.52	6.16	6.15

These results indicate that the minimum value of λ is approximately 6.13, and it follows that $K = 0.56$. Since it has been shown that the value $K = 1.29$ is required for stability, the flange is evidently improperly proportioned.

It is interesting to observe that if the lip is eliminated from the flange (i.e., $A = B = 0$), then a numerical analysis similar to the preceding shows that K is increased to 0.61. This demonstration that a lip is not invariably a stabilizing agent does not appear paradoxical if one considers that a lip in itself is a column with little inherent stability and that, consequently, an action may result in which the tendency for the lip to buckle actually reduces the stability of the combination.

No general inferences concerning the structural usefulness of a lip should be drawn from the present example, but the numerical methods that have been illustrated should serve to determine, in any specific case, whether or not a lip increases the stringer crippling stress. It should be observed that, even though a lip slightly reduces the crippling stress, it may effectively increase section properties that control the flexural or torsional buckling loads.

Appendix

Mathematical Theory

Since Timoshenko[1] has expounded the differential-equation theory of buckling of axially loaded rectangular plates, it suffices here to outline the course that has been followed.

The mathematical formulation of the problem requires the establishment of conditions under which the differential equation

$$\frac{\gamma^2}{m^4} w_{\xi\xi\xi\xi} + \frac{2\gamma}{m^2} w_{\xi\xi\eta\eta} + w_{\eta\eta\eta\eta} = -\frac{\lambda\gamma}{m^2} w_{\xi\xi} \tag{8}$$

has a nontrivial solution that conforms to the boundary conditions

$$(\gamma/m^2)w_{\xi\xi} + \nu w_{\eta\eta} = 0 \tag{9}$$

on the edges $\xi = 0$ and $\xi = \pi$;

$$w_{\eta\eta} + (\nu\gamma/m^2)w_{\xi\xi} = \kappa w_{\eta} \tag{10}$$

on the edge $\eta = 0$;

$$w_{\eta\eta\eta} + (2 - \nu)\frac{\gamma}{m^2} w_{\xi\xi\eta} = \frac{A\gamma^2}{m^4} w_{\xi\xi\xi} + \frac{B\lambda\gamma}{m^2} w_{\xi\xi} \tag{11}$$

on the edge $\eta = 1$.

In the derivation of Eq. (11), the torsional stiffness of the flange has been neglected.

It may be shown that the deflection function w must have the form

$$w = f(\eta) \sin m\xi \tag{12}$$

With Eq. (8) this relation yields an ordinary differential equation in η that has the general solution

$$f(\eta) = C_1 e^{\alpha\eta} + C_2 e^{-\alpha\eta} + C_3 \cos\beta\eta + C_4 \sin\beta\eta \tag{13}$$

in which

$$\alpha = \sqrt{\sqrt{\lambda\gamma} + \gamma}, \qquad \beta = \sqrt{\sqrt{\lambda\gamma} - \gamma} \tag{14}$$

The boundary conditions—Eqs. (9), (10), and (11)—furnish, with Eqs. (12) and (13), four linear, homogeneous, algebraic equations that admit nonzero values for the constants C_1, C_2, C_3, C_4 if, and only if, the determinant of the equations vanishes. The expansion of the determinant then yields a finite equation that can be expressed in the form of Eq. (4) when the functions f, g, and h have the following definitions:

$$\left.\begin{aligned} f &= \sqrt{\frac{\gamma}{\lambda}}\,\frac{[\lambda - (1-\nu)^2\gamma] + [\lambda + (1-\nu)^2\gamma]\cosh\alpha\cos\beta + \gamma[\lambda(1-2\nu) - \gamma(1-\nu)^2]\,\dfrac{\sinh\alpha}{\alpha}\dfrac{\sin\beta}{\beta}}{(\sinh\alpha/\alpha)\cos\beta - \cosh\alpha\,(\sin\beta/\beta)} \\ g &= -\lambda + \frac{(\alpha^2 - \nu\gamma)^2(\sinh\alpha/\alpha)\cos\beta - (\beta^2 + \nu\gamma)^2\cosh\alpha\,(\sin\beta/\beta)}{\gamma[(\sinh\alpha/\alpha)\cos\beta - \cosh\alpha\,(\sin\beta/\beta)]} \\ h &= \frac{2\sqrt{\lambda\gamma}\,(\sinh\alpha/\alpha)(\sin\beta/\beta)}{(\sinh\alpha/\alpha)\cos\beta - \cosh\alpha(\sin\beta/\beta)} \end{aligned}\right\} \tag{15}$$

Tabular values of these functions for the case $\nu = 0.30$ have been given in Tables 1, 2, and 3.

References

[1] Timoshenko, S., *Theory of Elastic Stability*, 1st Ed., pp. 337–350 and Fig. 185; McGraw-Hill Book Company, Inc., New York, 1936.

[2] Langhaar, H. L., *Design of Hat-Type Plate-Stringer Combinations*, Automotive and Aviation Industries, Vol. 91, No. 11, pp. 28–32, December 1, 1944.

Aileron Reversal Speed by Influence Coefficients and Matrix Iteration

WILLIAM T. THOMSON*
Ryan Aeronautical Company

ABSTRACT

Methods most frequently used in determining the aileron reversal speed are briefly reviewed. An alternative method of determining the reversal speed, making use of influence coefficients and matrix iteration, is presented.

INTRODUCTION

LOSS OF AILERON EFFECTIVENESS in developing roll results from the torsional flexibility of the wing. When an aileron is deflected downward, the increase in lift of the wing is partially compensated by the twisting of the wing resulting from the nose-down pitching torque. Since the torsional stiffness of the wing is independent of the speed, while the twisting torque increases as the square of the speed, it is evident that there is a critical speed at which the effect of the aileron will be completely canceled by the twisting of the wing, thereby resulting in a zero rolling moment. Beyond this critical speed the effect of the aileron will be the reverse of that for normal operation and, hence, the name "aileron reversal speed."

The aileron reversal speed is used as one of the design criteria of an airplane. In order to ensure sufficient aileron control at high speeds, present specifications require that the reversal speed exceed the maximum dive speed by at least 15 per cent. The reversal speed is also used in calculating the rolling performance of the airplane.

METHODS OF CALCULATION

Several methods are available for calculating the aileron reversal speed. The British use a method based on the semirigid theory developed by Pugsley[1] and Cox.[2] The equation for the reversal speed developed by Pugsley may be expressed as follows:

$$V_R = K\sqrt{m_\theta / {}^1/_2\rho s c^2}$$

where m_θ and c are the torsional stiffness and chord at the mid-aileron section; s is the semispan; ρ is the air density; and K is a constant depending on the aerodynamic coefficients determined by the wing-aileron configuration. Both the two- and three-dimensional cases are covered by the proper evaluation of K. For the three-dimensional case, Hirst's[3] simplified method can be used for evaluating K.

In the United States, a method presented by Shornick[4] of the Army Air Forces has been adopted. In this method the wing is divided into a number of rigid spanwise segments joined elastically. By assuming a mode of wing twist for the condition of zero rolling moment, the integral set up for the twisting of the wing is solved by tabular method and successive approximation. The aerodynamic coefficients used in Shornick's tabular form are for open-gap ailerons hinged at the leading edge, and modifications are necessary for aerodynamically balanced ailerons with seal.

In the following section a third method making use of influence coefficients and matrix iteration is suggested by the author. The procedure is analogous to Biot's[5] method of determining the wing divergence speed, and the equations reduce to that of divergence when $\beta = 0$. Both the open-gap aileron hinged at the leading edge and the aerodynamically balanced ailerons with seal are taken care of by the proper evaluation of the aerodynamic coefficients. These aerodynamic coefficients should be obtained from wind-tunnel data whenever possible; however, theoretical expressions reduced from Theodorsen[6] and Kussner[7] are presented in the Appendix.

DEVELOPMENT OF EQUATIONS

Consider a wing divided into n spanwise segments. Letting β be the aileron deflection and α the change in the torsional angle due to β, the increment of lift and pitching torque of any section produced by β can be written as

$$L_i = {}^1/_2\rho V^2 c_i(a_L\alpha_i + b_L\beta)\,\Delta x_i \qquad (1)$$

$$T_i = {}^1/_2\rho V^2 c_i^2(a_T\alpha_i + b_T\beta)\,\Delta x_i \qquad (2)$$

where a and b are aerodynamic coefficients depending on the wing-aileron configuration, and c_i the average chord of the ith section.

At the reversal speed the rolling moment obtained by summing up the lift times lever arm over both wings must vanish

$$M_R = 2\sum_{i=1}^{n} L_i x_i \Delta x_i = 0 \qquad (3)$$

which results in the following relation

Received August 17, 1945.

* Formerly Research Engineer in Charge of Vibration and Flutter Analysis. Now Associate Professor of Mechanics, University of Wisconsin.

$$\beta_R = -(a_L \sum_{i=1}^{n} c_i \alpha_i x_i \Delta x_i)/(b_L \sum_{i=s'}^{s''} c_i x_i \Delta x_i) \quad (4)$$

Eq. (4) assumes β to be constant over the aileron span, and, since $\beta = 0$ over the rest of the wing, the summation indicated in the denominator extends only over the aileron span.

Substituting Eq. (4) into Eq. (2), the twisting torque of the ith section at reversal may be expressed as

$$T_i = {}^1/_2\rho V^2 c_i^2 \{a_T \alpha_i - G \sum_{i=1}^{n} c_i \alpha_i x_i \Delta x_i\} \Delta x_i \quad (5)$$

where

$$G = a_L b_T / b_L \sum_{i=s'}^{s''} c_i x_i \Delta x_i \quad (6)$$

a constant depending only on the wing-aileron configuration.

The change in the angle of twist at any section k can be expressed in terms of the torsional influence coefficients ϕ_{ki} defined as the angle of twist at k due to a unit twisting torque at i.

$$\alpha_k = T_1\phi_{k1} + T_2\phi_{k2} + \ldots T_n\phi_{kn} = \sum_{i=1}^{n} T_i\phi_{ki} \quad (7)$$

Substituting Eq. (5) in Eq. (7)

$$\alpha_k = {}^1/_2\rho V^2 \sum_{i=1}^{n} c_i^2 \{a_T \alpha_i - G \sum_{i=1}^{n} c_i \alpha_i x_i \Delta x_i\} \phi_{ki} \Delta x_i \quad (8)$$

By expanding and rearranging, the above equation may be presented in the form

$$\alpha_k = {}^1/_2\rho V^2 \sum_{i=1}^{n} Q_{ki} \alpha_i \quad (9)$$

where

$$Q_{ki} = a_T c_i^2 \phi_{ki} \Delta x_i - G c_i x_i \Delta x_i \sum_{i=1}^{n} c_i^2 \phi_{ki} \Delta x_i \quad (10)$$

Eqs. (9) and (10) may be interpreted as follows. When $\beta = 0$, the second term of Eq. (10) vanishes and Eq. (9) reduces to that of divergence given by

$$\alpha_k = {}^1/_2\rho V^2 \sum_{i=1}^{n} a_T c_i^2 \phi_{ki} \Delta x_i \quad (11)$$

The second term of Eq. (10) is therefore the contribution due to the aileron deflection which alters the divergence speed determined from the set of equations expressed by Eq. (11).

The n equations represented by Eq. (9) will be satisfied by n values of V: however, only the lowest root corresponding to the lowest speed is of practical interest.

Solution by Matrix Iteration

The solution of the n equations indicated by Eq. (9) can be conveniently carried out by matrix iteration. Assuming a unit angle at the tip section, the n equations may be arranged in matrix form as follows

$$\frac{1}{{}^1/_2\rho V^2} \begin{vmatrix} \alpha_1 \\ \alpha_2 \\ \cdot \\ \cdot \\ \cdot \\ \alpha_n \end{vmatrix} = \begin{vmatrix} Q_{11}Q_{12} \ldots Q_{1n} \\ Q_{21}Q_{22} \ldots Q_{2n} \\ \cdot \\ \cdot \\ \cdot \\ Q_{n1}Q_{n2} \ldots Q_{nn} \end{vmatrix} \begin{vmatrix} \alpha_1 \\ \alpha_2 \\ \cdot \\ \cdot \\ \cdot \\ 1.0 \end{vmatrix} = \begin{vmatrix} a_1 \\ a_2 \\ \cdot \\ \cdot \\ \cdot \\ a_n \end{vmatrix} \quad (12)$$

where the operations to be performed are indicated by Eq. (9). Assuming any reasonable twist distribution with unit tip value, the column matrix obtained at the right side is normalized and compared to that on the left side. Using the new deflection mode so obtained, the process is repeated until the modes stabilize. Generally, three or four repetitions are sufficient because of the rapid convergence of the process.

The determination of the critical reversal speed is obvious by examination of Eq. (12). Taking the results of the final iteration

$$1/{}^1/_2\rho V^2 = a_n$$

the reversal speed is determined from

$$V_R = \sqrt{2/\rho a_n} \quad (13)$$

The matrix process will always result in the lowest mode, since the convergence to higher modes is possible only by additional constraint of the orthogonality principle.

Comments on Numerical Computation

The numerical computations may be carried out by the following procedure. Number the wing sections, starting with 1.0 at the root and ending with n at the tip. Because of the reciprocity theorem, the influence coefficients are symmetrical about the diagonal of the matrix—i.e., $\phi_{ki} = \phi_{ik}$. Also, ϕ_{ki} will be the same for all values of i greater than k, since the same torque is transmitted to section k when the torque is applied outboard of k. It is evident then that only n different values of ϕ appear in the matrix, all of which may be determined from a single test by applying the torque at the wing tip. Numerical values for Q_{ki} may then be determined by arranging the numbers in tabular form corresponding to the position in the matrix equation. Having set up the matrix equation, the iteration process may be carried out in a relatively short time with a computing machine.

The reversal speed is always lower than the divergence speed, since b_T is negative for the usual wing-aileron configuration. For aerodynamically balanced ailerons with seal, the coefficient b_T is considerably smaller than that of the open-gap aileron hinged at the leading edge, and the reversal speed approaches the divergence speed as b_T approaches zero. The divergence speed can be determined from Eq. (11) in matrix form.

Appendix

Theoretical expressions for the aerodynamic coefficients of Eqs. (1) and (2) are given for two types of ailerons.

Type I Aileron

Open gap hinged at leading edge

$$a_L = 2\pi$$
$$b_L = 2T_{10}$$
$$a_T = \pi(1/2 + a)$$
$$b_T = T_{10}(1/2 + a) - [(T_4 + T_{10})/2]$$

Type II Aileron

Aerodynamically balanced with seal

$$a_L = 2\pi$$
$$b_L = 2[T_{10} - (c - e)\varphi_{12}]$$
$$a_T = \pi(1/2 + a)$$
$$b_T = [T_{10} - (c - e)\varphi_{12}]\left(\frac{1}{2} + a\right) - \left[\frac{T_4 + T_{10}}{2} + (c - e)\varphi_{15}\right]$$

where

e = distance from mid-chord of wing to leading edge of aileron as a fraction of the semichord of wing

a = distance from mid-chord of wing to elastic axis of wing as a fraction of the semichord of wing (positive if elastic axis is aft of mid-chord)

c = distance from mid-chord of wing to aileron hinge as fraction of semichord of wing

These coefficients may be calculated by referring to Figs. 1, 2, and 3.

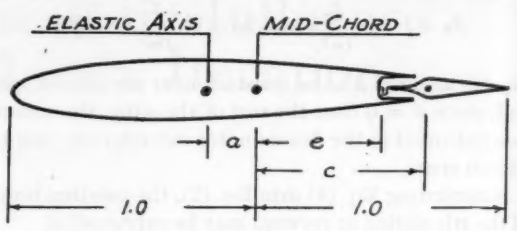

Fig. 1.

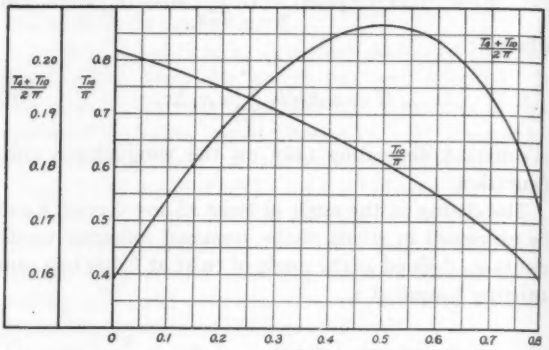

Fig. 2.

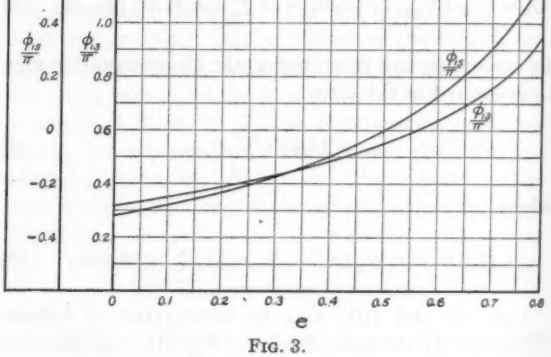

Fig. 3.

References

[1] Pugsley, A. G., *Aerodynamic Characteristics of a Semi-Rigid Wing*, R. & M. No. 1490, June, 1932.

[2] Cox, H. R., and Pugsley, A. G., *Theory of Loss of Lateral Control Due to Wing Twisting*, R. & M. No. 1506, October, 1932.

[3] Hirst, D. M., *Calculation of the Critical Reversal Speeds of Wings*, R. & M. No. 1567, September, 1933.

[4] Shornick, L. H., *The Computation of the Critical Speed of Aileron Reversal, Wing Torsional Divergence, and Wing-Aileron Divergence*, A.A.F. Material Center, Engineering Division Memorandum Report, Eng. M 51/vF18. Add. 1, December, 1942.

[5] Biot, M. A., *Flutter Analysis of Wing Carrying Large Concentrated Weights*, GALCIT Report No. 1A, January, 1942.

[6] Theodorsen, T., *General Theory of Aerodynamic Instability & Mechanism of Flutter*, N.A.C.A. Report No. 496, 1934.

[7] Kussner, H. G., and Schwarz, I., *The Oscillating Wing with Aerodynamically Balanced Elevators*, N.A.C.A. T.M. No. 991, October, 1941.

[8] Flax, A. H., *The Influence of Structural Deformation on Airplane Characteristics*, Journal of the Aeronautical Sciences, Vol. 12, No. 1, January, 1945.

A Method for the Stress Analysis of Helicopter Blades

DANIEL O. DOMMASCH*

Civil Aeronautics Administration

ABSTRACT

The method of analysis presented herein is applicable to both fixed and hinged rotors. Although the equations developed apply directly to rectangular blades, the method may be extended to cover blades having other shapes.[4]

Up to this time, no "exact" general solution has been found for even the simplest form of the differential equation governing rotor bending moments, although solutions can be determined for certain combinations of constants (these solutions are not general). Because of the lack of a general exact solution, various approximate methods such as series, perturbation methods, etc., were tried, but convergence was poor in most cases, necessitating the use of an unwieldy number of terms.

The solution presented in this paper is based on the method of finite differences and depends on the evaluation of a number of simultaneous linear equations. The method leads to a rapid determination of the bending moment at any point on the blade.

SYMBOLS

E = Young's modulus (lbs. per sq.in.)
I = moment of Inertia (in.^{4})
A = cross-section Area of Blade (sq.in.)
w = unit weight (lbs. per in.^{3})
g = 386 in. per sec.^{2}
ω = rotational velocity (rad. per sec.)
C.F. = centrifugal force
dm = differential mass
ϑ = cone angle
Z = axis of rotation
r = axis normal to Z
ξ = undeflected blade axis
ζ = axis normal to ξ
S = length of blade
P = axial load
S_s = shear
M = moment
u, v = running coordinates
B = $(Aw/g)\omega^2 \cos\vartheta$, (lbs. per sq.in.)
C = $\frac{1}{EI}\left(\frac{w_s}{6S} - \frac{B\sin\vartheta}{6}\right)$, (1/in.^{4})
M_d = hinge damping moment
D = $B\cos\vartheta/EI$, (1/in.^{4})
w_s = tip loading (lbs. per in.)
x = (ξ/S)
φ = $d\zeta/d\xi$
B.C. = boundary conditions
F = $w_s/12EI\,S^2$, (1/in.^{3})
G = $B\sin\vartheta/6EI$, (1/in.^{4})
α = $3CS^4$
β = $DS^4/2$
γ = $4FS^3$
λ = $3GS^4$
$f(a)$ = value of function at a
f_a' = first derivative of f relative to x
η = $S^3 nAw/EI$
n = load factor

Received July 23, 1945.

* Aeronautical Engineer.

INTRODUCTION

THE EQUATIONS DEVELOPED BELOW hold for blades of rectangular plan form; the development for other plan forms follow the same general outline.[4] At this point it is noted that the assumption normally made in beam theory that $EId^2\zeta/d\xi^2 = M$, is also made here. This assumption implies small deflections and negligible lengthening of the blade under load. Because of the small deflection notion, the angle for freely hinged blades must be chosen carefully (see Eq. 24).

In applying this method, certain preliminary work is required, namely:

(1) Determine the blade principal axes.

(2) Resolve the air load relative to these axes (the total thrust may be assumed to cause bending about the principal axis of minimum inertia).

In line with the assumption generally made in propeller analysis, only the air load normal to the principal axis of minimum inertia need be assumed as acting.[1]

Derivation of the Differential Equation

Referring to Fig. 1 and terminology:

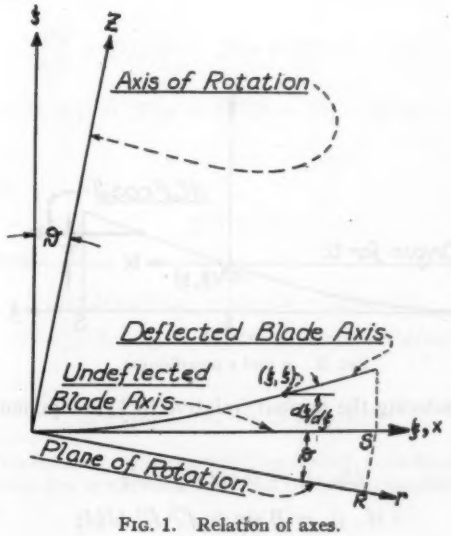

FIG. 1. Relation of axes.

$$dm = (Aw/g)d\xi$$
$$d\text{C.F.} = r\omega^2 dm$$
$$d\text{C.F.} = (Aw/g)r\omega^2 d\xi$$

Let $B = (Aw/g)\omega^2 \cos\vartheta$, then, since $r = \xi\cos\vartheta$, we have:

$$d\text{C.F.} = B\xi d\xi$$

At any point ξ, the total C.F. is

$$\text{C.F.}\xi = B\int_S^\xi \xi d\xi = B/2(\xi^2 - S^2) \qquad (1)$$

where the negative value of C.F. is due to the point S being the origin of integration.

Moment Due to C.F. About Any Point

To determine the moment about the point (ξ, ζ) due to C.F., the C.F. may be broken into components normal to and parallel to the ξ axis. (See Fig. 2.)

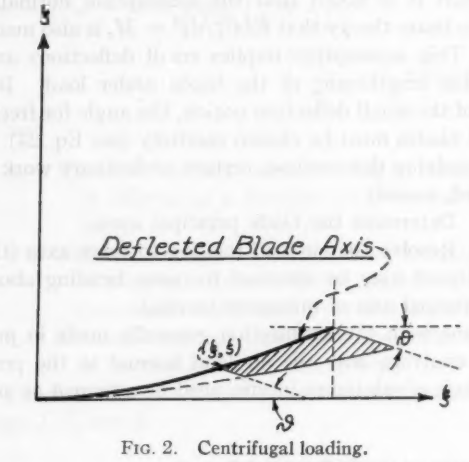

Fig. 2. Centrifugal loading.

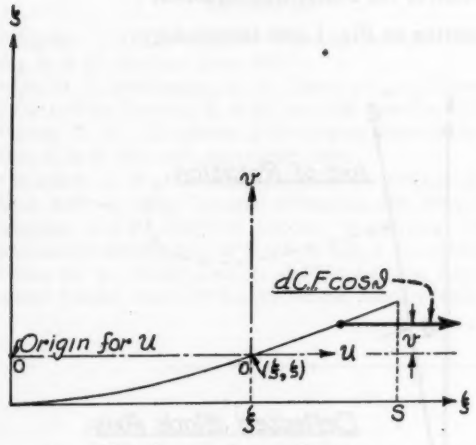

Fig. 3. u and v coordinates.

Considering the normal (relative to ξ) component of C.F.,

$$(S_{\xi,\,0})_v = B\sin\vartheta\int_S^\xi \xi d\xi$$
$$(M_{\xi,\,0})_v = B\sin\vartheta\int_S^\xi\int_S^\xi \xi d\xi d\xi$$

$$(S_{\xi,\,0})_v = (B\sin\vartheta/2)(\xi^2 - S^2) \qquad (2)$$
$$(M_{\xi,\,0})_v = (B\sin\vartheta/6)(2S^3 + \xi^3 - 3S^2\xi) \qquad (3)$$

Considering now the parallel component of C.F.

$$P = \text{axial load} = \text{C.F.}\cos\vartheta = (B\cos\vartheta/2)(\xi^2 - S^2) \qquad (4)$$

Moment about (ξ, ζ) of dC.F. $\cos\vartheta$ is (see Fig. 3):

$$dM_h = d\text{C.F.}\cos\vartheta(v)$$

but in terms of u and v, dC.F. $= Budu$, hence:

$$dM_h = B\cos\vartheta\, vudu$$
$$M_h = B\cos\vartheta\int_S^\xi vudu \qquad (5)$$

Moment Due to Air Load

The moment due to a known air-load distribution may readily be found. Depending on the down-wash distribution, blade twist, etc., the air loading may vary from an approximately triangular distribution to some nth degree parabolic distribution or may be defined by a trigonometric or power series. Two simple cases are considered here: (1) triangular and (2) second degree parabolic.

(1) *Triangular Distribution (See Fig. 4)*

If tip load $= w_s$, then $w_\xi = (w_s/S)\xi$, and

$$S_A = \frac{w_s}{S}\int_S^\xi \xi d\xi = \frac{w_s}{2S}(\xi^2 - S^2) \qquad (6)$$

$$M_A = \frac{w_s}{S}\int_S^\xi\int_S^\xi \xi d\xi d\xi = \frac{w_s}{6S}(2S^3 + \xi^3 - 3S^2\xi) \qquad (7)$$

(2) *Parabolic Distribution*

Again let w_s = tip load, then $w_\xi = (w_s/S^2)\xi^2$, and

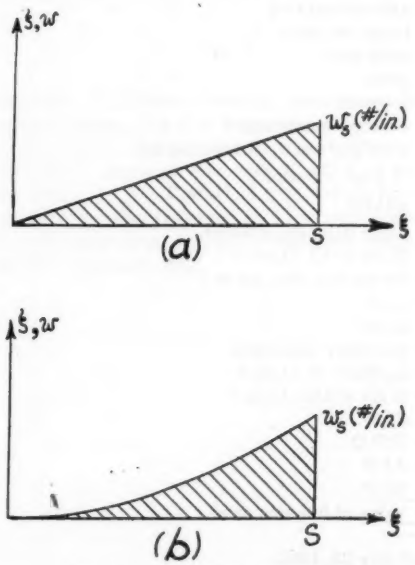

Fig. 4. Air loadings considered.

$$S_A = \frac{w_s}{S^2}\int_S^\xi \xi^2 d\xi = \frac{w_s}{3S^2}(\xi^3 - S^3) \quad (6a)$$

$$M_A = \frac{w_s}{S^2}\int_S^\xi\int_S^\xi \xi^2 d\xi d\xi = \frac{w_s}{12S^2}(3S^4 + \xi^4 - 4S^3\xi) \quad (7a)$$

Total Moment

(1) *Triangular Air-Load Distribution*

$$M_{\xi,\,\zeta} = -(3) + (5) + (7)$$

$$M = \left(\frac{w_s}{6S} - \frac{B\sin\vartheta}{6}\right)(2S^3 + \xi^3 - 3S^2\xi) + B\cos\vartheta\int_S^\xi vdu \quad (8)$$

Since $M/EI = (d^2\zeta/d\xi^2)$, we have

$$\frac{d^2\zeta}{d\xi^2} = \frac{1}{EI}\left(\frac{w_s}{6S} - \frac{B\sin\vartheta}{6}\right)(2S^3 + \xi^3 - 3S^2\xi) + \frac{B\cos\vartheta}{EI}\int_S^\xi vdu \quad (9)$$

Let

$$C = \frac{1}{EI}\left(\frac{w_s}{6S} - \frac{B\sin\vartheta}{6}\right) \quad (10)$$

$$D = \frac{B\cos\vartheta}{EI} \quad (11)$$

Then:

$$\frac{d^2\zeta}{d\xi^2} = C(2S^3 + \xi^3 - 3S^2\xi) + D\int_S^\xi vdu \quad (12)$$

(2) *Parabolic Air-Load Distribution*

$$M = -(3) + (5) + (7a)$$

$$M = \frac{w_s}{12S^2}(3S^4 + \xi^4 - 4S^3\xi) - \frac{B\sin\vartheta}{6}\times(2S^3 + \xi^3 - 3S^2\xi) + B\cos\vartheta\int_S^\xi vdu \quad (8a)$$

$$\frac{d^2\zeta}{d\xi^2} = \frac{w_s}{12EIS^2}(3S^4 + \xi^4 - 4S^3\xi) - \frac{B\sin\vartheta}{6EI}(2S^3 + \xi^3 - 3S^2\xi) + \frac{B\cos\vartheta}{EI}\int_S^\xi vdu \quad (9a)$$

Let

$$F = w_s/(12EIS^2);\ G = \frac{B\sin\vartheta}{6EI} \quad (10a)$$

Then:

$$\frac{d^2\zeta}{d\xi^2} = F(3S^4 + \xi^4 - 4S^3\xi) - G(2S^3 + \xi^3 - 3S^2\xi) + D\int_S^\xi vdu \quad (12a)$$

Transformation

Prior to reduction of Eqs. (12) and (12a), note that the B.C. are as follows:

(A) *Fixed Blades*

$$\zeta(0) = \zeta_\xi'(0) = \zeta_\xi''(0) = 0$$

(B) *Hinged Blades*

$$\zeta(0) = \zeta_\xi''(0) = \zeta_\xi''(S) = 0$$

no hinge damping.

$$\zeta(0) = \zeta_\xi''(S) = 0;\ \xi_\xi''(0) = M_d/EI$$

with hinge damping.

Eqs. (12) and (12a) may be simplified by considering the following:[2]

$$\frac{d}{d\xi}\int_S^\xi vudu = \int_S^\xi \frac{d}{d\xi}(vu)du + [v(\xi)\xi]\frac{d\xi}{d\xi} - [v(S)\xi]\frac{dS}{d\xi}$$

Now: $v = \zeta(u) - \zeta(\xi)$. Hence, $v(\xi) = \zeta(\xi) - \zeta(\xi) = 0$; also, $dS/d\xi = 0$, since S is constant.

Since u does not depend on ξ,

$$(d/d\xi)(vu)du = udu(dv/d\xi)$$

$$dv/d\xi = d[\zeta(u) - \zeta(\xi)]/d\xi = -d\zeta/d\xi$$

Hence,

$$\frac{d}{d\xi}\int_S^\xi vudu = -\frac{d\zeta}{d\xi}\int_S^\xi udu = -\left(\frac{d\zeta}{d\xi}\right)\tfrac{1}{2}(\xi^2 - S^2) \quad (13)^*$$

Making use of Eq. (13) and differentiating Eqs. (12) and (12a), one obtains:

$$\frac{d^3\zeta}{d\xi^3} = 3C(\xi^2 - S^2) - D/2(\xi^2 - S^2)\frac{d\zeta}{d\xi} \quad (14)$$

$$\frac{d^3\zeta}{d\xi^3} = 4F(\xi^3 - S^3) - 3G(\xi^2 - S^2) - D/2(\xi^2 - S^2)\frac{d\zeta}{d\xi} \quad (14a)$$

Let

$$\varphi = d\zeta/d\xi \quad (15)$$

Then:

$$\frac{d^2\varphi}{d\xi^2} + D/2(\xi^2 - S^2)\varphi = 3C(\xi^2 - S^2) \quad (16)$$

$$\frac{d^2\varphi}{d\xi^2} + D/2(\xi^2 - S^2)\varphi = 4F(\xi^3 - S^3) - 3G(\xi^2 - S^2) \quad (16a)$$

Let

$$\xi/S = x \quad (17)$$

Note:

$$(d\varphi/d\xi)(d\xi/dx) = d\varphi/dx = S(d\varphi/d\xi)$$

$$(d/dx)S(d\varphi/d\xi) = (d/dx)(d\varphi/dx) = d^2\varphi/dx^2$$

But

$$S(d/dx)(d\varphi/d\xi) = S^2(d^2\varphi/d\xi^2)$$

---

* This equation, when multiplied by $B\cos\vartheta$, gives the equivalent shear due to the centrifugal load component parallel to the ξ axis.

Hence,

$$(d^2\varphi/dx^2)(1/S^2) = d^2\varphi/d\xi^2 \tag{18}$$

Let

$$\varphi'' = d^2\varphi/dx^2 \tag{19}$$

Then Eqs. (16) and (16a) become

$$\varphi'' + (DS^4/2)(x^2 - 1)\varphi = 3CS^4(x^2 - 1) \tag{20}$$

$$\varphi'' + (DS^4/2)(x^2 - 1)\varphi = 4FS^5(x^3 - 1) - 3GS^4(x^2 - 1) \tag{20a}$$

Finally, let

$$\left.\begin{aligned} \beta &= DS^4/2, \quad \gamma = 4FS^5 \\ \alpha &= 3CS^4, \quad \lambda = 3GS^4 \end{aligned}\right\} \tag{21}$$

And Eqs. (20) and (20a) become

$$\varphi'' + \beta(x^2 - 1)\varphi = \alpha(x^2 - 1) \tag{22}$$

$$\varphi'' + \beta(x^2 - 1)\varphi = \gamma(x^3 - 1) - \lambda(x^2 - 1) \tag{22a}$$

The B.C. on $\varphi(x)$ are:

(A) Fixed Blades

$$\varphi(0) = \varphi'(1) = 0$$

(B) Hinged Blades

$$\varphi'(0) = \varphi'(1) = 0$$

no hinge moment.

$$\varphi'(0) = SM_d/EI; \quad \varphi'(1) = 0$$

with hinge damping.

Note that

$$M = EI\frac{d^2\zeta}{d\xi^2} = EI\frac{d\varphi}{d\xi} = \frac{EI}{S}\frac{d\varphi}{dx} \tag{23}$$

Also

$$\varphi = d\zeta/d\xi; \quad \zeta = \int_0^\xi \varphi\, d\xi = S\int_0^x \varphi\, dx$$

At this point it is noted that the angle ϑ is given for fixed blades as the initial dihedral angle (if any); for freely hinged blades, ϑ is determined by the condition that the moment at the root must be zero. The angle, ϑ, which satisfies this condition is given by Eqs. (24) and (24a).

(1) Triangular Loading

$$\sin 2\vartheta = 2gw_s/SwA\omega^2 \tag{24}$$

(2) Parabolic Loading

$$\sin 2\vartheta = {}^3/_2(w_s g/SwA\omega^2) \tag{24a}$$

It is interesting to note that Eq. (24) automatically gives zero bending over the entire blade. This follows from the fact that the assumed air-load distribution in this case is geometrically similar to the distribution of centrifugal load and it is possible for the blade to align itself with the total load resultant without flexure.

Development of Finite Difference Equations[3]

A number of methods were tried in an effort to determine an "exact" solution to Eqs. (22) and (22a). However, except for the fictitious case of $\beta = -1$ (implies negative dihedral, very stiff rotor), none was found. Series solutions were found but the convergence was generally considered too poor in the working range of β to make the series solution of practical interest.

As a consequence, the method of finite differences was tried, and it was found that this method gave accurate results with minimum labor.

As an aid to those not acquainted with difference solutions of differential equations, the development of the difference equations is outlined below. (See Fig. 5.)

The slope at the point φ_n for any continuous function $\varphi(x)$ may be presented by

$$\varphi_n' = (\Delta\varphi/\Delta x)_n \cong (\varphi_{n+1} - \varphi_{n-1})/2\,\Delta x \tag{25}$$

The rate of change of slope, $\Delta^2\varphi/\Delta x^2$, is then expressed:

Table 1

1 Point	2 x	3 x^2	4 $x^2 - 1$	5 ④ × Δx^2	6 $-\alpha \times$ ⑤ $\times 10^3$	7 $-\beta \times$ ⑤	8 ⑦ − 2
0	0	0	−1.0000	−0.00250000	5.00000	0.1750000	−2.1750000
1	0.05	0.0025	−0.9975	−0.00249375	4.98750	0.1745625	−2.1745625
2	0.10	0.0100	−0.9900	−0.00247500	4.95000	0.1732500	−2.1732500
3	0.15	0.0225	−0.9775	−0.00244375	4.88750	0.1710625	−2.1710625
4	0.20	0.0400	−0.9600	−0.00240000	4.80000	0.1680000	−2.1680000
5	0.25	0.0625	−0.9375	−0.00234375	4.68750	0.1640625	−2.1640625
6	0.30	0.0900	−0.9100	−0.00227500	4.55000	0.1592500	−2.1592500
7	0.35	0.1225	−0.8775	−0.00219375	4.38750	0.1535625	−2.1535625
8	0.40	0.1600	−0.8400	−0.00210000	4.20000	0.1470000	−2.1470000
9	0.45	0.2025	−0.7975	−0.00199375	3.98750	0.1395625	−2.1395625
10	0.50	0.2500	−0.7500	−0.00187500	3.75000	0.1312500	−2.1312500
11	0.55	0.3025	−0.6975	−0.00174375	3.48750	0.1220625	−2.1220625
12	0.60	0.3600	−0.6400	−0.00160000	3.20000	0.1120000	−2.1120000
13	0.65	0.4225	−0.5775	−0.00144375	2.88750	0.1010625	−2.1010625
14	0.70	0.4900	−0.5100	−0.00127500	2.55000	0.0892500	−2.0892500
15	0.75	0.5625	−0.4375	−0.00109375	2.18750	0.0765625	−2.0765625
16	0.80	0.6400	−0.3600	−0.00090000	1.80000	0.0630000	−2.0630000
17	0.85	0.7225	−0.2775	−0.00069375	1.38750	0.0485625	−2.0485625
18	0.90	0.8100	−0.1900	−0.00047500	0.95000	0.0332500	−2.0332500
19	0.95	0.9025	−0.0975	−0.00024375	0.4875	0.0170625	−2.0170625
20	1.00	1.0000	0.0000	0.00000000	0	0	0

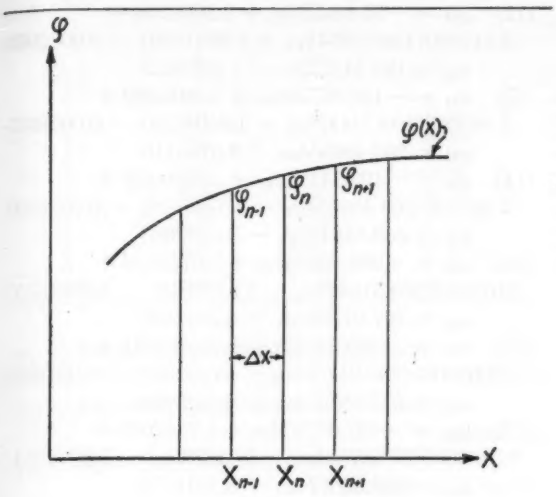

FIG. 5.

$$\varphi_n'' = \left(\frac{\Delta^2\varphi}{\Delta x^2}\right)_n \cong \left(\frac{\varphi_{n+1} - \varphi_n}{\Delta x} - \frac{\varphi_n - \varphi_{n-1}}{\Delta x}\right)/x\Delta$$

$$(\Delta^2\varphi/\Delta x^2)_n = (\varphi_{n+1} - 2\varphi_n + \varphi_{n-1})/\Delta x^2 \qquad (26)$$

As $\Delta x \to 0$, Eqs. (25) and (26) approach the exact derivatives; however, for a continuous function without singularity, even large values of Δx give excellent approximations to the exact solution.

Noting that $\varphi'' \cong \Delta^2\varphi/\Delta x^2$, Eqs. (22) and (22a) may be written:

$$\varphi_{n+1} + \varphi_{n-1} + \varphi_n[\beta\Delta x^2(x^2 - 1) - 2] = \alpha\Delta x^2(x^2 - 1) \qquad (27)$$

$$\varphi_{n+1} + \varphi_{n-1} + \varphi_n[\beta\Delta x^2(x^2 - 1) - 2] = \gamma\Delta x^2(x^3 - 1) - \lambda\Delta x^2(x^2 - 1) \qquad (27a)$$

The method of solving these equations is illustrated below by means of three related problems.

ILLUSTRATIVE EXAMPLES

Consider the following rotor blade.

$S = 20$ ft. $= 240$ in.
chord $= 2$ ft. $= 24$ in.
thickness (maximum) $= 15$ per cent $C = 3.6$ in. $= b$
$A^1 = 0.74\,bh = 0.74(3.6)(24) = 63.94$ sq.in.
$I^1 = 0.0472\,bh^3 = 0.0472(24)(3.6)^3 = 52.85$ in.^{4}
Solid wood construction, $E = 1{,}500{,}000$ lbs. per sq.in.
$w_s = 700$ lbs. per ft. $= 58.2$ lbs. per in. (assumed)
$w = 0.60(62.4) = 37.44$ lbs. per ft.$^3 = 0.0216$ lbs. per in.^{3}
$g = 32.2(12) = 386$ in. per sec.^{2}
$w_s/S = 58.2/240 = 0.242$ lbs. per sq.in. (may vary from 0 to 0.25 approximately)
$\omega = 300$ r.p.m./60 $(2\pi) \cong 30$ rad. per sec.
$\omega^2 = 900$
$\sin 2\vartheta$(0 to 0.5); ϑ, 0° to 15°

$$B = \frac{Aw}{g}\omega^2\cos\vartheta \cong \frac{(63.94)(0.0216)}{386.0}(900)(1) = 3.22$$

lbs. per sq.in.

$$C = (1/EI)[(w_s/6S) - (B\sin\vartheta/6)]$$

$$\frac{1}{EI} = \frac{1}{(1.5)(5.285)} \times 10^{-7} = 0.1261 \times 10^{-7}$$

Since w_s/S may vary from 0 to 0.25 and $B\sin\vartheta$ from 0 to 0.483 (approximately 0.5),

C ranges from $+0.53 \times 10^{-9}$ to -1.1×10^{-9}, 1/in.^{4}

$$D = \frac{B\cos\vartheta}{EI} = 3.22(1)(0.1261)(10^{-7}) = 40.6 \times 10^{-9}$$

$\alpha = 3CS^4$; $S^4 = (2.40)^4 \times 10^8 = 33.20 \times 10^8$
$\alpha = +1.76$ to -3.65

$$\beta = \frac{DS^4}{2} = \frac{40.6}{2} \times 10^{-9} \times 3.32 \times 10^9 = 67.4$$

For a hinged blade:

$$\vartheta = \text{arc sin } (0.242/3.22) = \text{arc sin } 0.0752 = 4°\,19'$$

Example 1

It is desired to determine the bending moment in a fixed blade having $\beta = 70$, $\alpha = 2$, and loaded by a triangular air-load distribution.

The quantities $[\alpha(\Delta x^2)(x^2 - 1)]$ and $[\beta(\Delta x^2) \times (x^2 - 1) - 2]$ are calculated below for $\Delta x = 0.05$.

From Table 1 and Eq. (27), the following set of linear equations is obtained.

(1) $\varphi_2 + \varphi_0 - 2.174563\varphi_1 = -0.00498750$
(2) $\varphi_3 + \varphi_1 - 2.173250\varphi_2 = -0.00495000$
(3) $\varphi_4 + \varphi_2 - 2.171063\varphi_3 = -0.00488750$

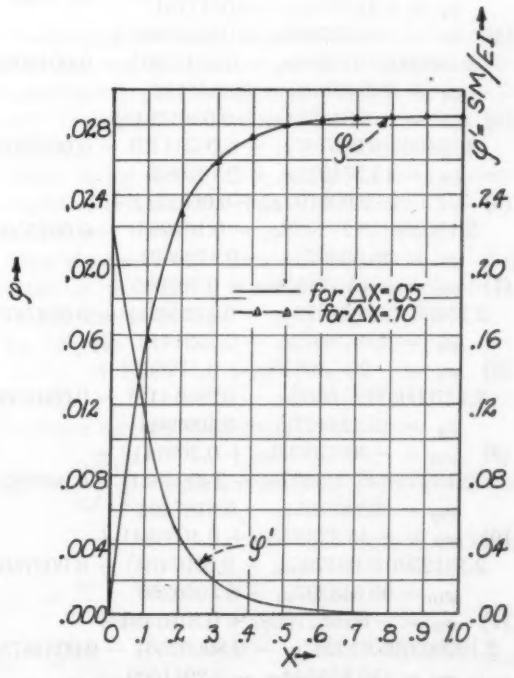

FIG. 6. Curves showing relation between φ and x and φ' and x.

$$
\begin{aligned}
&(4)\ \varphi_5 + \varphi_3 - 2.168000\varphi_4 = -0.00480000\\
&(5)\ \varphi_6 + \varphi_4 - 2.164063\varphi_5 = -0.00468750\\
&(6)\ \varphi_7 + \varphi_5 - 2.159250\varphi_6 = -0.00455000\\
&(7)\ \varphi_8 + \varphi_6 - 2.153563\varphi_7 = -0.00438750\\
&(8)\ \varphi_9 + \varphi_7 - 2.147000\varphi_8 = -0.00442000\\
&(9)\ \varphi_{10} + \varphi_8 - 2.139563\varphi_9 = -0.00398750\\
&(10)\ \varphi_{11} + \varphi_9 - 2.131250\varphi_{10} = -0.00375000\\
&(11)\ \varphi_{12} + \varphi_{10} - 2.122063\varphi_{11} = -0.00348750\\
&(12)\ \varphi_{13} + \varphi_{11} - 2.112000\varphi_{12} = -0.00320000\\
&(13)\ \varphi_{14} + \varphi_{12} - 2.101063\varphi_{13} = -0.00288750\\
&(14)\ \varphi_{15} + \varphi_{13} - 2.089250\varphi_{14} = -0.00255000\\
&(15)\ \varphi_{16} + \varphi_{14} - 2.076563\varphi_{15} = -0.00218750\\
&(16)\ \varphi_{17} + \varphi_{15} - 2.063000\varphi_{16} = -0.00180000\\
&(17)\ \varphi_{18} + \varphi_{16} - 2.048563\varphi_{17} = -0.00138750\\
&(18)\ \varphi_{19} + \varphi_{17} - 2.033250\varphi_{18} = -0.00095000\\
&(19)\ \varphi_{20} + \varphi_{18} - 2.017063\varphi_{19} = -0.00048750\\
&(20)\ \varphi_{21} + \varphi_{19} - 2\varphi_{20} = 0
\end{aligned}
$$

The B.C. are $\varphi(0) = 0;\ \varphi' = 0$

$$\varphi(0) = 0 \rightarrow \varphi_0 = 0$$

$$\varphi'(1) = 0 \rightarrow (\varphi_{21} - \varphi_{19})/2\,\Delta x = 0$$

$$\varphi_{21} = \varphi_{19}$$

Eq. (20) gives $2\varphi_{19} - 2\varphi_{20} = 0$; or $\varphi_{19} = \varphi_{20}$.

The above system of equations is easily solved as follows:

$$
\begin{aligned}
&(1)\ \varphi_2 = 2.174563\varphi_1 - 0.0049875\\
&(2)\ \varphi_3 = -\varphi_1 + 2.173250(2.174563\varphi_1 - 0.0049875) - 0.0049500\\
&\qquad \varphi_3 = 3.725869\varphi_1 - 0.0157891\\
&(3)\ \varphi_4 = -2.174563\varphi_1 + 0.0049875 + 2.171063(3.725869\varphi_1 - 0.0157891) - 0.00488750\\
&\qquad \varphi_4 = 5.914514\varphi_1 - 0.0341791\\
&(4)\ \varphi_5 = -3.725869\varphi_1 + 0.0157891 + 2.168000(5.914514\varphi_1 - 0.0341791) - 0.0048000\\
&\qquad \varphi_5 = 9.096797\varphi_1 - 0.0631112\\
&(5)\ \varphi_6 = -5.914514\varphi_1 + 0.0341791 + 2.164063(9.096797\varphi_1 - 0.0631112) - 0.0046875\\
&\qquad \varphi_6 = 13.771528\varphi_1 - 0.107085\\
&(6)\ \varphi_7 = -9.096797\varphi_1 + 0.0631112 + 2.159250(13.771528\varphi_1 - 0.107085) - 0.0045500\\
&\qquad \varphi_7 = 20.639375\varphi_1 - 0.1726621\\
&(7)\ \varphi_8 = -13.771528\varphi_1 + 0.107085 + 2.153563(20.639375\varphi_1 - 0.1726621) - 0.0043875\\
&\qquad \varphi_8 = 30.676666\varphi_1 - 0.2691412\\
&(8)\ \varphi_9 = -20.639375\varphi_1 + 0.1726621 + 2.147000(30.676666\varphi_1 - 0.2691412) - 0.0042000\\
&\qquad \varphi_9 = 45.223427\varphi_1 - 0.4093841\\
&(9)\ \varphi_{10} = -30.676666\varphi_1 + 0.2691412 + 2.139563(45.223427\varphi_1 - 0.4093841) - 0.0039875\\
&\qquad \varphi_{10} = 66.081705\varphi_1 - 0.6107494\\
&(10)\ \varphi_{11} = -45.223427\varphi_1 + 0.4093841 + 2.131250(66.081705\varphi_1 - 0.6107494) - 0.0037500\\
&\qquad \varphi_{11} = 95.613207\varphi_1 - 0.8960256\\
&(11)\ \varphi_{12} = -66.081705\varphi_1 + 0.6107494 + 2.122063(95.613207\varphi_1 - 0.8960256) - 0.00348750\\
&\qquad \varphi_{12} = 136.815544\varphi_1 - 1.2941609\\
&(12)\ \varphi_{13} = -95.613207\varphi_1 + 0.8960256 + 2.112000(136.815544\varphi_1 - 1.2941609) - 0.0032000\\
&\qquad \varphi_{13} = 193.341222\varphi_1 - 1.8404422\\
&(13)\ \varphi_{14} = -136.815544\varphi_1 + 1.2941609 + 2.101063(193.341222\varphi_1 - 1.8404422) - 0.0028875\\
&\qquad \varphi_{14} = 269.406554\varphi_1 - 2.5756116\\
&(14)\ \varphi_{15} = -193.341222\varphi_1 + 1.8404422 + 2.089250(269.406554\varphi_1 - 2.5756116) - 0.0025500\\
&\qquad \varphi_{15} = 369.516421\varphi_1 - 3.5432043\\
&(15)\ \varphi_{16} = -269.406554\varphi_1 + 2.5756116 + 2.076563(369.516421\varphi_1 - 3.5432043) - 0.00218750\\
&\qquad \varphi_{16} = 497.917574\varphi_1 - 4.7842629\\
&(16)\ \varphi_{17} = -369.516421\varphi_1 + 3.5432043 + 2.063000(497.917574\varphi_1 - 4.7842629) - 0.0018000\\
&\qquad \varphi_{17} = 657.687534\varphi_1 - 6.3285301\\
&(17)\ \varphi_{18} = -497.917574\varphi_1 + 4.7842629 + 2.048563(657.687534\varphi_1 - 6.3285301) - 0.0013875\\
&\qquad \varphi_{18} = 849.396774\varphi_1 - 8.1815172\\
&(18)\ \varphi_{19} = -657.687534\varphi_1 + 6.3285301 + 2.033250(849.396774\varphi_1 - 8.1815172) - 0.00095000\\
&\qquad \varphi_{19} = 1069.348457\varphi_1 - 10.3074897\\
&(19)\ 849.396774\varphi_1 - 8.1815172 - 1.017063(1069.348457\varphi_1 - 10.3074897) + 0.0004875 = 0
\end{aligned}
$$

$$\varphi_1 = \frac{2.3023367}{238.197976} = 0.0096656$$

Note: It can be shown that for this type of loading φ_1 is a direct function of α, and the following can be written.

$$\varphi_1/\alpha = 0.0048328 \quad (\beta = 70)$$

Further, φ at any point is linearly dependent on α, with the consequence that φ' and M are also linearly dependent on α. It follows that, knowing M for one α, M can be determined directly for any other α.

Recapitulating:

$$
\begin{aligned}
\varphi_1 &= 0.0096656\\
\varphi_2 &= 2.174563(0.0096656) - 0.0049875 = 0.016031\\
\varphi_3 &= 3.725869(0.0096656) - 0.0157891 = 0.020224\\
\varphi_4 &= 5.914514(0.0096656) - 0.0341791 = 0.022988\\
\varphi_5 &= 9.096797(0.0096656) - 0.0631112 = 0.024815\\
\varphi_6 &= 13.771528(0.0096656) - 0.107085 = 0.026025\\
\varphi_7 &= 20.639375(0.0096656) - 0.1726621 = 0.026830\\
\varphi_8 &= 30.676666(0.0096656) - 0.2691412 = 0.027367\\
\varphi_9 &= 45.223427(0.0096656) - 0.4093841 = 0.027728\\
\varphi_{10} &= 66.081705(0.0096656) - 0.6107494 = 0.027970\\
\varphi_{11} &= 95.613207(0.0096656) - 0.8960256 = 0.028133\\
\varphi_{12} &= 136.815544(0.0096656) - 1.2941609 = 0.028243\\
\varphi_{13} &= 193.341222(0.0096656) - 1.8404422 = 0.028317\\
\varphi_{14} &= 269.406554(0.0096656) - 2.5756116 = 0.028364\\
\varphi_{15} &= 369.516421(0.0096656) - 3.5432043 = 0.028394\\
\varphi_{16} &= 497.917574(0.0096656) - 4.7842629 = 0.028409
\end{aligned}
$$

TABLE 2

1 Point	2 x	3 x^2	4 $x^2 - 1$	5 ④ × Δx^2	6 $\alpha \times$ ⑤	7 $\beta \times$ ⑤	8 ⑦ − 2
0	0	0	−1	−0.100	−0.0200	−0.7000	−2.7000
1	0.1	0.01	−0.99	−0.0099	−0.0198	−0.6930	−2.6930
2	0.2	0.04	−0.96	−0.0096	−0.0192	−0.6720	−2.6720
3	0.3	0.09	−0.91	−0.0091	−0.0182	−0.6370	−2.6370
4	0.4	0.16	−0.84	−0.0084	−0.0168	−0.5880	−2.5880
5	0.5	0.25	−0.75	−0.0075	−0.0150	−0.5250	−2.5250
6	0.6	0.36	−0.64	−0.0064	−0.0128	−0.4480	−2.4480
7	0.7	0.49	−0.51	−0.0051	−0.0102	−0.3570	−2.3570
8	0.8	0.64	−0.36	−0.0036	−0.0072	−0.2520	−2.2520
9	0.9	0.81	−0.19	−0.0019	−0.0038	−0.1330	−2.1330
10	1.0	1.00	0	0.0000	0.0000	+0.0000	−2.0000

$\varphi_{17} = 657.687534(0.0096656) - 6.3285301 = 0.028415$

$\varphi_{18} = 849.396774(0.0096656) - 8.1815172 = 0.028412$

$\varphi_{19} = \varphi_{20} = 1069.348457(0.0096656) - 10.3074897 = 0.028405$

The moments at the stations considered will be determined later; however, in order to determine the effect of larger Δx, φ will be determined first for $\Delta x = 0.1$.

Example 2

Same as Example 1 except for $\Delta x = 0.1$.
From Table 2, the following system of equations results:

(1) $\varphi_2 + \varphi_0 - 2.693\varphi_1 = -0.0198$
(2) $\varphi_3 + \varphi_1 - 2.672\varphi_2 = -0.0192$
(3) $\varphi_4 + \varphi_2 - 2.637\varphi_3 = -0.0182$
(4) $\varphi_5 + \varphi_3 - 2.588\varphi_4 = -0.0168$
(5) $\varphi_6 + \varphi_4 - 2.525\varphi_5 = -0.0150$
(6) $\varphi_7 + \varphi_5 - 2.448\varphi_6 = -0.0128$
(7) $\varphi_8 + \varphi_6 - 2.357\varphi_7 = -0.0102$
(8) $\varphi_9 + \varphi_7 - 2.252\varphi_8 = -0.0072$
(9) $\varphi_{10} + \varphi_8 - 2.133\varphi_9 = -0.0038$
(10) $\varphi_{11} + \varphi_9 - 2.000\varphi_{10} = -0.0000$

The B.C. give $\varphi_0 = 0$ and $\varphi_{11} = \varphi_9 = \varphi_{10} = 0$.
Solving:

(1) $\varphi_2 = 2.693\varphi_1 - 0.0198$
(2) $\varphi_3 = -\varphi_1 + 2.672(2.693\varphi_1 - 0.0198) - 0.0192$
$\varphi_3 = 6.195696\varphi_1 - 0.0721056$
(3) $\varphi_4 = -2.693\varphi_1 + 0.0198 + 2.637(6.195696\varphi_1 - 0.0721056) - 0.0182$
$\varphi_4 = 13.645050\varphi_1 - 0.1885425$
(4) $\varphi_5 = -6.195696\varphi_1 + 0.0721056 + 2.588(13.645050\varphi_1 - 0.1885425) - 0.0168$
$\varphi_5 = 29.117693\varphi_1 - 0.4326424$
(5) $\varphi_6 = 13.64505\varphi_1 + 0.1885425 + 2.525(29.117693\varphi_1 - 0.4326424) - 0.0150$
$\varphi_6 = 59.877125\varphi_1 - 0.9188796$
(6) $\varphi_7 = -29.117693\varphi_1 + 0.4326424 + 2.448(59.877125\varphi_1 - 0.9188796) - 0.0128$
$\varphi_7 = 117.461509\varphi_1 - 1.8295749$
(7) $\varphi_8 = -59.877125\varphi_1 + 0.9188796 + 2.357(117.461509\varphi_1 - 1.8295749) - 0.0102$
$\varphi_8 = 216.979652\varphi_1 - 3.4036284$
(8) $\varphi_9 = -117.461509\varphi_1 + 1.8295749 + 2.252(216.979652\varphi_1 - 3.4036284) - 0.0072$
$\varphi_9 = 371.176667\varphi_1 - 5.8425963$
(9) $216.979652\varphi_1 - 3.4036284 - 1.133(371.176667\varphi_1 - 5.8425963) + 0.0038 = 0$

$$\varphi_1 = \frac{3.2198332}{203.563512} = 0.0158173;$$

$$\frac{\varphi_1}{\alpha} = 0.00790865$$

Recapitulating:

$\varphi_1 = 0.0158173$
$\varphi_2 = 2.693(0.0158173) - 0.0198 = 0.02280$
$\varphi_3 = 6.195696(0.0158173) - 0.0721056 = 0.02589$
$\varphi_4 = 13.645050(0.0158173) - 0.1885425 = 0.02729$
$\varphi_5 = 29.117693(0.0158173) - 0.4326424 = 0.02792$
$\varphi_6 = 59.877125(0.0158178) - 0.9188796 = 0.02821$
$\varphi_7 = 117.461509(0.0158173) - 1.8295749 = 0.02835$
$\varphi_8 = 216.979652(0.0158173) - 3.4036284 = 0.02840$
$\varphi_9 = 371.176667(0.0158173) - 5.8425963 = 0.02842$
$\varphi_{10} = \varphi_9 = 0.02842$

Comparing the above with the results obtained for $\Delta x = 0.05$, one notes that there is a maximum error of $1^1/_8$ per cent in φ caused by an increase in Δx from 0.05 to 0.1 (considerably less work is involved in using $\Delta x = 0.1$).

Note: φ_1 for $\Delta x = 0.1 = \varphi_2$ for $\Delta x = 0.05$, etc.

A plot of φ versus x for $\Delta x = 0.05$ and $\Delta x = 0.1$ is given below.

Since the two curves for φ fall almost on top of one another, $\varphi' = SM/EI$ is determined for $\Delta x = 0.05$ only and plotted in Fig. 6.

Eq. 25 gives

$$\varphi_n' = (\varphi_{n+1} - \varphi_{n-1})/2\,\Delta x$$

φ_0' is taken directly from the plot of φ.

$$\varphi_0' = \frac{0.004}{0.018} = 0.222 \left(\text{check } \varphi_0' \cong \frac{\varphi_1}{\Delta x} = 0.0096656 \div 0.05 = 0.193312\right)$$

$$\varphi_1' = \frac{\varphi_2 - \varphi_0}{2\Delta x} = \frac{0.016031}{0.1} = 0.16031$$

$$\varphi_2' = \frac{\varphi_3 - \varphi_1}{2\,\Delta x} = \frac{0.020224 - 0.0096656}{0.1} = 0.10558$$

$$\varphi_3' = \frac{\varphi_4 - \varphi_2}{2\Delta x} = \frac{0.022988 - 0.016031}{0.1} = 0.06957$$

$$\varphi_4' = \frac{\varphi_5 - \varphi_3}{2\Delta x} = \frac{0.024815 - 0.020224}{0.1} = 0.04591$$

$$\varphi_5' = \frac{\varphi_6 - \varphi_4}{2\Delta x} = \frac{0.026025 - 0.022988}{0.1} = 0.03037$$

$$\varphi_6' = \frac{\varphi_7 - \varphi_5}{2\Delta x} = \frac{0.026830 - 0.024815}{0.1} = 0.02015$$

$$\varphi_7' = \frac{\varphi_8 - \varphi_6}{2\Delta x} = \frac{0.027367 - 0.026025}{0.1} = 0.01342$$

$$\varphi_8' = \frac{\varphi_9 - \varphi_7}{2\Delta x} = \frac{0.027728 - 0.026830}{0.1} = 0.00898$$

$$\varphi_9' = \frac{\varphi_{10} - \varphi_8}{2\Delta x} = \frac{0.027970 - 0.027367}{0.1} = 0.00603$$

$$\varphi_{10}' = \frac{\varphi_{11} - \varphi_9}{2\Delta x} = \frac{0.028133 - 0.027728}{0.1} = 0.00405$$

$$\varphi_{11}' = \frac{\varphi_{12} - \varphi_{10}}{2\Delta x} = \frac{0.028243 - 0.027970}{0.1} = 0.00273$$

$$\varphi_{12}' = \frac{\varphi_{13} - \varphi_{11}}{2\Delta x} = \frac{0.028317 - 0.028133}{0.1} = 0.00184$$

$$\varphi_{13}' = \frac{\varphi_{14} - \varphi_{12}}{2\Delta x} = \frac{0.028364 - 0.028243}{0.1} = 0.0012$$

$$\varphi_{14}' = \frac{\varphi_{15} - \varphi_{13}}{2\Delta x} = \frac{0.028394 - 0.028317}{0.1} = 0.00077$$

$$\varphi_{15}' = \frac{\varphi_{16} - \varphi_{14}}{2\Delta x} = \frac{0.028409 - 0.028364}{0.1} = 0.00045$$

$$\varphi_{16}' = \frac{\varphi_{17} - \varphi_{15}}{2\Delta x} = \frac{0.028415 - 0.028394}{0.1} = 0.00021$$

$$\varphi_{17}' = \frac{\varphi_{18} - \varphi_{16}}{2\Delta x} = \frac{0.028412 - 0.028409}{0.1} = 0$$

$$\varphi_{18}' = \frac{\varphi_{19} - \varphi_{17}}{2\Delta x} = \frac{0.028405 - 0.028415}{0.1} = 0$$

$$\varphi_{19}' = \frac{\varphi_{20} - \varphi_{18}}{2\Delta x} = \frac{0.028405 - 0.028412}{0.1} = 0$$

$$\varphi_{20}' = 0$$

Example 3*

Same as Example 2 except for freely hinged rotor. The system of equations is the same as that given in Example 2; however, the B.C. are: $\varphi'(0) = \varphi'(1) = 0$; these give $\varphi_0 = \varphi_1$; $\varphi_9 = \varphi_{10}$.

Solving:

(1) $\varphi_2 = +1.693\varphi_1 - 0.0198$

(2) $\varphi_3 = -\varphi_1 + 2.672(1.693\varphi_1 - 0.0198) - 0.0192$
$\varphi_3 = 3.523696\varphi_1 - 0.0721056$

(3) $\varphi_4 = -1.692\varphi_1 + 0.0198 + 0.0198 + 2.637(3.523696\varphi_1 - 0.0721056) - 0.0182$
$\varphi_4 = 7.5989864\varphi_1 - 0.1885425$

(4) $\varphi_5 = -3.523696\varphi_1 + 0.0721056 + 2.588(7.598986\varphi_1 - 0.1885425) - 0.0168$
$\varphi_5 = 16.142480\varphi_1 - 0.4326424$

(5) $\varphi_6 = -7.598986\varphi_1 + 0.1885425 + 2.525(16.142480\varphi_1 - 0.4326424) - 0.0150$
$\varphi_6 = 33.160776\varphi_1 - 0.9188796$

(6) $\varphi_7 = -16.142480\varphi + 0.4326424 + 2.448(33.160776\varphi_1 - 0.9188796) - 0.0128$
$\varphi_7 = 65.035010\varphi_1 - 1.8295749$

(7) $\varphi_8 = -33.160776\varphi_1 + 0.9188796 + 2.357(65.035010\varphi_1 - 1.8295749) - 0.0102$
$\varphi_8 = 120.126743\varphi_1 - 3.4036284$

(8) $\varphi_9 = -65.035010\varphi_1 + 1.8295749 + 2.252(120.126743\varphi_1 - 3.4036284) - 0.0072$
$\varphi_9 = 205.490415\varphi_1 - 5.8425963$

(9) $120.126743\varphi_1 - 3.4036284 - 1.133(205.490415\varphi_1 - 5.8425963) - 0.0038$

$\varphi_1 = 3.2198332/112.693897 = 0.0285715$

$\varphi_{1/\alpha} = 0.0142857$

Recapitulating:

$\varphi_0 = \varphi_1 = 0.0285715$

$\varphi_2 = 1.693000(0.0285715) - 0.0198 = 0.0285715$

$\varphi_3 = 3.523696(0.0285715) - 0.0721056 = 0.0285717$

$\varphi_4 = 7.598986(0.0285715) - 0.1885425 = 0.0285719$

$\varphi_5 = 16.142480(0.0285715) - 0.4326424 = 0.028725$

$\varphi_6 = 33.160776(0.0285715) - 0.9188796 = 0.0285735$

$\varphi_7 = 65.035010(0.0285715) - 1.8295749 = 0.0285729$

$\varphi_8 = 120.126743(0.0285715) - 3.4036234 = 0.0285728$

$\varphi_{10} = \varphi_9 = 205.490415(0.0285715) - 5.8425963 = 0.0285731$

The above result is interesting, since it indicates that an incorrect choice of ϑ did not give an incorrect answer. In the above problem flapping inertia, coriolis and gyroscopic loads were not considered. If the net distribution of these loads combined with air load were geometrically similar to the centrifugal load distribution, the condition of zero moment all along the blade would still exist even if these loads were considered. If the load distributions were not similar, small bending moments would exist, since, in this case, the blade would have to flex in order to satisfy the boundary conditions. The effect of a hinge damping moment is considered in the Appendix.

Conclusions

(1) The method of finite differences leads to a rapid determination of rotor bending moments.

(2) For constant chord (rectangular plan form) blades of uniform section and weight, loaded with a

* Eq. (24) for this case gives $\alpha = 0$; however, to determine the effect of an incorrect choice of ϑ, α is taken as 2. Note that $\alpha = 0$, with the B.C. $\varphi'(0) = \varphi'(1)$ automatically gives $\varphi' = 0$ at all points.

triangular load, the bending moments are directly proportional to α and, hence, to the tip loading.

Appendix

I. *Summary of Formulas for Untapered Blades*

Axial Load:

$$P_t = \frac{B\cos\vartheta}{2}(\xi^2 - S^2) - \frac{B\sin\vartheta}{2}(\xi^2 - S^2)\frac{d\zeta}{d\xi}$$

Shear with triangular air load:

$$S_s = \left(\frac{w_s}{2S} - \frac{B\sin\vartheta}{2}\right)(\xi^2 - S^2) - \frac{B\cos\vartheta}{2}(\xi^2 - S^2)\frac{d\zeta}{d\xi}$$

Shear with parabolic air load:

$$S_s = \frac{w_s}{3S^2}(\xi^3 - S^3) - \frac{B\sin\vartheta}{2}(\xi^2 - S^2) - \frac{B\cos\vartheta}{2}(\xi^2 - S^2)\frac{d\zeta}{d\xi}$$

Bending Moment:

$$M = (EI/S)(d\varphi/dx);\ \varphi' = d\varphi/dx$$

Deflection:

$$\zeta = S\int_0^x \varphi dx$$

II. *Effect of Blade Dead Weight*

For a rectangular blade of uniform section and weight, the dead-weight inertia loading is uniform and has a running value of: ndW, where n = load factor and dW = differential blade weight; but, $dW = Awd\xi$; hence, $ndW = nAwd\xi$.

$$S_n = \text{inertia shear} = nAw\int_S^\xi d\xi = nAw(\xi - S)$$

$$M_i = nAw\int^\xi\int_S^\xi d\xi d\xi = \frac{nAw}{2}(\xi^2 + S^2 - 2S\xi)$$

The inertia moment acts in opposition to the air-load moment; hence Eqs. (22) and (22a) become:

$$\varphi'' + \beta(x^2 - 1)\varphi = \alpha(x^2 - 1) - \eta(x - 1) \qquad \text{(II—22)}$$

$$\varphi'' + \beta(x^2 - 1)\varphi = \gamma(x^3 - 1) - \lambda(x^2 - 1) - \eta(x - 1) \qquad \text{(II—22a)}$$

where $\eta = S^3nAw/EI$.

III. *Effects of Hinge Damping*

Since the magnitude of a hinge damping moment is dependent on the angular flapping velocity and not alone on the blade position, the angle, ϑ (and, hence, α), is indeterminate when hinge moments due to damping are present. The moment distribution can be determined, however, if an assumed value of ϑ is used.

The method of determining the bending moment at any point with hinge damping follows exactly the procedure of the illustrative examples with the exception of consideration of the B.C.—in this case,

$$\frac{EI}{S}\varphi_0' = M_d;\quad \varphi_0' = SM_d/EI$$

Assuming a straight line between φ_1 and φ_0:

$$(\varphi_1 - \varphi_0)/\Delta x = SM_d/EI$$
$$\varphi_1 = SM_d\Delta x/EI + \varphi_0$$

Knowing the relation between φ_0 and φ_1, the remaining φ_n are readily determined.

References

[1] Weick, Fred E., *Aircraft Propeller Design*, 1st Ed.; McGraw-Hill Book Company, Inc., New York, 1930.

[2] Pierce, B. O., *A Short Table of Integrals;* Ginn and Company, Boston, 1929.

[3] Stoker, J. J., *Bending and Buckling of Elastic Plates—Lectures*, pp. 29 and 30; New York University, 1941.

[4] Dommasch, Daniel O., *The General Equations for the Analysis of Rotor or Propeller Blades*, presented at the Fourteenth Annual Meeting of the Institute of the Aeronautical Sciences, New York, January 28–31, 1946. Author's Note: This last reference presents a generalized extension of the theory developed in the present paper and considers such variables as blade taper, variable EI, variable weight, blade hinge offset, arbitrary air load, and inertia load distribution and is not restricted to blade shapes definable analytically.

Influence of Different Factors on Buckling Loads of Curved Thin Aluminum-Alloy Sheets for Monocoque Constructions

GEORGES WELTER*

École Polytechnique de Montreal

ABSTRACT

Aerodynamic requirements of smooth surfaces and fair contours for both wings and fuselage have made aeronautical engineers conscious of the buckling problems associated with the design of semimonocoque (sheet-stringer) construction. This paper discusses the fundamental principles involved in increasing the buckling strength of the sheet. Test results show a 50 to 70 per cent increase in ultimate buckling load obtained by changes in the configuration of the sheet, which resulted in more load being carried in the supported edges and less in the unsupported central region. Although several suggestions are made, the practical method of achieving the desired results is left to the ingenuity of the designer. As a sidelight, these tests emphasize the necessity for well-controlled end and side conditions if consistent results are to be obtained in panel testing.

INTRODUCTION

IN ORDER TO THROW some additional light on the problem of pure monocoque construction, which is intimately related to the buckling of sheets in compression, a few problems concerning the behavior of thin curved aluminum-alloy panels of different shape and width, as well as the influence of different loading conditions, were investigated. In connection with an investigation titled "Curved Aluminum-Alloy Sheets in Compression for Monocoque Constructions,"[1] this additional work was carried out on duralumin sheets (17ST) of 0.032-in. thickness with a radius of curvature of 24 in. and a free length between grips of 9 in. The following points were investigated.

(1) Influence of different shapes of panels on buckling loads.

(2) Clearance between the ends of the panels and the loading tables.

(3) Width of panels and width of supported edges in relation to buckling and maximum loads.

(4) Influence of clearance between the supported edges of the sheet and the width between the teeth of the guides.

The guides used had, if not otherwise stated, teeth of $^1/_2$-in. depth, spaced $^1/_2$ in. apart (see Fig. 5 of reference 1). The tests were carried out on a 60,000-lb. Baldwin-Southwark-Tate-Emery testing machine using a loading range of 12,000 lbs.

Received November 9, 1944. Revised and resubmitted October 30, 1945.

* Professor of Applied Mechanics.

INFLUENCE OF DIFFERENT SHAPES OF PANELS ON BUCKLING LOADS

Thin sheets used as structural elements in stressed skin constructions show, in general, low buckling stresses compared to the ultimate loads they can carry. It can be supposed that the compression stress on the loaded edge is more or less uniformly distributed in the pure elastic range up to the critical buckling load. But after buckling takes place, the greatest part of the sheet (the central part), representing more than two-thirds of the width of the sheet, is, as already shown[1] for panels without guides, not able to carry an additional load. After buckling, this part of the sheet has practically no additional load-carrying capacity. Depending upon the stiffness of the testing machine, the maximum buckling load suddenly falls down a certain percentage (22–50 per cent) of this load and, despite this automatic unloading of the panels, their supported edges are not in the same proportion unloaded; on the contrary, the edge stress increases during this automatic unloading. This can be easily observed by the readings of the extensometers recording the edge strain. Furthermore, the edges of the panels cannot take part in the buckling process itself since they are supported and are forced by the guides to remain straight.

The total deflection of the sheet takes place normally in two distinct parts:

(1) The completely elastic deformation up to the maximum buckling load; this is the straight stress-strain part AB of the usual load-deformation diagram, as shown in Fig. 1, diagram *a*.

(2) From the buckling load to the ultimate load the stress-strain diagram (part CD) is curved and shows permanent deformations which gradually increase with higher loads.

The airplane designer is concerned with (a) initial buckling and whether it is elastic or permanent and (b) ultimate strength. Although elastic buckling of wings in normal flight condition has been permitted in the past, there is considerable evidence that the buckles have produced adverse pressure gradients on the wings and control surfaces, both at high speed and at high load factor, and designers are realizing the necessity for eliminating buckles.

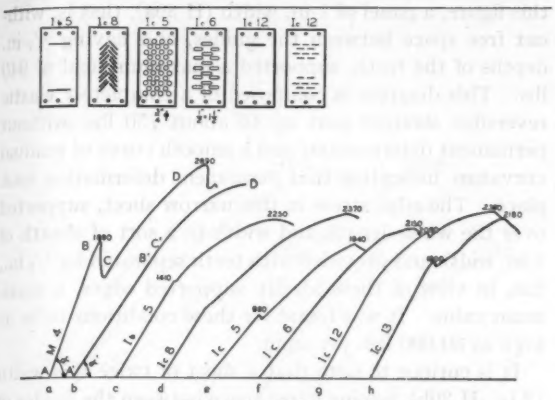

FIG. 1. Influence of shape of panels.

If in a loaded thin sheet, a distribution of the compressive stresses could be obtained in such a way that the ultimate load is reached without buckling taking place, then a favorable solution to this basic problem could be found. If it were possible to transform the discontinuity of the diagram during the loading process (Fig. 1, diagram *a*) into an uninterrupted line with an elastic range up to maximum load, this embarrassing problem would no longer exist for the constructor, whether or not buckling can take place. This would mean a stress-strain diagram as shown in Fig. 1, diagram *b*, having possibly an elastic range A′–B′ as high as in point B, diagram *a*, for the usual panels and about the same maximum load in D. It is quite natural that the slope of the elastic part A′–B′ would in this case be somewhat smaller ($\alpha' < \alpha$). It seems that this would represent a more elastic and stable skin construction as opposed to the fairly stiff and instable body materials used in present panels.

As shown in Fig. 1, diagrams *c* to *h*, preliminary attempts have been made to attain this aim. By changing the shape, especially that of the central part of the panels, it may be expected that some improvement in this respect can be obtained. About 30 panels, each one with a different distribution of the central longitudinal internal forces, were tested for this purpose. This was achieved by making a few horizontal jigsaw incisions of different lengths located at different spots in the central part of the sheets, as well as by incisions located at an angle of 45° to the loading direction. In addition, some discharging central openings of varying sizes, differing in number and orientation, vertical slots to limit the spreading of the buckle, transverse slots, slots at the base and at the top of the plates, were made, as well as longitudinal overlapping slots, as represented in Figs. 2–4.

It can be stated that by this means the shape of the load deflection diagram can be changed appreciably in the required direction, so that a more or less uninterrupted compression curve can be obtained. Some sheets, especially those with horizontal slots, show a fairly straight load deflection diagram up to about 1,500 lbs. (for sheets of 0.032-in. thickness and 6-in. width, as shown in Fig. 1, *c*, *g*, *h*). Some of these panels had only an unpronounced buckle and showed a small difference of slope between the pure elastic range and the parts of permanent deformation in the diagram (Schemes Ic 5 and Ic 6, Fig. 1).

Clearance Between the Ends of the Panels and the Loading Tables

Investigations of greater practical interest seem to be those conducted in a similar direction on normal panels without, however, appreciably changing their geometric shape. A more regular distribution of the unit stress over the whole width of the panels can be attained in the following manner. If the panel is fastened so that the unsupported central parts are not loaded uniformly over the whole width, that is, less intensely

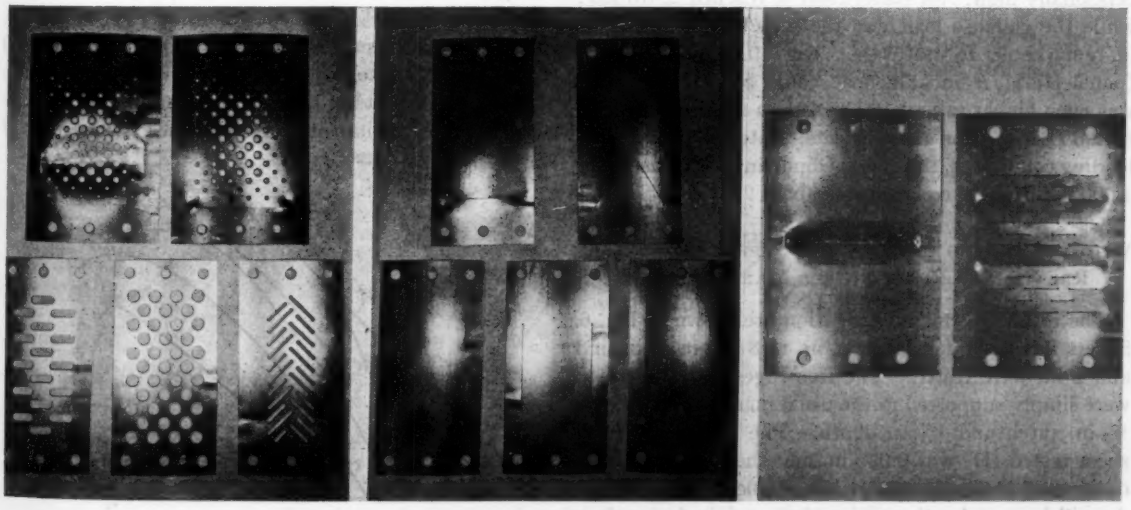

FIGS. 2, 3, and 4.

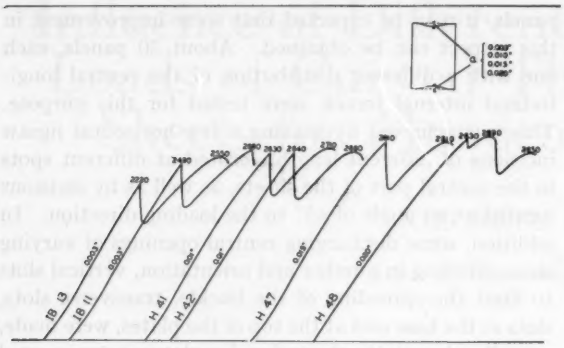

FIG. 5. Influence of shape of panel.

in the middle than in the restrained edges, the buckling will probably take place at a higher load compared to the normally uniformly loaded panels at their ends. In fact, by introducing the end loads gradually into the panels, starting from the two restrained edges toward the central part, the maximum buckling load can be shifted appreciably toward much higher values. With this in mind, the central part of the panel was loaded gradually and less intensely than the supported edges. A clearance of only a few thousandths of an inch on both ends of the panels, decreasing from the center part toward the edges, which were loaded over a width of about $1^1/_2$ in., plainly had the expected effect. As shown in Fig. 5, with a clearance of about 0.003 in. only (diagram IB 13, IB 11), a buckling load of 2,220 to 2,490 lbs. with an ultimate load of 2,550 and 2,660 lbs. was reached; for a clearance of 0.01 in., this load was extremely regular for two panels—in one case it was as high as 2,630 lbs. (panel H-41), in the other (panel H-42) it was 2,640 lbs. It is interesting to note that this last buckling load is only 20 lbs. lower than the ultimate load of 2,660 lbs. reached during the buckling test. By providing the panels with a still greater clearance of 0.015 in. at both ends, the buckling load was exceptionally high; for panel H-47 it reached 2,810 lbs., while the collapse load was the same (2,810 lbs.). It is remarkable to note that with 0.02-in. clearance (panel H-48), a buckling load could be reached which was even higher (about 180 lbs.) than the ultimate load of 2,650 lbs. For these sheets, tested under normal loading conditions, the average buckling load was about 1,660 lbs. and the collapse load about 2,700 to 2,800 lbs.

WIDTH OF PANELS AND WIDTH OF SUPPORTED EDGES IN RELATION TO BUCKLING AND MAXIMUM LOADS

The results of this investigation are shown in Fig. 6. Sheets having widths of 1 in. up to 8 in., in steps of 1 and 2 in. were tested. The free edges of these panels were simply supported in the usual manner by guides of $^1/_2$-in. pitch and $^1/_2$-in. depth. The thickness of the sheet tested (H) was 0.032 in. and the specimens were designated H 39a, H 39b, H 45b, H 39c, H 24 and H 40. As will be seen by the copies of the original records in this figure, a panel of 1-in. width (H 39a), that is, without free space between the guides, and having $^1/_2$-in. depths of the teeth, supported a maximum load of 940 lbs. This diagram is composed of a completely elastic reversible straight part up to about 750 lbs. without permanent deformations and a smooth curve of gradual curvature indicating that permanent deformation took place. The edge stress in this narrow sheet, supported over the whole length and width in a sort of sheath of 1-in. width and provided with teeth separated by $^1/_2$ in., has, in view of these ideally supported edges, a maximum value. It was found for these conditions to be as high as 30,000 lbs. per sq.in.

It is curious to note that a sheet of twice this width (2 in.–H 39b), having a free space between the guides of 1 in., showed a maximum load of nearly double the value measured for the sheet of 1-in. width; about 1,840 lbs. were recorded, corresponding to an edge stress of 28,700 lbs. per sq.in. This means that the guides of $^1/_2$-in. depth can be supposed to act on a depth of more than $^1/_2$ in. A free space of at least another $^1/_2$ in. outside the guides seems to protect the panel from buckling in its middle part; this record may be considered to be straight up to a load of about 900 lbs., where a discontinuity in the chart took place. For a greater width of 3 in. (H 45b), this protection of the guides was already less effective; the diagram shows, at about 1,200 lbs., the beginning of a small buckle and the maximum load with 2,370 lbs. is only about 30 per cent higher than that for the panel of 2-in. width. A check test for another panel of the same width gave a maximum load of about 2,380 lbs. (H 45a). A more distinct buckle, shown in the stress-strain record, was observed with panel H 39c of 4-in. width. At 1,230 lbs. the first buckle took place and a maximum load of 2,580 lbs. was reached. The usual shape of the stress-strain diagram was obtained in this test series with a sheet of 6-in. width (H 24) showing a pronounced buckle at 1,790 lbs. and an ultimate load of 2,720 lbs. Furthermore, a sheet of 8-in. width, according to record H 40, had two buckles, one at 1,860 lbs. and another at 1,880 lbs. The ultimate load of this sheet was 2,930 lbs.

From the results of another test completing the preceding investigation, it can be deduced what part of

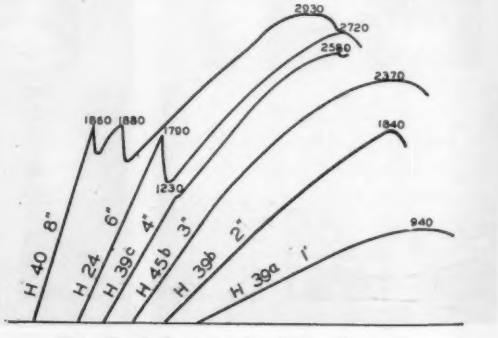

FIG. 6. Influence of width of panels.

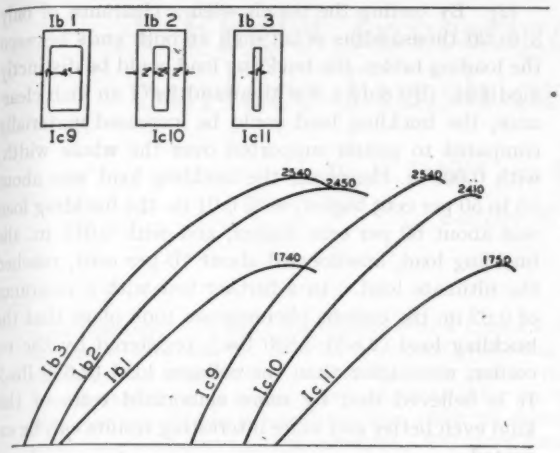

FIG. 7. Influence of width of panels.

the total load the supported edges may carry without buckling in the central part of the sheet. Sheets of 6-in. width, provided with a central free space of 1-, 2-, and 4-in. width, were tested. The remaining supported edges of these panels designated Ib 1, Ib 2, and Ib 3, were of $2^1/_2$-, 2-, and 1-in. width. According to Fig. 7, a panel with a central free space of 4-in. width showed no buckle and carried a maximum load of 1,740 lbs. (Ib 1); a panel with a free space of 2 in. (Ib 2) carried 2,450 lbs., and with 1-in. width (Ib 3) carried 2,540 lbs. All three sheets did not show any buckling at lower loads. Check tests made with three identical shaped panels (Ic 9, 10, and 11) showed practically the same results (Fig. 7).

Influence of Clearance Between the Supported Edges of the Sheets and the Teeth of the Guides

The clearance of the guiding slots for sheets of 0.020-in. thickness as well as for sheets up to 0.050-in. thickness, has been established by other investigators with ±0.002 in. That means ±10 per cent for thin sheets and about ±6 per cent for thick sheets. However, if the usual fairly appreciable variation of the thicknesses of these sheets is taken into consideration, where differences of about 10 per cent in a single sheet have been measured the clearance between the guides and the effective thickness of the individual panels becomes much greater and equally of much greater importance. Furthermore, since commercial tolerances of ±0.0025 in. are admissible for these sheets, which may measure from 0.0295-in. to 0.0345-in. thickness, it is obvious that the clearance between the guides and the supported edges of the sheets may also vary in fairly wide limits.

Since in the preceding test series it could be observed that the test results at buckling loads and at ultimate loads seemed somewhat influenced by the clearance of the guides and their adjustment, as well as by the thickness of the sheets tested, the following supplementary investigation has been carried out.

The normal guides with $^1/_2$-in. pitch were adjusted with $^1/_2$-in. depth in three different ways. Three tests (N 14, 15, and 16) were made with guides clamped strongly on the edges of the sheets, so that not only was there no clearance between the sheet and the guides but the latter were fixed so tightly that the sheet could not glide in the guides.

Fig. 8 shows stress-strain records of these three panels. The buckling loads, varying between 1,600 and 1,640 lbs., are fairly regular and the ultimate loads which these panels can carry are from 2,960 to 3,200 lbs.

Four other tests with panels cut out of the same sheet N (39, 40, 31, 32) were carried out in the normal way. That is, the guides were adjusted on each panel with a minimum of clearance, sufficient, however, to permit the panel to glide easily in the guides. Since the panels tested varied appreciably in thickness (0.031 to 0.034 in.) the adjustment of the guides was made individually for each sheet in such a way that the guides could just glide by their own weight on the edges of the panels. Apart from one panel (N 32 with 1,580 lbs.), the buckling loads for these tests were higher than the preceding values. Three panels showed buckling loads of 1,720, 1,810, and 1,990 lbs., with an average value of 1,775 lbs., that is, about 150 lbs. higher than those of the preceding series. On the other hand, the ultimate loads,

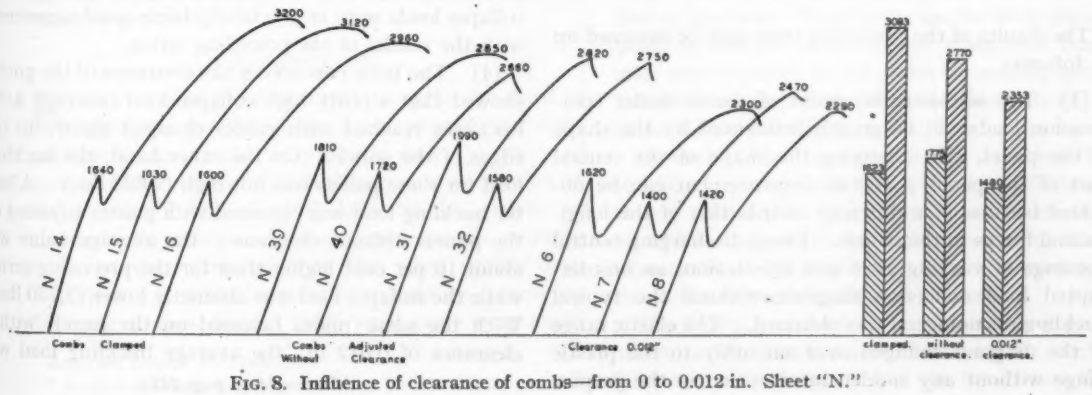

FIG. 8. Influence of clearance of combs—from 0 to 0.012 in. Sheet "N."

varying between 2,660 and 2,850 lbs., were distinctly lower than those for the panels with strongly clamped guides.

The third test series was made with a somewhat exaggerated clearance between the guides and the edges of the panel. The guides were preliminarily adjusted on a sheet of 0.045-in. thickness, and afterward used on panels with 0.033-in. thickness, so that a clearance of about 0.012 in. was used during these tests.

As may be seen by Fig. 8, the records of panels N 6, 7, and 8 show a buckling load that is distinctly lower than that for panels tested with normally adjusted guides, as used in the preceding series (N 39, 40, 31, 32). The buckle took place between 1,400 and 1,620 lbs. The average value for this test series is only 1,480 lbs. compared with 1,775 lbs. for normally adjusted guides with a maximum value of 1,990 lbs. The buckling loads of sheets with exaggerated clearance are distinctly lower than those for strongly clamped guides as shown by the first series.

An even more pronounced difference between these three ways of adjusting the guides on the panels could be observed for the ultimate loads. From an average ultimate load of 3,093 lbs. for tightly clamped guides, this load falls down to an average of 2,770 lbs. for normally adjusted guides and for guides adjusted with a clearance of 0.012 in. the average ultimate load is as low as 2,353 lbs.

From these tests and records it becomes obvious that the influence of the clearance of the guides supporting the free edges of the panels cannot be neglected, either in further investigations or in theoretic calculations concerning the maximum buckling loads of panels. It seems that it may become necessary to adjust the guides individually to each sheet and even to each edge of the panel, in order to obtain reliable results in compression tests of this sort. Guides with a nonadjustable slot and a given tolerance do not appear to give the highest possible accuracy. Guides with variable slots, enabling them to be adjusted to the edge thickness of each individual panel, should be used in further investigations.

Test Results

The results of the preceding tests may be summed up as follows:

(1) The stress-strain record of panels under compression loads can be greatly influenced by the shape of the panel. By changing the shape of the central part of the panel, a certain improvement can be obtained because of a different distribution of the longitudinal forces in the panels. Using discharging central openings of varying sizes and orientation, an uninterrupted load deflection diagram without the typical buckling phenomenon was obtained. The elastic range of the diagram changed over smoothly to the plastic range without any sudden interruption in the graphs.

(2) By testing the panels with a clearance of only 3 to 20 thousandths of an inch at both ends between the loading tables, the buckling load could be distinctly modified. By only a few thousandths of an inch clearance, the buckling load could be increased materially compared to panels supported over the whole width; with 0.003-in. clearance, the buckling load was about 35 to 50 per cent higher, with 0.01 in. the buckling load was about 60 per cent higher, and with 0.015 in. the buckling load, ameliorated about 70 per cent, reached the ultimate load. In a further test with a clearance of 0.02 in. the curious phenomenon took place that the buckling load (2,830–3,890 lbs.), registered by the recorder, was higher than the collapse load (2,650 lbs.). It is believed that by more elaborated tests of this kind even better and more interesting results can be expected.

(3) The width of the panels is of the greatest influence on their load-carrying capacity, as well as on the shape of their load deflection diagram. Because of the restrainers, the smaller the panels are in width, the more resistant they are. The collapse load of the 1-in. width panel was as high as 940 lbs., reaching nearly 30,000 lbs. per sq.in.; no buckling effect took place and the proportional limit in compression was attained for this panel at about 23,000 lbs. per sq.in. For the panel of 2-in. width, the collapse load reached was nearly twice that of the 1-in. sheet, while the proportional limit was only about 25 per cent higher. With a further increase in the width of the panels (3 and 4 in.) the collapse load increased more slowly and a distinct discontinuity in the diagram indicated that the buckling load was reached at 1,230 lbs. for the sheet of 4-in. width. Panels with a width of two-thirds of their free length showed the characteristic upper and lower buckling load, while for larger panels (8 in.) a double buckling effect at 1,860 and 1,880 lbs. took place with only a small increase for the collapse load. Compared to the 4-in. panel, this load was only 15 per cent higher for an increase of the width of 100 per cent.

Quite different loading diagrams were obtained with panels of different width by taking the middle part of the panels out. In all these cases, no buckling took place, the shape of the diagram was quite different, and collapse loads were in practically fairly good agreement with the results of the preceding series.

(4) The tests concerning the clearance of the guides showed that a fairly high collapse load (average 3,093 lbs.) was reached with guides clamped tightly to the edges of the panels. On the other hand, the buckling load for these panels was not high (1,623 lbs.). A better buckling load was obtained with guides adjusted on the panels without clearance; the average value was about 10 per cent higher than for the preceding series, while the collapse load was distinctly lower (2,770 lbs.). With the same guides fastened on the panels with a clearance of 0.012 in., the average buckling load was

(*Continued on page 217*)

A Flight Investigation of the Effects of Surface Finish on Wing Profile Drag

W. H. DAY* AND J. M. SCHWARZBACH*

Curtiss-Wright Corporation

ABSTRACT

An investigation in flight was conducted on a Curtiss P-40F airplane to determine the effect on the section profile drag of smoothing the wing surface. A total and static pressure rake, located aft of the wing trailing edge in the wake of the test section, measured the loss in momentum from which the sectional profile drag coefficient (c_{d_0}) was calculated. The airfoil section at the plane of measurement was approximately an NACA 2212.8 profile. For each surface finish condition, data were taken at values of airplane lift coefficient varying between $C_L = 0.15$ and $C_L = 0.35$. The corresponding Mach Numbers were between $M = 0.28$ and $M = 0.41$.

The surface finish smoothness has a large effect on the profile drag coefficient. At an airplane lift coefficient of $C_L = 0.16$ ($RN = 16.5 \times 10^6$, $M = 0.405$), four degrees of wing surface smoothness produced the following values of c_{d_0}:

Fresh camouflage paint (standard production type finish)	$c_{d_0} = 0.0088$
Above paint after several days weathering	$c_{d_0} = 0.0083$
Above paint sanded and pumiced	$c_{d_0} = 0.0078$
Wing surface filled and smoothed to obtain as aerodynamically smooth a surface as possible	$c_{d_0} = 0.0064$

Calculations made on the basis of these data indicate that an appreciable improvement in performance could be obtained merely by smoothing the factory-finished wing.

Two flights, one with a thick mud layer on the wing and the other with a somewhat lighter layer, indicated the necessity of flying with clean wings. The thin layer of mud caused a drag increase above the production wing of about $\Delta c_{d_0} = 0.0035$, while the addition of the heavy mud caused the profile drag to be slightly more than double that of the factory-finished wing. These surfaces were tested to show what might be expected in actual combat service.

This investigation also indicated that calculations made with the simplified Silverstein-Katzoff integrating equation,[1] corrected for compressibility, yielded values of profile drag coefficient substantially equal to those calculated by use of a more exact equation that required lengthy point-by-point integrations across the wake to determine c_{d_0}.

INTRODUCTION

RECENT TESTS HAVE SHOWN that over one-third of the total parasite drag of a modern fighter-type airplane is due to the wing profile drag. A series of measurements in flight on a representative section of the Curtiss P-40F wing (NACA 2212.8 airfoil) at moderate Reynolds and Mach numbers was recently made to determine whether the wing profile drag coefficient, c_{d_0}, could be reduced merely by improving the wing surface finish. Additional tests were made with the wing surface covered with two different thicknesses of mud to approximate service conditions often encountered.

During the investigation, a comparison was made of the drag coefficients calculated by Silverstein and Katzoff's simplified[1] and exact equations in an attempt to determine the accuracy of the simplified equation.

Received August 10, 1945.

* Aerodynamicists, Airplane Division, Buffalo Plant.

INSTRUMENTATION

The flight measurements were made on a representative section of the left wing of a Curtiss P-40F airplane. The wing profile drag coefficients were calculated from measurements of the momentum loss in the wake. The loss in momentum was obtained from measurements of the static and total pressure in the wake. A rake mounted $0.16c$ aft of the wing about 108 in. outboard of the airplane centerline on a cantilever strut fastened through the upper surface to the ribs near the trailing edge, as shown in Fig. 1, was used to measure the pressures. The wing chord at this station was approximately 78.15 in. The pressures were recorded by a photo-observer, located in the baggage compartment, which contained a liquid manometer, altimeter, airspeed indicator, and chronometer. The pilot recorded the free air temperatures, which were measured by a calibrated thermocouple located on the underside of the wing.

FLIGHT PROCEDURE

Twelve flights were made at approximately 5,000-ft. density altitude. The first flight was made to locate the rake in the center of the wake and to determine, by means of long light yarn streamers, the direction of airflow at the rake. Small tufts on the wing surface indicated an absence of noticeable transverse flow. The rake was centered in the wake for subsequent flights, and the total and static pressure tubes were adjusted to be parallel to the direction of airflow.

On each of the remaining flights, data were taken at stabilized, true air speeds varying from 200 to approximately 330 m.p.h. in increments of about 20 m.p.h. In addition, the first and last runs during each flight were made at 100 m.p.h. to enable the pilot to record the calibrated outside air temperature.

The flights were made in air as smooth as possible to minimize the acceleration effects on the manometer fluid, but some fluctuation of the liquid persisted. In

FIG. 1. Profile drag rake mounted on the Curtiss P-40F wing.

most cases, the amplitude was small and was c_{d_0} computed from averaged liquid levels. This averaged liquid level was determined from the theoretical deflection of the free stream static pressure below the free stream total head liquid level which should have existed to correspond to the indicated air-speed reading. The compressibility and air-speed pitot-static tube interference corrections were included in the calculations. This averaged, theoretical value checked the actual liquid deflections used for computation, and it had been determined previously that the manometer level fluctuation occurred simultaneously in all of the tubes. In the few cases where the liquid level fluctuation was appreciable, the data were discarded.

The inclusion of "dampers," consisting of porous plugs of copper or glass wool in the lower sections of the manometer tubes, helped to alleviate the fluctuation of the liquid levels with no effect on the manometer readings.

The photo-observer instruments were calibrated at frequent intervals. Tests in the Curtiss-Buffalo 8-ft. wind tunnel showed negligible interference effects on the rake static-pressure readings from the supporting strut. At the start and finish of each flight the actual rake tube locations were measured, and these values were used to plot the corresponding recorded pressures. The take-off weight and fuel consumption were measured during the flight to allow calculation of airplane lift coefficient (C_L).

Surface Finishes

Flights were made with six different types of surface finish on the wing test panel. The test section of the wing is shown in Fig. 2. The first surface tested was the regular camouflage paint as applied to the production airplane in the factory. This surface was modified in three ways. Finally, to simulate the worst conditions that might be encountered in actual combat operation from small advanced air bases, two tests were

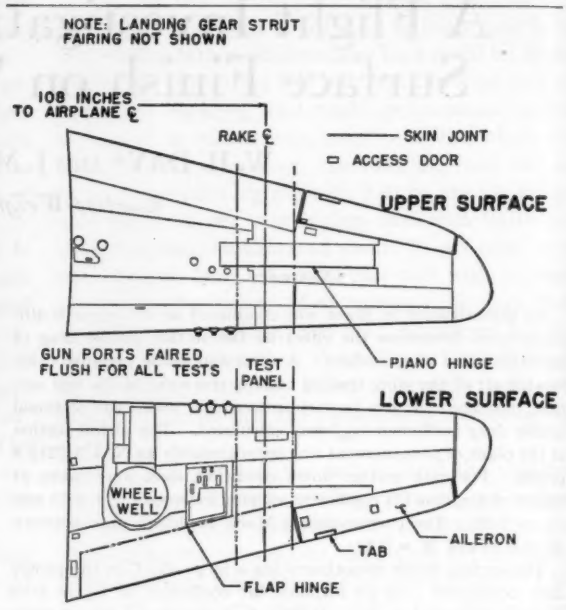

FIG. 2.

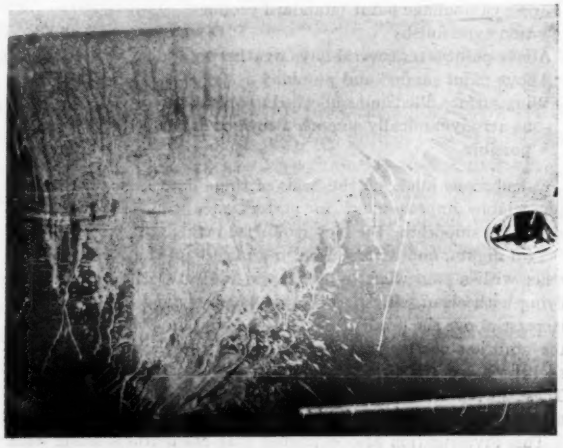

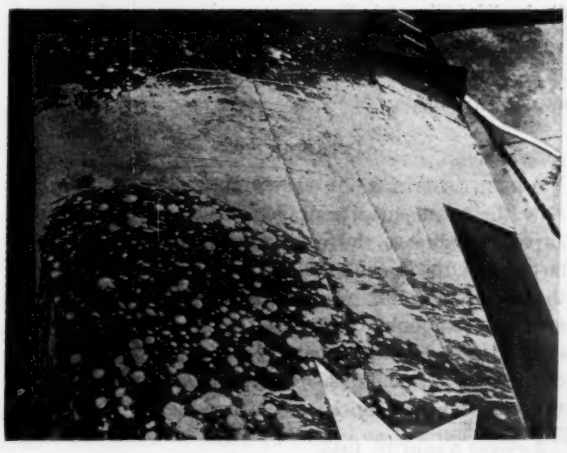

FIG. 3. Curtiss P-40F wing test section with a thick irregular mud layer (Finish 2).

run with mud applied to the surface—first in a thick layer and then in a thin layer. The six finishes are described as follows:

(1) Freshly Painted Production Camouflage Paint

This was the actual production finish that was applied to the airplanes leaving the factory. The texture of the surface was rough and sandpapery. No attempt was made to fill or smooth the skin joints, ammunition door and flap piano-type hinges, rivets, or other protuberances. A Ω-shaped wire (plane of wire perpendicular to the flight path), extending about $^1/_4$ in. above the surface at the ammunition door hinge, was not removed.

(2) Production Paint with Thick Layer of Mud

A thick irregular layer of mud was applied over Finish 1 as shown in Fig. 3.

(3) Weathered Production Paint

The mud of Finish 2 was removed by water and the surface left to weather for several days, leaving a finish that was not so rough to the touch as Finish 1. The Ω-shaped wire at the ammunition door hinge was made flush with the surface and remained so for the remainder of the program.

(4) Thin Mud Layer on Production Paint

A light layer of mud was applied to Finish 3. It was thinner than Finish 2, but it did have small pebbles and other irregularities imbedded in it as shown in Fig. 4.

(5) Sanded and Pumiced Paint

The production paint was sanded smooth with No. 320 (wet) sandpaper followed by a rubbing with wet rags and pumice. There was no filling of the irregularities or smoothing of protuberances; the paint was made just as smooth as possible.

(6) Aerodynamically Smooth Surface

All of the surface irregularities including piano hinges, skin joints, rivets, ejection chutes, and the covered gun ports were filled with glazing putty and sanded. The surface was pumiced with long chordwise strokes until it felt perfectly smooth. Every care was taken to keep the surface clean and free from imperfections for all flights with this particular surface.

Results and Discussion

Surface Finish Effect on Wing Profile Drag

The variation of section profile drag with airplane lift coefficient is shown in Fig. 5. The test Mach Numbers and Reynolds Numbers are also presented.

The wing with the production finish of freshly applied camouflaged paint (Finish 1) had a profile drag coefficient of about $c_{d_0} = 0.0088$ in the high-speed range ($C_L = 0.15$ to 0.18). Allowing the paint to weather and making the Ω hinge wire flush with the wing surface (Finish 3) caused a drag decrease of about $\Delta c_{d_0} = 0.0005$ as shown by the curves in Fig. 5. This slight profile drag decrease with weathering is confirmed by results of speed-power calibration-type flight tests on several fighter airplanes. An examination of the two surfaces revealed that the weathered paint looked and felt somewhat smoother to the touch.

FIG. 4. Curtiss P-40F wing test section with a thin mud layer (Finish 4).

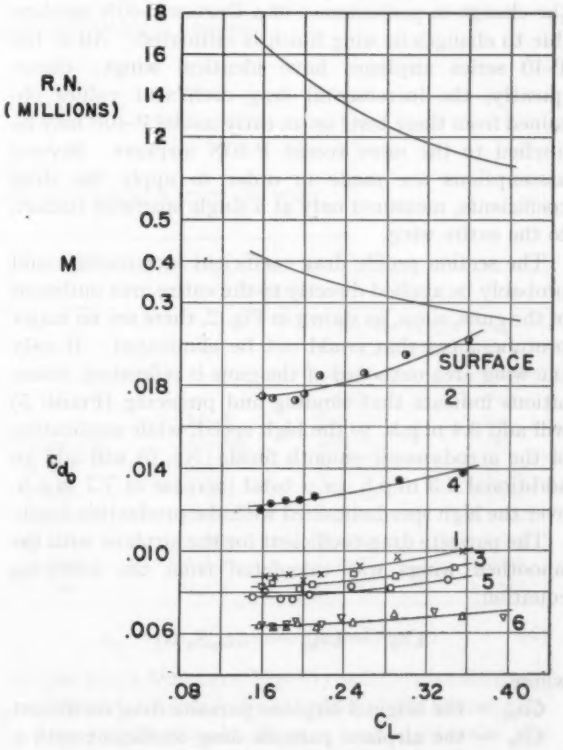

FIG. 5.

A further decrease of $\Delta c_{d_0} = 0.0005$ was obtained by wet-sanding and pumicing the paint surface (Finish 5). The resultant paint was extremely smooth, but the unfilled rivet depressions, hinges, and lap joints were still present. A decrease in wing profile drag of about $\Delta c_{d_0} = 0.0010$ seems to be all that would be obtained by merely smoothing the production finish paint.

Filling the irregularities, fairing the surface contour, and then carefully painting and polishing the wing (Finish 6) reduced the drag coefficient to about $c_{d_0} = 0.0064$. This value was checked by four separate flights.

The addition of a comparatively thin coating of mud (Finish 4) to the wing increased the drag coefficient to $c_{d_0} = 0.0125$. A heavy, irregular mud application (Finish 2) more than doubled the drag of the production finished section.

These results show the relation of surface finish to the drag coefficient for an NACA 2212.8 airfoil. It had been long thought that comparatively small drag decreases could be obtained by smoothing a conventional-type airfoil. These results show, however, that a smooth wing is essential to the attainment of low drag, even on a conventional airfoil. Of course, the need for a smooth wing is even greater if the new N.A.C.A. low-drag airfoils are employed.

Estimation of Change in High Speed Due to Smoothing the Wing

As an example of the application of the flight c_{d_0} data the change in performance of a Curtiss P-40N airplane due to changes in wing finish is estimated. All of the P-40 series airplanes have identical wings; consequently, the incremental drag coefficient values obtained from these tests on an early model P-40F may be applied to the more recent P-40N airplane. Several assumptions are made in order to apply the drag coefficients, measured only at a single spanwise station, to the entire wing.

The section profile drag coefficient increments could probably be applied directly to the entire area outboard of the guns, since, as shown in Fig. 2, there are no major protuberances that could not be eliminated. If only the wing area outboard of the guns is refinished, calculations indicate that sanding and pumicing (Finish 5) will add 3.4 m.p.h. to the high speed, while application of the aerodynamic smooth finish (No. 6) will add an additional 4.3 m.p.h. or a total increase of 7.7 m.p.h. over the high speed obtained with the production finish.

The parasite drag coefficient for the airplane with the smoothed wings was calculated from the following equation:

$$C_{D_p} = C_{D_{p_0}} - (\Delta c_{d_0} S_a / S)$$

where

$C_{D_{p_0}}$ = the original airplane parasite drag coefficient
C_{D_p} = the airplane parasite drag coefficient with a changed wing finish
S_a = the wing area affected by the smoothing process
S = the total wing area

Regular methods of calculation were then used to estimate the high speed.

It is more difficult to judge the drag reductions that may actually be attained by smoothing the entire wing, since the exact effect of the slipstream is unknown. If, because of turbulence in the slipstream, transition occurs at or close to the wing leading edge, then the effect of smoothing the surface in the turbulent boundary layer area can be estimated only roughly. The presence of the guns and wheel fairings and other large protuberances on this portion of the wing is another factor preventing the application of the measured section drag data.

Flight tests made on the airfoil with Finish 6 and transition induced at $0.10c$ on both the upper and lower surfaces yielded a drag coefficient in the high-speed range of about $c_{d_0} = 0.0077$.

Two assumptions were made in order to estimate the high speed increase that might be obtained by applying the aerodynamically smooth finish (No. 6) to the entire P-40 wing.

(1) The low profile drag coefficient obtained from these tests of Finish No. 6 apply to the entire wing area outboard of the guns.

(2) The drag coefficient obtained from the tests with transition fixed at 10 per cent chord is realized over the inboard wing area except for those areas affected by protuberances, wheel pockets, landing gear, etc., where there is no drag decrease.

The calculated increase in high speed, then, is 9 m.p.h.

The validity of these calculations has been approximately verified by flight tests of various airplanes, including several P-40's with the entire wing finished in various ways.

The wing finish on each production airplane is not exactly the same. It is dependent upon the painter, atmospheric conditions, care taken in handling the airplane, and other factors. Overspray, a condition that results in a rougher surface, may be present to a greater or lesser degree. All these variables tend to make the exact prediction of the gain in high speed or improvement of other performance items of a specific airplane difficult and prevent an exact comparison of increments obtained from different tests.

The values estimated herein are of use as an indication of the gain that might be expected on the P-40 airplane, but they also illustrate the general tendency toward improved performance that might be obtained with any airplane merely by constructing smooth wings. It is obvious that, if the production wing finish is poor to start with, more of a gain will be realized by smoothing the wing than if a consistently good finish is always produced by standard shop practice.

Comparison of Methods

Several equations have been derived to calculate the section profile drag coefficient from measurements of the total and static pressures in the wake and in the free stream.

Jones[2] derived an equation that neglects the effect of compressibility.

$$c_{d_0} = \frac{2}{c}\int^{w}\sqrt{\frac{H_1 - p_1}{H_0 - p_0}}\left(1 - \sqrt{\frac{H_1 - p_0}{H_0 - p_0}}\right)dy \quad (1)$$

where

H_0 = free stream total pressure
H_1 = total pressure in wake
p_0 = free stream static pressure
p_1 = static pressure in wake
c = local wing chord
$\int^{w}$ = integrate across the wake
dy = elemental distance across wake

Silverstein and Katzoff[1] derived a simplified equation for calculating c_{d_0} based on the assumption of a cosine squared wake shape but also neglecting the effects of compressibility. They substitute for the point-by-point calculation of the integrand in the Jones equation and subsequent integration across the wake, a "summary" equation including a factor, F_1, which is dependent on the maximum and average pressure losses in the wake.

$$c_{d_0} = F_1\frac{W}{c}\frac{(H_0 - H_1)_{\text{average}}}{(H_0 - p_0)} \quad (2)$$

where W is the width of the wake.

Values of F_1 were obtained by simultaneous solution of Eqs. (1) and (2) for wakes having cosine squared shapes and various maximum and average pressure losses in the wake.

They also derived an equation requiring an integration across the wake which takes into account the effects of compressibility, including the density decrease in the wing wake due to the temperature rise at high Mach Numbers.

$$c_{d_0} = \frac{2}{c}\int^{w}\sqrt{\frac{p_1^{1/\gamma}}{p_0}\frac{(H_1 - p_1)(1+\eta_0)}{(H_0 - p_0)(1+\eta_1)}}\left\{\sqrt{\left[1 + 0.202M_0^2\frac{(H_1 - p_0)(1+\eta_0)}{(H_0 - p_0)(1+\eta_2)}\right]\Big/(1 + 0.202M_0^2)} - \sqrt{\frac{(H_1 - p_0)(1+\eta_0)}{(H_0 - p_0)(1+\eta_2)}}\right\}dy \quad (3)$$

where

γ = ratio of the specific heat at constant pressure to that at constant volume
$1 + \eta_0 = 1 + {}^1/_4M_0^2 + {}^1/_{40}M_0^4 + \ldots$
$1 + \eta_1 = 1 + {}^1/_4M_1^2 + {}^1/_{40}M_1^4 + \ldots$
$1 + \eta_2 = 1 + {}^1/_4M_2^2 + {}^1/_{40}M_2^4 + \ldots$
M_0 = Mach Number of the free stream
M_1 = Mach Number in the wake at the measuring plane
M_2 = Mach Number in the wake at an infinite distance downstream from the wing

TABLE 1

Airplane C_L	Section Profile Drag Coefficient, c_{d_0} Calculated with Eq. (1)	Calculated with Eq. (2)
0.347	0.0094	0.0096
0.290	0.0090	0.0092
0.249	0.0092	0.0092
0.209	0.0087	0.0087
0.196	0.0090	0.0089
0.159	0.0087	0.0092

A correction for the effect of compressibility, (F_c/F_1), which may be applied to drag coefficients calculated with Eqs. (1) or (2), was derived by Silverstein and Katzoff from Eq. (3) on the basis of the cosine squared wake shape. The corrected drag coefficient is expressed as

TABLE 2

Airplane C_L	Mach Number	Section Profile Drag Coefficient, c_{d_0} Calculated with Eqs. (2) and (3)	Calculated with Eq. (4)
0.347	0.280	0.0093	0.0092
0.290	0.306	0.0088	0.0088
0.249	0.329	0.0088	0.0089
0.209	0.359	0.0083	0.0084
0.196	0.396	0.0085	0.0082
0.159	0.408	0.0084	0.0083

$$c_{d_0} = (F_c/F_1)\ (\text{incompressible } c_{d_0}) \quad (4)$$

At low Mach Numbers, Eqs. (1) and (2) give accurate c_{d_0} values and differ only by the error in the assumption of a cosine squared wake shape. A comparison of the

(*Continued on page 217*)

Static Displacement and Coupled Frequencies of a Twisted Bar

R. J. DUNHOLTER*
University of Cincinnati

Introduction

THE ELASTIC BODY CONSIDERED is a straight bar with constant rectangular cross section and an initial structural twist of θ (constant) radians per unit of length. The object of the paper is twofold: (1) to calculate the static displacement components $u(z)$ and $v(z)$ in the direction of the principal axes u and v at each section due to the uniform loads w_u and w_v also in the direction of the principal axes; (2) to approximate by the energy method, using the displacement functions mentioned in (1), the first two natural frequencies of the bar. The method used is applicable to any end conditions but only the fixed-free case is considered. In the case of a fixed-free bar without twist the two fundamental frequencies corresponding to vibrations normal and parallel to the minor principal axis v are given by the formulas

$$\omega_u = 3.52\sqrt{EI_v/\gamma L^4}$$

$$\omega_v = 3.52\sqrt{r}\sqrt{EI_v/\gamma L^4}$$

where $r = I_u/I_v$ and γ is the mass per unit length of bar. In the case of the bar with an initial structural twist these two fundamentals will be coupled.

The coefficients replacing those given above for the untwisted bar are obtained by the energy method. It is known that the functions representing the normal modes are solutions of the variational equation

$$\delta(T - U) = 0 \tag{1}$$

where T and U are the kinetic and potential energies, respectively. If T and U are evaluated for an assumed displacement function satisfying the boundary conditions, then Eq. (1) furnishes approximate values for the natural frequencies.[1, 2] A function that can be expected to give good values for the two coupled fundamental frequencies of the twisted bar is the function representing the static displacement due to uniform loads w_u and w_v in the direction of the principal axes u and v, respectively, at each section.

The fundamental formulas from which the component displacement functions are obtained are

$$EI_v[(d^2u/dz^2) - 2\theta(dv/dz) - \theta^2u] = -M_v \tag{2}$$

$$EI_u[(d^2v/dz^2) + 2\theta(du/dz) - \theta^2v] = +M_u \tag{3}$$

These are a special case of more general formulas for bars with initial variable twist and initial curvature discussed and derived in detail by A. E. H. Love[3] and H. Reissner.[4] For completeness a brief derivation of the formulas is given in the next section.

Derivation of Fundamental Formulas

The differential equation for the displacement of a bar may be written in the form

$$EI\kappa = M \tag{4}$$

where κ is the curvature of the plane displacement curve and M is the bending moment. In the case of an untwisted bar with loads along both principal axes it is customary to apply Eq. (4) to the two projections of the space displacement curve. For a twisted bar with small rate of twist θ it is assumed to be a good approximation to apply Eq. (4) to the projections of the space curve on the u, z and v, z axes at each section (Fig. 1).

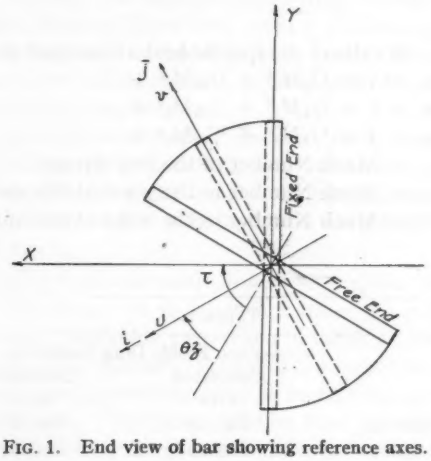

FIG. 1. End view of bar showing reference axes.

The curvatures κ of the two projections at each section can be calculated directly or, more simply, as follows.

Let $\boldsymbol{r}$ be the position vector of a point on the space displacement curve. Then

$$\boldsymbol{r} = u(z)\boldsymbol{i} + v(z)\boldsymbol{j} + z\boldsymbol{k} \tag{5}$$

where $\boldsymbol{i}, \boldsymbol{j}, \boldsymbol{k}$ is a right-hand set of unit vectors. If s is distance measured along the curve and if the displacement is assumed to be small so that $ds/dz = 1$, then

$$d\boldsymbol{r}/dz = (d\boldsymbol{r}/ds)(ds/dz) = \boldsymbol{T} \tag{6}$$

Received June 29, 1945.

* Assistant Professor of Mathematics.

$$d^2\mathbf{r}/ds^2 = (d\mathbf{T}/ds)(ds/dz) = d\mathbf{T}/dz = \kappa\mathbf{N} \quad (7)$$

where $\mathbf{T}$ and $\mathbf{N}$ are the unit tangent and unit principal normal vectors, respectively.

Before applying Eqs (6) and (7) to Eq. (5) it should be noted that

$$d\mathbf{i}/dz = \theta\mathbf{j} \text{ and } d\mathbf{j}/dz = -\theta\mathbf{i}$$

Now by differentiating Eq. (5) twice with respect to z it is easily shown that

$$\kappa\mathbf{N} = \left(\frac{d^2u}{dz^2} - 2\theta\frac{dv}{dz} - \theta^2u\right)\mathbf{i} + \left(\frac{d^2v}{dz^2} + 2\theta\frac{du}{dz} - \theta^2v\right)\mathbf{j} \quad (8)$$

It is apparent now that the components on the right of Eq. (8) are the curvatures of the projections of the space curve on the u, z and v, z planes, respectively, at section z. Substitution of these values in Eq. (4) gives the formulas (2) and (3).

Bending Moments and Shears

M_u and M_v are the moments of the loads between section z and the free end with respect to the u and v axes, respectively, at section z. M_u is positive if, as a vector, it points in the direction of the u axis. The same right-hand rule applies to M_v.

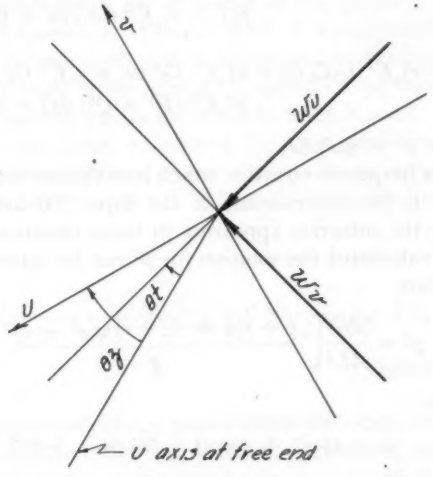

Fig. 2. End view of bar showing axes at section $z = z$ and loads w_u and w_v at section $z = t$.

The following formulas are obtained with reference to Fig. 2.

$$M_u = w_v\int_0^z (z-t)\cos\theta\,(z-t)\,dt - w_u\int_0^z (z-t)\sin\theta(z-t)\,dt$$

$$M_v = -w_u\int_0^z (z-t)\cos\theta(z-t)\,dt - w_v\int_0^z (z-t)\sin\theta(z-t)\,dt$$

$$V_u = w_v\int_0^z \sin\theta(z-t)\,dt + w_u\int_0^z \cos\theta(z-t)\,dt$$

$$V_v = w_v\int_0^z \cos\theta(z-t)\,dt - w_u\int_0^z \sin\theta(z-t)\,dt$$

The second derivatives with respect to z can be expressed in the forms

$$D^2M_u = -\theta^2M_u - 2\theta V_u + w_v$$
$$D^2M_v = -\theta^2M_v - 2\theta V_v - w_u$$
$$D^2V_u = -\theta^2V_u + \theta w_v$$
$$D^2V_v = -\theta^2V_v - \theta w_u$$

where $D = d/dz$.

If V_u and V_v are eliminated from the above expressions, one obtains M_u and M_v in the operational forms

$$M_u = -\theta^2w_v/(D^2+\theta^2)^2 \quad (9)$$

$$M_v = +\theta^2w_u/(D^2+\theta^2)^2 \quad (10)$$

Displacement Functions

The expressions for M_u and M_v given in Eqs. (9) and (10) are now substituted in the Eqs. (2) and (3). The differential equations of the component displacement functions $u(z)$ and $v(z)$, expressed in operational form, are

$$(D^2-\theta^2)u - 2\theta Dv = -\theta^2a/(D^2+\theta^2)^2 \quad (11)$$

$$2\theta Du + (D^2-\theta^2)v = -\theta^2b/(D^2+\theta^2)^2 \quad (12)$$

where $a = w_u/EI_v$, $b = w_v/EI_u$.

There are eight boundary conditions. The slope and displacement at the fixed end of the bar are zero. Thus,

(1) $u = 0, z = L$ (3) $Du = 0, z = L$
(2) $v = 0, z = L$ (4) $Dv = 0, z = L$

Since M_u and M_v are zero at the free end it follows from Eqs. (2) and (3) that

(5) $(D^2-\theta^2)u - 2\theta Dv = 0,\ z = 0$
(6) $2\theta Du + (D^2-\theta^2)v = 0,\ z = 0$

The shears V_u and V_v are also zero at the free end. Then from the formulas for M_u and M_v one observes that

$$DM_u = +\theta M_v + V_v = 0, z = 0$$
$$DM_v = -\theta M_u - V_u = 0, z = 0$$

The last two boundary conditions are now obtained by differentiating Eqs. (2) and (3) once with respect to z. Thus,

(7) $D(D^2-\theta^2)u - 2\theta D^2v = 0, z = 0$
(8) $2\theta D^2u + D(D^2-\theta^2)v = 0, z = 0$

Eqs. (11) and (12) can now be solved. From Eq. (11)

$$v = \frac{(D^2+\theta^2)^2(D^2-\theta^2)u + \theta^2a}{2\theta D(D^2+\theta^2)^2}$$

Substituting this value of v in Eq. (12), one obtains

$$(D^2+\theta^2)^4u = \theta^4a \quad (13)$$

The complete solution of Eq. (13) can be expressed in the form

$$u = R(A + Bz + Cz^2 + Dz^3)e^{i\theta z} + a/\theta^4 \quad (14)$$

where R indicates the real part of the expression following and A, B, C, D are complex constants. It is easily shown that corresponding to u given by Eq. (14)

$$v = Ri(A + Bz + Cz^2 + Dz^3)e^{i\theta z} + b/\theta^4 \quad (15)$$

where, as in Eq. (14), i is the imaginary unit.

$$P = \frac{1}{\theta^4}\left[1 - \cos\theta(L-z) + \frac{1}{2}\theta^2(L-z)^2\cos\theta z - \theta(L-z)\sin\theta(L-z) + \frac{1}{6}\theta^3(L-z)^2(2L+z)\sin\theta z\right] \quad (18)$$

$$Q = \frac{1}{\theta^4}\left[\sin\theta(L-z) - \theta(L-z)\cos\theta(L-z) + \frac{1}{2}\theta^2(L-z)^2\sin\theta z - \frac{1}{6}\theta^3(L-z)^2(2L+z)\cos\theta z\right] \quad (19)$$

If in Eqs. (16) and (17) one substitutes $\theta = 0$ the expressions P and Q have the indeterminate form 0/0. However, it is easily shown that

$$\lim_{\theta\to 0} P = (3L^4 - 4L^3z + z^4)/24$$
$$\lim_{\theta\to 0} Q = 0$$

Thus, u and v will reduce when $\theta \to 0$ to the familiar formula for the displacement of a cantilever bar due to a uniform load.

Coupled Fundamental Frequencies

The total potential energy of the oscillation, considering bending only, is

$$U = \int_0^L (M_v^2/2EI_v)\,dz + \int^L (M_u^2/2EI_u)\,dz$$

where M_v and M_u are determined by Eqs. (2) and (3). Using the displacement functions $u(z)$ and $v(z)$ given by Eqs. (16) and (17) one obtains

$$M_v = -EI_v(P''a + Q''b - \theta^2Pa - \theta^2Qb - 2\theta P'b + 2\theta Q'a)$$

$$M_u = +EI_u(P''b - Q''a - \theta^2Pb + \theta^2Qa + 2\theta P'a + 2\theta Q'b)$$

where the primes denote differentiation with respect to z. Or

$$M_v = -EI_v(aC_1 + bC_2)$$
$$M_u = +EI_u(bC_1 - aC_2)$$

where

$$C_1 = P'' + 2\theta Q' - \theta^2P \quad (20)$$

$$C_2 = Q'' - 2\theta P' - \theta^2Q \quad (21)$$

Thus,

$$U = \frac{EI_v}{2}\int_0^L (aC_1 + bC_2)^2\,dz + \frac{EI_u}{2}\int_0^L (bC_1 - aC_2)^2\,dz$$

The total kinetic energy of the oscillation is

The eight real constants are determined by the eight boundary conditions given. The final solutions for u and v are

$$u = Pa + Qb \quad (16)$$

$$v = Pb - Qa \quad (17)$$

where

$$T = \tfrac{1}{2}\gamma\omega^2\int_0^L (u^2 + v^2)\,dz$$
$$= \tfrac{1}{2}\gamma\omega^2\int_0^L (P^2 + Q^2)(a^2 + b^2)\,dz \quad (22)$$

where ω is the frequency of the oscillation. The quantity $(T - U)$ must now be minimized considering a and b as the variables. The two equations obtained by differentiating $(T - U)$ partially with respect to a and b are

$$a[\int_0^L C_1^2\,dz + r\int_0^L C_2^2\,dz - p^2\int_0^L (P^2 + Q^2)\,dz] + b(1-r)\int_0^L C_1C_2\,dz = 0 \quad (23)$$

$$a(1-r)\int_0^L C_1C_2\,dz + b[\int_0^L C_2^2\,dz + r\int_0^L C_1^2\,dz - p^2\int_0^L (P^2 + Q^2)\,dz] = 0 \quad (24)$$

where $p^2 = \gamma\omega^2/EI_v$.

The frequency equation which is of the second degree in p^2 is the determinant of the Eqs. (23) and (24). After the integrals appearing in these equations have been calculated the solution for p^2 can be expressed in the form

$$p^2 = \frac{35\tau^4}{4L^4}\left[\frac{(1+r)d \pm (1-r)\sqrt{e^2 + 4f^2}}{g}\right] \quad (25)$$

where

$$d = 48\tau(1 + \cos\tau) - 96\sin\tau + 8\tau^3 \quad (26)$$

$$e = -96\sin\tau + 6(5 - 2\tau^2)\sin 2\tau - 36\tau\cos 2\tau + 48\tau(1 + \cos\tau) - 24\tau \quad (27)$$

$$f = -33 + 48\cos\tau + 24\tau\sin\tau - 3(5 - 2\tau^2)\cos 2\tau - 18\tau\sin 2\tau \quad (28)$$

$$g = (1{,}680\tau + 420\tau^3 + 21\tau^5 + 11\tau^7) - (3{,}360 + 210\tau^4)\times\sin\tau + (1{,}680\tau - 140\tau^3 + 77\tau^5)\cos\tau \quad (29)$$

and $\tau = \theta L$.

The following coefficients of $\sqrt{EI_v/\gamma L^4}$ were calculated for $r = 16$:

$\tau = 0$; 3.53 and 14.12
$\tau = 0.8$; 3.68 and 14.0

$\tau = \pi/2$; 3.96 and 14.0
$\tau = \pi$; 5.5 and 13.6
$\tau = 2\pi$; 9.6 and 11.5

The exact values for $\tau = 0$ are 3.52 and 14.08.

As $\tau \to \infty$ the coefficients approach the common value 10.4. For $\tau = 1$ Eq. (25) gives nearly the same value, around 3.55, for all the above values of τ.

Conclusion

The preceding analysis is assumed to be valid only for small values of the rate of twist θ. However, Eq. (25) shows that the coefficients depend only on the total twist τ and, hence, large values of τ can be considered provided the corresponding L is large. The effect of coupling due to twist is relatively small for values of τ as high as 90°. It should be noted that the two fundamental frequencies converge to a common value as the twist increases; the smaller increases in value while the larger one decreases.

References

[1] Temple, G., and Bickley, W. G., *Rayleigh's Principle*, p. 150; Oxford University Press, London, 1933.

[2] von Kármán, Th., and Biot, M. A., *Mathematical Methods in Engineering*, p. 353; McGraw-Hill Book Company New York, 1940.

[3] Love, A. E. H., *The Mathematical Theory of Elasticity*, 4th Ed., p. 381; Cambridge University Press, London, 1934.

[4] Reissner, H., *Formänderung, Spannung und kleine Schwingungen von Staben mit anfänglicher Krümmung und Verwindung, die um eine Querachse rotieren*, Ingenieur Archiv, Vol. 4, p. 557, 1933.

Buckling Loads of Curved Thin Aluminum-Alloy Sheets

(*Continued from page 208*)

about 15 per cent and the average collapse load about 20 per cent lower than those for guides fastened without clearance.

From the results of these tests it becomes obvious that the influence of the clearance of the guides is of material importance. Guides with a nonadjustable slot and a given tolerance do not seem to give the highest possible loads of the panels; it appears to be necessary to adjust the guides individually to each panel.

Another test series, concerning the basic question of the detrimental influence of any eccentricity on curved panels, has been carried out. It could be shown that, contrary to the general consideration admitting that the slightest eccentricity of the panels is extremely harmful to their mechanical resistance under axial thrust, a local eccentricity of the panels up to as much as several tenths of an inch remains without marked influence on the buckling load or even on the collapse load. Because of their special character, details about these test results can only be published at a later date.

Reference

[1] Welter, G., Journal of the Aeronautical Sciences, Vol. 12, No. 3, pp. 357–369, July, 1945.

Effects of Surface Finish on Wing Profile Drag

(*Continued from page 213*)

drag coefficients calculated from Curtiss flight-test data, Table 1, as well as other unpublished comparisons, indicates that the cosine squared wake shape assumption is valid for normal wing wakes. At moderate Mach Numbers Eqs. (1) and (2) yield a c_{d_0} value that is higher than the actual drag coefficient.

The drag coefficients that are calculated by methods that include the effects of compressibility are presented in Table 2.

A comparison between the drag coefficients calculated with Eq. (3) and those obtained by correcting the drag coefficients in Table 1 by the Silverstein-Katzoff compressibility factor (F_c/F_1) shows that the two compare closely.

The conclusion may be drawn that use of the simplified Silverstein-Katzoff integrating equation yields drag coefficients that compare favorably with those calcuated with the longer, exact equations.

References

[1] Silverstein, A., and Katzoff, S., *A Simplified Method of Determining Wing Profile Drag in Flight*, Journal of the Aeronautical Sciences, Vol. VII, No. 7, pp. 295–301, May, 1940.

[2] Jones, B. M., *Measurement of Profile Drag by the Pilot-Traverse Method*, British R. & M. No. 1688, January, 1936.

Airfoil Theory for Rotary Wing Aircraft

RUFUS ISAACS*

United Aircraft Corporation

Introduction

In the author's previous paper, "Airfoil Theory for Flows of Variable Velocity,"† hereinafter referred to as AT, there was developed an airfoil theory for a stream with a greatly varying velocity. In particular, the lift was explicitly given for the case where the velocity consisted of a sinusoidal variation superposed on a constant velocity.

The chief application in mind of such a theory was rotary wing aircraft. In the present paper the theory, insofar as this application goes, will be completed. Specifically it includes the following addenda to AT: The angle of attack as well as the velocity is variable and the aerodynamic moment is computed in addition to the lift. The lift and moment are given specifically for the case where the angle of attack is also of the form constant plus sinusoidal variation; the frequency being the same as for the velocity variation but the amplitude and phase are arbitrary. The result is in the form of a complete Fourier series, as some applications call for a knowledge of certain higher harmonics.

To save a great deal of needless duplication the chain of ideas in AT will be followed closely; most of the content of this paper stresses the modifications necessary.

General Theory

The hypotheses of this section are the same as the corresponding section of AT except that α is now a function of the time. Eq. (1) of AT then becomes

$$v = \alpha w + x\dot{\alpha} + v_T(x, t) \tag{1'}$$

The reasoning of AT is unchanged until the equating to zero of the net flow through the plate. Then the system (10) is replaced by

$$\begin{aligned} c_1 &= b_2 - b_0 - 2\alpha w \\ c_2 &= b_3 - b_1 - b\dot{\alpha} \\ c_n &= b_{n+1} - b_{n-1} \quad (n = 3, 4, \ldots) \end{aligned} \tag{10'}$$

and likewise

$$c_0 = 2\alpha w + b\dot{\alpha} + b_0 + b_1 \tag{12'}$$

This leads to the final relation (in the periodic form),

$$b\pi(2\alpha w + b\dot{\alpha}) = \Gamma(t) + \int_0^\infty \Gamma'(t-\lambda)\left[\sqrt{\frac{2b}{W(t) - W(t-\lambda)} + 1} - 1\right] d\lambda \tag{14'}$$

The left side will be designated by $g(t)$. Making the same transformation as in AT,

$$\Gamma(t) = Q(W)$$

Eq. (14′) assumes the form

$$g(t) = Q(W) + \int_0^\infty Q'(W-\lambda)[\sqrt{(2b/\lambda) + 1} - 1]d\lambda \tag{16'}$$

The usual problem is: given $w(t)$ and $\alpha(t)$, to find $\Gamma(t)$. This now admits of a precise mathematical formulation as follows: $g(t)$ is a known function. By integration $W(t)$ is known and this may be inverted in general to give t as a function of W. Substituting its value in $g(t)$, there is obtained g as a function of W. Eq. (16′) is then an integral equation with Q as the unknown function, whose solution, when W is replaced by $W(t)$, solves the problem.

For later purposes, there is obtained by making the usual transformation

$$b_n = -\frac{1}{\pi b}\int_0^\infty Q'(W-\lambda)\left[\frac{(a - \sqrt{a^2-1})^n}{\sqrt{a^2-1}}\right]d\lambda \tag{16''}$$

where $a = 1 + (\lambda/b)$.

The Case of Rotary Wing Aircraft

Now $g(t)$ will be taken as a periodic function of circular frequency ω. And so for some complex $g_n(-\infty < n < \infty)$, $g(t)$ may be written

$$\sum_n g_n e^{in\tau}$$

with $\tau = \omega t$. Then, as in Eq. (17) of AT, $Q(W)$ may be written as

$$\sum_n a_n e^{in(\omega/w_0)W} \tag{17'}$$

where w_0 is the mean value of $w(t)$.

Inserting these series in Eq. (16′) and proceeding as in AT, there results

$$\sum_n g_n e^{in\tau} = \sum_n A_n e^{in(\omega/w_0)W}$$

Received April 2, 1945.

* Senior Analytical Engineer, Hamilton Standard Propellers Division. Now Assistant Professor Department of Mathematics, University of Notre Dame.

† Journal of the Aeronautical Sciences, Vol. 12, No. 1, January, 1945.

where $A_n = R_n a_n$ and

$$R_0 = 1$$

$$R_n = \psi\left(\frac{nb\omega}{w_0}\right) = \psi(nk), \ (n > 0)$$

$$R_{-n} = \bar{R}_n$$

ψ is given by AT, Eq. (19).

w and W are now taken as the same specific functions as on AT, page 114. Then applying the same technique as in AT there is obtained

$$A_n = \frac{1}{2\pi}\sum_m g_m \int_0^{2\pi}(1 + \sigma \sin\tau)e^{i(m-n)\tau}e^{in\sigma\cos\tau}\,d\tau$$

Then by well-known expressions for Bessel functions

$$A_0 = g_0 - (\sigma/2i)(g_1 - \bar{g}_1)$$

$$A_n = \frac{i^n}{n}\sum_m m g_m i^{-m} J_{n-m}(n\sigma), \ (n \neq 0)$$

It is now time to take a more explicit expression for $\alpha(t)$ such as will be encountered in connection with rotary wing aircraft. Thus

$$\alpha = \alpha_0(1 + \beta_1 \sin\tau + \beta_2 \cos\tau)$$

Let

$$h = 2b\pi\alpha_0 = (2b)(C_L/2)$$

where C_L is the mean lift coefficient, i.e., for angle of attack α_0.

Then from a short calculation

$$g_0 = w_0 h[1 + (\sigma/2)\beta_1]$$

$$g_1 = -\bar{g}_{-1} = \frac{w_0 h}{2i}\left[\sigma + (\beta_1 + i\beta_2)\left(1 + \frac{ik}{2}\right)\right]$$

$$g_2 = \bar{g}_{-2} = -(w_0 h\sigma/4)(\beta_1 + i\beta_2)$$

$$g_n = 0, \ (|n| > 2)$$

It follows further

$$A_0/hw_0 = 1 + (\sigma^2/2) + \sigma[\beta_1 - \beta_2\,(k/4)]$$

and using the abbreviations

$$J_n = J_n(n\sigma)$$

$$J^n = J_{n+1}(n\sigma) - J_{n-1}(n\sigma)$$

for $n \neq 0$

$$A_n = \frac{i^n}{n} w_0 h(H_n + iH_n')$$

with

$$H_n = {}^1/_2\, J^n\left(\sigma - \beta_1 - \beta_2\frac{k}{2}\right) - (2\beta_1/n\sigma)J_n$$

$$H_n' = {}_n\frac{\beta_2}{n} + \frac{J_n}{\sigma}\left[\beta_2(1 - \sigma^2) - \beta_1\frac{k}{2}\right]$$

Thus the A_n are known for this specific case. Then the a_n are, and from Eq. (17′) is obtained the circulation, so that the problem is now essentially solved.

Calculation of the Lift

AT can be followed without change until Eq. (25). In Eq. (26) the final $\alpha w'$ needs be replaced by $(\alpha w)'$. As further details consist of a routine application of the results in the earlier sections, they are omitted. Letting L_0 be the steady lift for the mean conditions, i.e., here

$$L_0 = \pi\alpha_0\rho w_0^2(2b) = h\rho w_0^2$$

and L the lift sought, the final result is

$$\frac{L}{L_0} = 1 + \frac{\sigma^2}{2} + \sigma\left(\beta_1 - \beta_2\frac{k}{4}\right) +$$

$$\left[\frac{k}{2}(\sigma + \beta_1) + l_1\right]\cos\tau + \left[\left(\sigma - \beta_2\frac{k}{2}\right)\left(1 + \frac{\sigma^2}{2}\right) +\right.$$

$$\left.\sigma^2\beta + l_1'\right]\sin\tau + \left(\frac{k}{2}\sigma\beta_2 + l_2\right)\cos 2\tau +$$

$$\left(\frac{k}{2}\sigma\beta + l_2'\right)\sin 2\tau + \sum_{n=3}^{\infty}(l_n\cos n\tau + l_n'\sin n\tau)$$

where

$$l_m + il_m' = -2mi^{-m}\sum_{n=1}^{\infty}\{F_n[J_{n+m}(n\sigma) - J_{n-m}(n\sigma)] +$$

$$iG_n[J_{n+m}(n\sigma) + J_{n-m}(n\sigma)]\}$$

$$F_n + iG_n = \frac{1}{n^2}[F(nk) + iG(nk)](H_n + iH_n')$$

H_n and H_n' as above

$\tau = \omega t$.

Computing the elementary lift for comparison

$$\frac{L_E}{L_0} = 1 + \frac{\sigma^2}{2} + \sigma\beta_1 + \beta_2\left(1 + \frac{\sigma^2}{4}\right)\cos\tau +$$

$$[2\sigma - \beta_1\,(1 + {}^3/_4\sigma^2)]\sin\tau + \ldots.$$

it should be noted that here, contrary to AT, the mean lift is not necessarily the same in both cases.

Calculation of the Moment

A climbing moment will be taken as positive. Following the procedure used hitherto, the moment M is decomposed into $M_I + M_J$, with

$$M_J = -\rho w\int_{-b}^{b}\gamma x\,dx$$

$$M_I = -(\rho/2)(d/dt)\int_{-b}^{b}(b^2 - x^2)\gamma\,dx$$

The integral in M_J has already occurred in the lift calculations of AT. From AT, Eq. (25), it is

$$b\Gamma - I = -\pi b^2\alpha w + ib\sum a_n S_n e^{inkW/b}$$

Thus I_1, the integral appearing in M_I, presents the only new difficulty. Evaluating it:

$$I_2 = b^3\int_0^\pi \sin^3\theta\gamma(\theta, t)\,d\theta$$
$$= {}^1/_2 b^3\int_0^\pi (1 - \cos 2\theta)\gamma(\theta, t)\sin\theta\,d\theta$$
$$= {}^1/_2 b^2\Gamma - (\pi/4)b^3 c_2$$
$$= {}^1/_2 b^2\Gamma + (\pi/4)b^4\dot{\alpha} - (\pi/4)b^3(b_3 - b_1)$$

Using Eq. (16″) and performing reductions by the usual techniques, there is obtained

$$I_2 = (\pi/4)b^4\dot{\alpha} + (b^2/2)\sum a_n T_n e^{inkW/b}$$

where

$$T_0 = 1$$
$$T_n = \zeta(nk),\ (n > 0)$$
$$T_{-n} = \bar{T}_n$$

and

$$\zeta(x) = 1 + i\int_0^\infty e^{-i\lambda}\times$$
$$\left[2\left(1 + \frac{\lambda}{x}\right)\sqrt{\left(1 + \frac{\lambda}{x}\right)^2 - 1} - 2\left(1 + \frac{\lambda}{x}\right)^2 + 1\right]d\lambda$$

Now, marshalling of the results leads to

$$M = \rho\pi b^3\alpha w^2 - \frac{\pi}{8}b^4\rho\dot{\alpha} - \rho bw\sum_{n\neq 0}A_n\times$$
$$\left(i\frac{S_n + {}^1/_4 nkT_n}{R_n}\right)e^{inkW/b}$$

In an appendix it will be shown that the expression in parentheses is equal to ${}^1/_2[1 - C(nk)]$.

Putting

$$M_0 = (b/2)L_0 = \rho\pi b^3\alpha_0 w_0^2 = (b/2)h\rho w_0^2$$

there is obtained

$$\frac{M}{M_0} = \frac{\alpha}{\alpha_0}\left(\frac{w}{w_0}\right)^2 + \frac{1}{8}k^2\left(\frac{\alpha}{\alpha_0}\right) + \frac{1}{i}\frac{d}{d\tau}\sum_{n\neq 0}\frac{i^n}{n^2}\times$$
$$(H_n + iH_n')[C(nk) - 1]e^{in(\tau - \cos\tau)}$$

All that remains is the arrangement as a Fourier series. This is a simple matter as it has already been done for the infinite series if the bracket is thought of as being replaced by $C(nk)$. Then the final result is

$$\frac{M}{M_0} = \left(1 + \frac{\sigma^2}{2} + \sigma\beta_1\right) + \left[\beta_2\left(1 + \frac{\sigma^2}{4} + \frac{k^2}{8}\right) + t_1\right]$$
$$\cos\tau + \left[2\sigma + \beta_1\left(1 + \frac{3}{4}\sigma^2 + \frac{k^2}{8}\right) + t_1'\right]\sin\tau +$$
$$\left[-\sigma\left(\frac{\sigma}{2} + \beta_1\right) + t_2\right]\cos 2\tau + (\sigma\beta_2 + t_2')\sin 2\tau +$$
$$\left(-\frac{\sigma^2\beta_2}{4} + t_3\right)\cos 3\tau + \left(-\frac{\sigma^2\beta_1}{4} + t_3'\right)\sin 3\tau +$$
$$\sum_{m=4}^{\infty}(t_m\cos m\tau + t_m'\sin m\tau)$$

where $t_m + it_m'$ is given by the same expression as $l_m + il_m'$ except that $F(nk)$ is to be replaced by $F(nk) - 1$.

Appendix

In the region R, $(I[x] \leq 0,\ x \neq 0)$ the following integrals exist

$$\xi(x) = x\int_0^\infty e^{-i\lambda x}(1 + \lambda - \sqrt{\lambda^2 + 2\lambda})\,d\lambda = x\alpha(x)$$
$$\zeta(x) = 1 + ix\int_0^\infty e^{-i\lambda x}[2(1 + \lambda)\sqrt{\lambda^2 + 2\lambda} - 2\lambda^2 - 4\lambda - 1]\,d\lambda$$

because both brackets $= 0(\lambda)$, $(\lambda \to \infty)$. Then for any region $I[x] \leq c < 0$

$$\zeta(x) = 1 - 2ix\alpha(x) + ix\int_0^\infty e^{-i\lambda x}[2\lambda(\sqrt{\lambda^2 + 2\lambda} - \lambda - 1) + 1]\,d\lambda = 2 - 2ix\alpha(x) + 2x\alpha'(x)$$

and so

$$\xi(x) + \frac{1}{4}x\zeta(x) = x\left[\left(1 - \frac{i}{2}x\right)\alpha(x) + \frac{x}{2}\alpha'(x) + \frac{1}{2}\right]$$

From the principles of analytic continuation this latter equality must be valid in R, in particular on the positive real axis. Here, from AT, Appendix II, Eq. (6),

$$\alpha(x) = -\frac{i}{x} - \frac{1}{x^2} - \frac{i}{x}\frac{\pi}{2}e^{ix}H_1^{(2)}(x)$$

Thus, a simple calculation gives

$$\xi(x) + \frac{1}{4}x\zeta(x) = -\frac{xi}{2}\frac{\pi}{2}e^{ix}\,H_0^{(2)}(x),\quad (x > 0)$$

Then, using Eqs. (5) and (7) from the same appendix, there is readily obtained

$$i\left[\frac{\xi(x) + {}^1/_4\zeta(x)}{\psi(x)}\right] = \frac{1}{2}\left[\frac{iH_0^{(2)}(x)}{H_1^{(2)}(x) + iH_0^{(2)}(x)}\right] =$$
$$\frac{1}{2}[C(x) - 1]$$

INSTITUTE of the AERONAUTICAL SCIENCES

President
ARTHUR E. RAYMOND

Vice-Presidents
P. R. BASSETT
J. H. KINDELBERGER
JOHN C. LESLIE
BURDETTE S. WRIGHT

Director
S. PAUL JOHNSTON

Executive Vice-President
BENNETT H. HORCHLER

Past-Presidents
J. C. HUNSAKER
CHARLES L. LAWRANCE
DONALD W. DOUGLAS
GLENN L. MARTIN
CLARK B. MILLIKAN
T. P. WRIGHT
GEORGE W. LEWIS
JAMES H. DOOLITTLE
FRANK W. CALDWELL
HALL L. HIBBARD
HUGH L. DRYDEN
R. H. FLEET
CHARLES H. COLVIN

Assistant to the President
GEORGE R. FORMAN

Secretary
ROBERT R. DEXTER

Treasurer
C. S. JONES

Controller
JOSEPH J. MAITAN

COUNCIL

LESTER D. GARDNER, *Chairman*

E. E. ALDRIN
PETER ALTMAN
REX B. BEISEL
LAWRENCE D. BELL
GEORGE W. BRADY
W. A. M. BURDEN
CHARLES H. COLVIN
JAMES H. DOOLITTLE
WILLIAM K. EBEL
SHERMAN M. FAIRCHILD
DONALD W. FINLAY
CHARLES FROESCH
LEROY R. GRUMMAN
R. PAUL HARRINGTON
W. WALLACE KELLETT
OTTO E. KIRCHNER
JEROME LEDERER
ROBERT J. MINSHALL
EARL D. OSBORN
ELMER A. SPERRY, JR.
ERNEST G. STOUT
FRED E. WEICK

ADVISORY COMMITTEE

W. M. ALLEN
WALTER BEECH
ERNEST R. BREECH
RALPH S. DAMON
DONALD W. DOUGLAS
R. H. FLEET
JACK FRYE
ROBERT E. GROSS
R. M. HAZEN
H. MANSFIELD HORNER
J. C. HUNSAKER
CROIL HUNTER
TH. VON KÁRMÁN
I. M. LADDON
P. W. LITCHFIELD
F. W. MAGIN
ALFRED MARCHEV
GLENN L. MARTIN
THOMAS A. MORGAN
R. C. MUIR
JOHN K. NORTHROP
W. A. PATTERSON
E. T. PRICE
F. W. REICHELDERFER
LAURANCE S. ROCKEFELLER
FRED H. ROHR
T. CLAUDE RYAN
GUY W. VAUGHAN
EDWARD P. WARNER

HONORARY MEMBERS

JOHN C. ADAMS
GRIFFITH BREWER
W. A. M. BURDEN
E. U. CONDON
L. C. CRAIGIE
IRA C. EAKER
HARRY F. GUGGENHEIM
HENRY G. HOUGHTON
GEORGE B. PEGRAM
L. WELCH POGUE
J. LAURENCE PRITCHARD
ARTHUR W. RADFORD
F. W. REICHELDERFER
H. B. SALLADA
CARL SPAATZ
L. C. STEVENS
NATHAN F. TWINING

HONORARY FELLOWS

H. H. ARNOLD
DONALD W. DOUGLAS
HUGH L. DRYDEN
W. F. DURAND
SIR RICHARD FAIREY
SIR ROY FEDDEN
J. C. HUNSAKER
SIR MELVILL JONES
GEORGE W. LEWIS
GLENN L. MARTIN
GEORGE J. MEAD
SIR FREDERICK HANDLEY PAGE
D. R. PYE
IGOR I. SIKORSKY
G. I. TAYLOR
TH. VON KÁRMÁN
EDWARD P. WARNER
ORVILLE WRIGHT
T. P. WRIGHT

BENEFACTORS

E. E. ALDRIN
HART O. BERG (Deceased)
W. A. M. BURDEN
E. L. CORD
DONALD W. DOUGLAS
SHERMAN M. FAIRCHILD
SIR RICHARD FAIREY
R. H. FLEET
FLORENCE GUGGENHEIM (Deceased)
C. D. HANSCOM
JOHN P. V. HEINMULLER
ALEXANDER KLEMIN
PAUL KOLLSMAN
BELLA C. LANDAUER
WILLIAM LANDAUER
GROVER LOENING
EDMUND C. LYNCH (Deceased)
F. W. MAGIN
GLENN L. MARTIN
GEORGE J. MEAD
S. A. REED (Deceased)
LAURANCE S. ROCKEFELLER
EDWARD P. WARNER

AMERICAN FELLOWS

JOHN D. AKERMAN
EDWIN E. ALDRIN
HARRY G. ARMSTRONG
KARL ARNSTEIN
J. L. ATWOOD
PAUL S. BAKER
RALPH S. BARNABY
P. R. BASSETT
WELLWOOD E. BEALL
REX B. BEISEL
G. M. BELLANCA
DON R. BERLIN
HENRY A. BERLINER
WILLIAM BOLLAY
B. C. BOULTON
GEORGE W. BRADY
LYMAN J. BRIGGS
W. G. BROMBACHER
CHARLES P. BURGESS
FRANK W. CALDWELL
KENNETH CAMPBELL
CHARLES H. CHATFIELD
ALLAN CHILTON
V. E. CLARK
FRANKLIN R. COLLBOHM
CHARLES H. COLVIN
KARL T. COMPTON
JOHN W. CROWLEY, JR.
RALPH S. DAMON
LUIS DE FLOREZ
SMITH J. DE FRANCE
J. P. DEN HARTOG
WALTER S. DIEHL
JAMES H. DOOLITTLE
C. S. DRAPER
IVAN H. DRIGGS
WILLIAM K. EBEL
C. L. EGTVEDT
FREDERIC FLADER
CHARLES FROESCH
JACK FRYE
GARLAND FULTON
LESTER D. GARDNER
RICHARD C. GAZLEY
MICHAEL E. GLUHAREFF
MELVIN N. GOUGH
LEROY R. GRUMMAN
HAROLD R. HARRIS
R. M. HAZEN
ALBERT F. HEGENBERGER
EDWARD H. HEINEMANN
S. D. HERON
HALL L. HIBBARD
L. S. HOBBS
PAUL E. HOVGAARD
WILLIAM HOVGAARD
ROBERT INSLEY
EASTMAN N. JACOBS
CLARENCE L. JOHNSON
ALEXANDER KARTVELI
PAUL H. KEMMER
J. H. KINDELBERGER
OTTO E. KIRCHNER
ARTHUR L. KLEIN
ALEXANDER KLEMIN
W. B. KLEMPERER
PAUL KOLLSMAN
OTTO C. KOPPEN
B. V. KORVIN-KROUKOVSKY
S. M. KRAUS
I. M. LADDON
E. S. LAND
CHARLES L. LAWRANCE
JOHN G. LEE
JOHN C. LESLIE
CHARLES A. LINDBERGH
WILLIAM LITTLEWOOD
GROVER LOENING
W. RANDOLPH LOVELACE, II
EUGENE E. LUNDQUIST
R. D. MACCART
JOHN R. MARKHAM
ERLE MARTIN
WM. H. MCAVOY
C. J. MCCARTHY
CLARK B. MILLIKAN
ROBERT J. MINSHALL
SANFORD A. MOSS
JOSEPH S. NEWELL
ALFRED S. NILES
JOHN K. NORTHROP
ARTHUR NUTT
SHATSWELL OBER
ROBERT R. OSBORN
W. BAILEY OSWALD
GEORGE A. PAGE, JR.
F. W. PAWLOWSKI
F. W. PENNOYER, JR.
A. A. PRIESTER
ARTHUR E. RAYMOND
F. W. REICHELDERFER
ELLIOTT G. REID
H. J. E. REID
H. C. RICHARDSON
LEONARD E. ROOT
C. E. ROSENDAHL
WILLIAM T. SCHWENDLER
JAMES M. SHOEMAKER
MAC SHORT
IGOR ALEXIS SIKORSKY
SELDEN B. SPANGLER
ELMER A. SPERRY, JR.
JOHN STACK
WILLIAM B. STOUT
HARRY A. SUTTON
C. FAYETTE TAYLOR
EDWARD S. TAYLOR
PHILIP B. TAYLOR
TH. THEODORSEN
T. E. TILLINGHAST
S. TIMOSHENKO
STARR TRUSCOTT
L. B. TUCKERMAN
RALPH H. UPSON
J. G. VINCENT
RICHARD VON MISES
FRANK L. WATTENDORF
P. V. H. WEEMS
FRED E. WEICK
R. D. WEYERBACHER
JOHN B. WHEATLEY
ANDREW V. WILLGOOS
DONALD H. WOOD
ROBERT J. WOODS
JOHN E. YOUNGER
ALBERT F. ZAHM
STEPHEN J. ZAND

An Appreciation

TO CORPORATE MEMBERS OF THE INSTITUTE OF THE AERONAUTICAL SCIENCES

Listed below are the leading aeronautical and industrial companies that make possible the publication of the *Journal of the Aeronautical Sciences*.

They enable the Institute to publish scientific and technical papers in the *Journal* and to devote its pages exclusively to editorial material.

Dues from individual members which would normally be used to publish this scientific and engineering monthly are thus released for additional services to the profession and industry.

The *Aeronautical Engineering Review* and the *Aeronautical Engineering Catalog*, together with the *Journal*, provide a comprehensive technical information service for the benefit of the aircraft and related industries.

ACADEMY OF AERONAUTICS
AERO INSURANCE UNDERWRITERS
AEROJET ENGINEERING CORPORATION
AEROQUIP CORPORATION
AGAWAM AIRCRAFT PRODUCTS, INC.
AIRCHOX COMPANY DIVISION, JOYCE AVIATION, INC.
AIRCRAFT RADIO CORPORATION
AIREON MANUFACTURING CORPORATION
AIRESEARCH MANUFACTURING COMPANY
AIRESEARCH MANUFACTURING COMPANY OF ARIZONA, INC.
AIREX MANUFACTURING COMPANY, INC.
ALLIS-CHALMERS MANUFACTURING COMPANY
ALLISON DIVISION, GENERAL MOTORS CORPORATION
ALUMINUM COMPANY OF AMERICA
AMERICAN AIRLINES SYSTEM
AMERICAN OVERSEAS AIRLINES, INC.
AMERICAN BOSCH CORPORATION
AMERICAN PHENOLIC CORPORATION
ASSOCIATED AVIATION UNDERWRITERS
ASSOCIATED FOUNDRIES & MANUFACTURERS, INC.
ATLAS SUPPLY COMPANY
BAKER STEEL & TUBE COMPANY
BEECH AIRCRAFT CORPORATION
BELL AIRCRAFT CORPORATION
BENDIX AVIATION CORPORATION
BENDIX PRODUCTS DIVISION
BENDIX RADIO CORPORATION
ECLIPSE-PIONEER DIVISION
EXPORT DIVISION
FRIEZ INSTRUMENT DIVISION
PACIFIC DIVISION
SCINTILLA MAGNETO COMPANY
THE BG CORPORATION
BOEING AIRCRAFT COMPANY
BOEING SCHOOL OF AERONAUTICS
BREEZE CORPORATIONS, INC.
ESSEX TOOL & DIE COMPANY
FEDERAL LABORATORIES, INC.
CAL-AERO TECHNICAL INSTITUTE, A DIVISION OF GRAND CENTRAL AIRPORT COMPANY
CARRIER CORPORATION
CESSNA AIRCRAFT COMPANY
CHANDLER-EVANS CORPORATION
CHASE NATIONAL BANK OF THE CITY OF NEW YORK
THE CLEVELAND GRAPHITE BRONZE COMPANY
THE CLEVELAND PNEUMATIC TOOL COMPANY
AUTOMOTIVE-AIRCRAFT DIVISION
CLIFFORD MANUFACTURING COMPANY
CONSOLIDATED VULTEE AIRCRAFT CORPORATION
NASHVILLE DIVISION
STINSON AIRCRAFT DIVISION
CONTINENTAL MOTORS CORPORATION
COX AND STEVENS AIRCRAFT CORPORATION
CULVER AIRCRAFT CORPORATION
CURTISS-WRIGHT CORPORATION
AIRPLANE DIVISION
DEVELOPMENT DIVISION
PROPELLER DIVISION
WRIGHT AERONAUTICAL CORPORATION
DOAK AIRCRAFT COMPANY, INC.
DOUGLAS AIRCRAFT COMPANY, INC.
EL SEGUNDO PLANT
LONG BEACH PLANT
THE DOW CHEMICAL COMPANY
DZUS FASTENER COMPANY, INC.
EASTERN AIR LINES, INC.
EATON MANUFACTURING COMPANY
THOMAS A. EDISON, INCORPORATED, INSTRUMENT DIVISION
EDO AIRCRAFT CORPORATION
THE ELECTRIC AUTO-LITE COMPANY
ELECTROL INCORPORATED
ENGINEERING AND RESEARCH CORPORATION
ETHYL CORPORATION
THE FAFNIR BEARING COMPANY
FAIRCHILD CAMERA & INSTRUMENT CORPORATION
FAIRCHILD AERIAL SURVEYS, INC.
FAIRCHILD ENGINE AND AIRPLANE CORPORATION
DURAMOLD DIVISION
FAIRCHILD AIRCRAFT DIVISION
RANGER AIRCRAFT ENGINES DIVISION
FEDERAL TELEPHONE AND RADIO CORPORATION
FIRESTONE AIRCRAFT COMPANY
FLEETWINGS DIVISION, KAISER CARGO, INC.
FLETCHER AVIATION CORPORATION
G & A AIRCRAFT, INC.
GENERAL AIRCRAFT EQUIPMENT, INC.
GENERAL AVIATION EQUIPMENT COMPANY, INC.
GENERAL ELECTRIC COMPANY
GENERAL INSTRUMENT CORPORATION
GENERAL MOTORS CORPORATION
AC SPARK PLUG DIVISION
AEROPRODUCTS DIVISION
BUICK MOTOR DIVISION
CADILLAC MOTOR CAR DIVISION
CHEVROLET MOTOR DIVISION
DELCO PRODUCTS DIVISION
DELCO-REMY DIVISION
EASTERN AIRCRAFT DIVISION
FISHER BODY DIVISION
FRIGIDAIRE DIVISION
HARRISON RADIATOR DIVISION
RESEARCH LABORATORIES DIVISION
ROCHESTER PRODUCTS DIVISION
THE B. F. GOODRICH COMPANY
THE GOODYEAR TIRE & RUBBER COMPANY
THE GRAY MANUFACTURING COMPANY
GRUMMAN AIRCRAFT ENGINEERING CORPORATION
GUIBERSON DIESEL ENGINE COMPANY
W. & L. E. GURLEY
HANNA ENGINEERING WORKS
HASKELITE MANUFACTURING CORPORATION
HAWAIIAN AIRLINES LIMITED
THE HILLIARD CORPORATION
THE INTERNATIONAL NICKEL COMPANY
JACK & HEINTZ, INC.
JACOBS AIRCRAFT ENGINE COMPANY
JOHNS-MANVILLE SALES CORPORATION
CASEY JONES SCHOOL OF AERONAUTICS, INC.
KELLETT AIRCRAFT CORPORATION
KENYON INSTRUMENT COMPANY, INC.
WALTER KIDDE & COMPANY, INC.
KOLLSMAN INSTRUMENT DIVISION, SQUARE D COMPANY
LANGLEY CORPORATION
LAVELLE AIRCRAFT CORPORATION
LEAR INCORPORATED
LIBERTY AIRCRAFT PRODUCTS CORPORATION
LINK AVIATION DEVICES, INC.
THE LIQUIDOMETER CORPORATION
LOCKHEED AIRCRAFT CORPORATION
LONGINES-WITTNAUER WATCH COMPANY, INC.
MAGNAFLUX CORPORATION
THE MARQUETTE METAL PRODUCTS COMPANY
THE GLENN L. MARTIN COMPANY
THE W. L. MAXSON CORPORATION
WARREN McARTHUR CORPORATION
McDONNELL AIRCRAFT CORPORATION
MENASCO MANUFACTURING COMPANY
MICROMATIC HONE CORPORATION
MINNEAPOLIS-HONEYWELL REGULATOR COMPANY
MOORE DROP FORGING COMPANY
NATIONAL CITY BANK OF NEW YORK
NATIONAL CREDIT OFFICE, INC.
THE NEW YORK AIR BRAKE COMPANY
NORMA-HOFFMANN BEARINGS CORPORATION
NORTH AMERICAN AVIATION, INC.
NORTH AMERICAN AVIATION, INC., OF TEXAS
NORTHROP AIRCRAFT, INC.
NORTHWEST AIRLINES, INC.
OTTO AVIATION CORPORATION
OWENS-CORNING FIBERGLAS CORPORATION
PAN AMERICAN WORLD AIRWAYS SYSTEM
THE PARKER APPLIANCE COMPANY
PENNSYLVANIA-CENTRAL AIRLINES CORPORATION
PESCO PRODUCTS COMPANY DIVISION, BORG-WARNER CORPORATION
PHILLIPS PETROLEUM COMPANY
PIONEER PARACHUTE COMPANY, INC.
THE PURE OIL COMPANY
REPUBLIC AVIATION CORPORATION
J. P. RIDDLE COMPANY
A. V. ROE CANADA LIMITED
JOHN A. ROEBLING'S SONS COMPANY
ROHR AIRCRAFT CORPORATION
ROOSEVELT FIELD, INC.
THE RYAN AERONAUTICAL COMPANY
SCIAKY BROTHERS
SCOTT AVIATION CORPORATION
SHELL OIL COMPANY, INC.
SIMMONDS AEROCESSORIES, INC.
SKYDYNE, INC.
SOCONY-VACUUM OIL COMPANY
SOLAR AIRCRAFT COMPANY
SPERRY GYROSCOPE COMPANY, INC.
SQUARE D COMPANY
STANDARD OIL COMPANY OF CALIFORNIA
STANDARD OIL COMPANY (INDIANA)
STANDARD OIL COMPANY OF NEW JERSEY
SWEDLOW AEROPLASTICS CORPORATION
TELEFLEX LIMITED
THE TEXAS COMPANY
THOMPSON PRODUCTS, INC.
TINNERMAN PRODUCTS, INC.
TITEFLEX, INC.
TRANSCONTINENTAL & WESTERN AIR, INC.
TRIPLETT & BARTON, INC.
UNION CARBIDE AND CARBON CORPORATION
BAKELITE CORPORATION
HAYNES STELLITE COMPANY
LINDE AIR PRODUCTS COMPANY
NATIONAL CARBON COMPANY
UNITED AIRCRAFT CORPORATION
CHANCE VOUGHT AIRCRAFT DIVISION
HAMILTON STANDARD PROPELLERS DIVISION
PRATT & WHITNEY AIRCRAFT DIVISION
PRATT & WHITNEY AIRCRAFT CORPORATION OF MISSOURI
SIKORSKY AIRCRAFT DIVISION
UNITED AIR LINES, INC.
UNITED STATES AVIATION UNDERWRITERS, INC
UNITED STATES RUBBER COMPANY
DOMINION RUBBER COMPANY, LTD.
THE VARIETY AIRCRAFT CORPORATION
VICKERS, INC.
VIDAL CORPORATION
THE WACO AIRCRAFT COMPANY
WARNER AIRCRAFT CORPORATION
THE WEATHERHEAD COMPANY
WESTERN AIR LINES, INC.
WESTINGHOUSE ELECTRIC CORPORATION
WESTON ELECTRICAL INSTRUMENT CORPORATION
WYMAN-GORDON COMPANY
YOUNG RADIATOR COMPANY

of the
ges ex-
neering
provide

ION
TEXAS

N

RATION
-WARNER

ON

ISION
ATION OF

, INC

RATION